39

SATELLITE & MESOMETEOROLOGY
RESEARCH PROJECT

Department of the Geophysical Sciences
The University of Chicago

THE ILLINOIS TORNADOES OF 17 AND 22 APRIL 1963

by

Joseph L. Goldman

SMRP Research Paper 39

January 1965

SATELLITE AND MESOMETEOROLOGY RESEARCH PROJECT
Department of the Geophysical Sciences
The University of Chicago

THE ILLINOIS TORNADOES OF 17 AND 22 APRIL 1963

SMRP Research Paper #39
January 1965

The research reported in this paper has been supported by the National Severe Storms Project, U. S. Weather Bureau, under grant CWB WBG - 20.

TABLE OF CONTENTS

THE ILLINOIS TORNADOES OF 17 AND 22 APRIL 1963

Joseph L. Goldman

Department of the Geophysical Sciences

The University of Chicago

Chicago, Illinois

ABSTRACT

Radar and photographic data are used to describe in detail the tornado of 17 April 1963 that struck the northern suburb of Kankakee, Illinois. Specific findings for the Kankakee Tornado include: (1) a detailed survey of the damage path with catalogued pictures taken of the damage while on the survey; (2) catalogued photographs of the tornado cloud system at various times and locations along the path, including a continuous distribution based on its photographic manifestations; (3) radar observations of the cloud system with computed cross sections through the echoes and a suggested distribution of giant hail encountered during the study; (4) speeds of the cloud system including an estimate of the relation between tornado and main cloud speeds along their respective paths; (5) the distribution of data points at which component motions of the cloud system were computed; and (6) the distribution of the vertical velocity component computed from motion pictures at four locations along the path, with two distributions of this component, normalized by using different indices. The methods used to survey damage, collect photographic data, and rectify photographs, as well as other techniques used in this study, are described in detail. Damage survey techniques were also applied to the limited data of the tornadoes of 22 April.

I. Introduction

In the pursuance of our aim to learn the structure of atmospheric phenomena, it sometimes behooves the researcher, normally satisfied with restricting himself to in-house type work, to confront personally the raw data used in his research by actively engaging in the field study associated with the gathering and reduction of the data. This is particularly true for those who are studying phenomena that are not adequately measured by existing data networks. Such has been the case in the study of the tornadoes that occurred on 17 and 22 April 1963.

When word was received that severe tornado damage had been wrought on a number of communities in Illinois and Indiana, it was decided that a survey should be made in order to locate precisely the path of the tornado and to correlate it with any meteorological evidence that might be obtained from surrounding data stations. The survey made by various members of the Mesometeorology Project is described in detail so

that the methods used can be evaluated and so that the energy expended in developing this process for obtaining data may be saved by this or other groups in similar undertakings. In addition, the methods used in obtaining visual (photographic) evidence of the tornado and the processes used in rectifying these data will also be described in detail. With the data obtained using these methods a concentrated effort is made to reveal the characteristic shape of the 17 April or Kankakee Tornado vortex and its changes with time and location along the damage path. As a result, the shape of the vortex and its translational movement and internal motion, as well as radar observational data of the entire storm cloud, are computed, analyzed, and/or correlated so that a more comprehensive view of the tornado's nature might be revealed.

As was described in a preliminary report of this study (Goldman and Fujita, 1963) the emphasis on photographic data collection was greater in the 17 April tornado, possibly accounted for by the fact that fewer photographs of the tornado clouds were obtained of the 22 April tornadoes. There were meteorological data stations which showed in their observations some effects of the tornado cyclone for the 22 April case; however, the addition of data collected for this case, other than that from the regular Weather Bureau network, made little difference in the surface meteorological analysis. Therefore, the analysis shown in the preliminary report of this study remains unchanged. Also, an examination of the upper air data for both cases resulted in the usual meteorological situation of strong vertical wind shear in the general area of the storm.

This study is a continuation of that reported in the preliminary study, and the locations of photographs with interpretive measurements of cloud elements in this study naturally supersede those of the preliminary study.

II. Survey of Damage Paths

Damage path surveys were made by three teams — two for 17 April comprised of three project members each, and one for 22 April of two members. Operating by automobile these groups used their odometers to calculate measurements from known road intersections to points of interest. It was found that the most expeditious method for completing the survey, especially of the 17 April path, was to assign each member of a team specific duties. The direction of the team was the responsibility of the navigator, who extrapolated the location of the path, noted its verified location and width, and kept notes on the distribution and orientation of significant debris. The driving was done by the pilot who also called out the odometer readings which were then noted by the navigator. All the picture taking was assigned to the photographer, who also recorded his locations and camera headings. In addition to these specific duties, all members of the team provided additional information as it was observed. Since no pictures were taken of the 22 April damage and since the paths extended through a more densely populated area, there was no necessity for assigning specific duties to the members of that team.

The general location of the 17 April damage path is shown in Fig. 1, which is a map of the affected area including the disposition of Weather Bureau stations about the path. As was explained in the preliminary report, the distribution of stations forms an ellipse with the path oriented along the major axis. The location of radar stations north and south of the path are depicted by antenna symbols.

The damage survey for the 17 April Tornado was begun in Bourbonnais, Illinois, the region of greatest population density along the path, and proceeded westward toward the origin of the damage path (see Fig. 2). The team surveying this part of the path consisted of Fujita as navigator, Kelley as pilot, and Arnold as photographer. In some instances the damage path could be determined only by a few fragments caught on fences since much of the debris had been cleared before the survey was instituted. The first day's survey continued westward to the gravel pits located north of Essex. Since no damage or debris was found west of the pits (shown in the figure) and since there were no eye witness accounts of any damage on the west side of the pits, the origin of the damage path was placed in that area. This is not meant to imply that the tornado circulation began in that region but only that the tornado circulation made its first contact with the ground in that area.

The portion of the damage path surveyed by the second team began at the intersection of U. S. Highway 54 with the path. This team was made up of Goldman as

navigator, Kelley as pilot, and Schwabach as photographer. Since a great part of this portion of the path extended through fields that had been cleared of debris immediately after the occurrence of the tornado, the surveyed damage consisted mainly of damaged farm buildings, fences, and uprooted or broken trees.

The points along the damage path from which photographs were taken by the survey teams are shown in Fig. 2; all of these photographs are catalogued and are available for reference. However, only a few have been selected to depict damage that might reveal some dynamic characteristics of the storm. These appear in a numbered sequence following Fig. 2. Some comments, nevertheless, regarding the more significant points of interest in the remaining unpublished damage photographs are made.*

From unpublished pictures 1 SE and 2 NW the width of the damage path is difficult to delineate since the tree damage is not continuous; picture 4 SW shows the first structural damage by the tornado. Picture 7 E suggests a widening area of damage; the series 8 NW through 12 NE reveals damage on the west bank of the Kankakee River. Confirmation of the tornado's northeast direction of motion may be seen by the damage on the opposite bank in the center of picture 12 NE. Pictures 14 W through 21 W are a panoramic view (in sequence) of the tornado's damage swath through a suburban housing development. Although the orientation of the debris in this series of pictures is not clearly uniform, the size of the area destroyed (revealed by missing houses) is a good indication of the width of the damage path.

The most severe property damage occurred at Olivet College: unpublished picture 23 SE shows exterior structural damage on the rear side of the administration building; pictures 27 SSW, 28 SSE, and 29 SE disclose damage to the campus trailer park; pictures 31 WSW and 32 SW show damage on the front side of the administration building. In addition to the exterior, substantial damage was inflicted on the interior walls of the building. The engineering specifications on the interior and exterior walls of the administration building are known and wind force could be computed by using such data. In this study, however, such computations are not made.

---

*In the discussion which follows references to damage photographs can be distinguished from later tornado pictures by their camera headings (e.g., picture 53 NNE). Also, in each case where the damage photograph is printed in this report a figure number reference is made; all other pictures are on file at the Satellite and Mesometeorology Research Project at the University of Chicago.

The next series of unpublished pictures, 33 SW through 38 N, show damage to the community of Exline, Illinois, where the principal effects were found on the south side of various structures. It should be noted that pictures 33 SW through 100 E were shot several days later than the preceeding pictures; the survey revealed that a great deal of the debris had been cleared or moved from its original orientation, so that it was necessary to rely on a tree and fence damage as the best evidence from which to derive qualitative examples of the direction of pressure and wind forces. Although the example is not unique, broken trees in picture 41 SSW may be seen toward the center of the path. Here also can be found an instance of debris removal, a small stump to the right of center (such trimmed stumps were later verified as being from broken trees).

On the east bank of the Kankakee River several small broken trees are evidence of the wind damage, and the house shown in picture 42 S of Fig. 3 had its roof removed and walls collapsed inward by the tornado. Again, wind directions at various points about the main damage could not be obtained since most of the large debris had been moved (see piled debris left of center). In picture 43 E an evergreen tree left of center is partially uprooted and leaning due east; tall telephone and power line supports (south side of road) had been replaced since the occurrence of the tornado; and a damaged barn barely discernable to the right of center can be seen in picture 44 SE. The orientation of debris at this point along the path was toward ENE or, more generally, along the path and toward its center. Picture 45 WSW, taken from east of the barn in 44 SE, includes damaged and totally destroyed trees oriented perpendicular to the path.

In picture 47 SE of Fig. 3 the orientation of the destroyed fence is evidence of cyclonic circulation; also, at this point, the width of the path could be determined with a high degree of accuracy from information obtained from the power line repairmen who were engaged in replacing the destroyed power lines. Since four supports at intervals of 135 ft were replaced paralleling a fence downed for a distance equal to 4 1/4 intervals (shown in the photograph by arrows), the lower limit of the diameter of the vortex is 540 ft. As was indicated previously, the fence leaned toward the west, north of a point along its length and toward the east, south of that point. The point was displaced toward the north of the center of its length, indicating asymmetry in the circular motion. In picture 48 N a damaged fence on the west side of the road leaned to the east. The differences between the orientation of fences on the east and west sides of roads were verified generally by surveyed damage farther along the path. Fences on the west side were either not damaged or pushed generally toward the east while those on the east side were either completely dismantled or oriented

to show counterclockwise circulation as in picture 47 SE (Fig. 3).

In one location a sizeable portion of macadam road surface was removed by the tornado; this is shown in picture 53 NNE of Fig. 4. As can be seen in the extreme right center of the picture, the macadam surface is strewn on the field east of the road. Both the north and south edges of the remaining road surface were straight enough to have been cut mechanically, and the orientation of both edges was east-west. In picture 54 ENE an uprooted tree lies south of the center of the damage path, oriented toward the center. Pictures 55 WNW and 56 ESE were taken in directions approximately parallel to the damage path. An eastward leaning fence in the center of 55 WNW may be noted as well as a consistent orientation of felled trees (perpendicular to and toward the center of the path) in 56 ESE. A first glance at the damage area of picture 58 S might seen to negate what was previously stated about fence damage; however, a perusal of the damaged fence on the west side of the road (right side of photo) would show it to be leaning toward the east and while new metal fence posts on the east side might be evidence of total destruction (at best they are indicative of an efficient proprietor). In 59 E, as well as in 60 E which is shown in Fig. 4, large trees are uprooted; considering their positions with regard to craters left by their roots, they appear to have been lifted and displaced before being dropped. Again their orientation is toward the center of the path; this phenomenon can be found also in picture 61 E which was taken from a distance to show the total width of the damage path. A lateral view of damage is shown also in pictures 62 ENE and 63 WNW where the tornado cut through a grove of trees, and in 64 ESE as it moved perpendicularly to another line of trees.

The variability in the direction of the tornado's damage path is probably shown best in picture 66 W of Fig. 5, although the quality of the photo is by no means good. Because of adverse weather conditions at the time of the shot, a time exposure was made but, as can be seen, the photographer moved, thereby producing the blurred image; yet the significant detail of the path is clearly shown by the dark region which extends toward the horizon and northward to the right where dried cornstalks in the field were obviously uprooted leaving a path of dark underlying soil. Although the variability in direction of path shown in 66 W (Fig. 5) extends over a length of one mile, the displacement of the path transverse to its general direction is too small to be indicated in the damage path of Fig. 2.

In picture 69 N of Fig. 5 the fence on the west side of the road is leaning eastward all along the section which is down; on the east side of the road the fence posts

had been newly erected. These facts seem to corroborate the evidence in pictures 47 SE (Fig. 3) and 48 N. Additional testimony to counterclockwise circulation may be seen in unpublished picture 72 SSE, where the fence on the east side of the road leaned both west and east consistent with counterclockwise circulation (westward leaning to the north of the path's center and eastward leaning to the south). One mile farther east, pictures 73 NE, 74 N, and 75 S show progressively increasing extent of damage; the path width at this point was easily determined from the almost total destruction of farm property, approximately two-tenths of a mile wide. At one mile east of this point, pictures 76 NE and 77 E depict the total destruction of a farmhouse. One may note the orientations of the uprooted tree in the center foreground of 76 NE and of the trees in 77 E — the trees which head northeast to the south of the center of the path and southeast north of the center. It is interesting that most of the dried corn stalks shown in these pictures were not from the field immediately west but, instead, from the field shown in picture 72 SSE and/or points even farther west. From the density of the stalks at the fence line, it appeared that they were all dropped or spewed out of the vortex simultaneously after being held in its circulation above the ground for at least one mile of path length. At one point in picture 83 E the tornado crossed the road (clearly shown by the orientation of fence posts on both sides of the road), and in 84 E and 85 WSW the tornado path runs south of the road and parallel to it. A house in 84 E and 85 WSW suffered damage, mainly to its roof and windows; however, there was little damage to its exterior and interior walls even though the dwelling was very close to the center of the path. The tornado then crossed to the north of the section road as evidenced by pictures 86 N and 87 NNW. In 88 SSW the path width may be estimated again from the beginning of a felled fence and trees south of the damage fence.

Unpublished pictures 89 NW and 90 W verify the change in direction of motion of the tornado from eastward to northeastward: the orientation of an uprooted tree in 89 NW is toward the south-southeast which is the same as the orientation of a large broken limb in picture 90 W; in picture 89 NW the edge of a crater left by an uprooted tree was not higher on its northern edge than on its southern edge and the part of the tap root remaining in the crater was directly beneath the lateral roots, again implying that the tree was pulled directly up and then dropped after a slight displacement. Picture 91 S shows the extent of the damage along the path and 92 NW contains an example of how debris had been cleared and stacked into neat piles. Pictures 93 NNW and 94 SSW show the south and north edges of the damage path at the point indicated in Fig. 2, and 95 E was taken from the western point of intersection

of the damage path with the road at the point where the tornado crossed the road to the south. Although the random orientation of the assorted debris shown in 95 E appears to be the result of the tornado, it was later concluded that some of the debris had been removed from road intersections in pictures 94 SSW and 95 E. Pictures 96 ESE and 97 WSW show damage to a large corn storage barn and surrounding structures. Since debris had again been moved, little information from the orientation of debris could be obtained.

Picture 98 N of Fig. 6 provides another clear view of fence damage showing counterclockwise circulation. Again, the fence is on the east side of the road, and the upright fence posts are closer to the northern edge than to the southern edge of the damage path. In picture 100 E, shown in Fig. 6, the recurving of the tornado's path is evident in the southward arc of the path of corn stalks left in the field. As can be seen in the foreground of the photograph, the dried stalks are wrapped around the damaged fence posts; east of the fence posts the stalks are strewn in small clumps following a general path across the field. Although it is not clear in the picture, the small clumps were located both north and south of the center of the path and were oriented in spiral-like ringlets extending inward to or outward from the center of the path.

The damage path of the 17 April tornado ended at the west side of highway #421 near Medaryville, Indiana. The last region where the tornado was in contact with the ground was a cornfield. According to an eyewitness, the debris, consisting mainly of corn stalks and husks, was strewn over an adjacent highway which was cleared immediately to permit the passage of traffic. Therefore, at the time of the survey, the cornfield had no sign of damage or strewn debris — the last visible evidence of the tornado being the roof damage (a few missing shingles) to a farmhouse immediately northeast of the field. Eyewitness accounts of the termination of the tornado were in general agreement that "the rope-like funnel moved snakelike through the cornfield and headed toward the farmhouse as it lifted into the dark cloud," wherefrom corn husks and stalks seemed to rain out of the dark cloud covering the highway and the bordering buildings north of Medaryville.

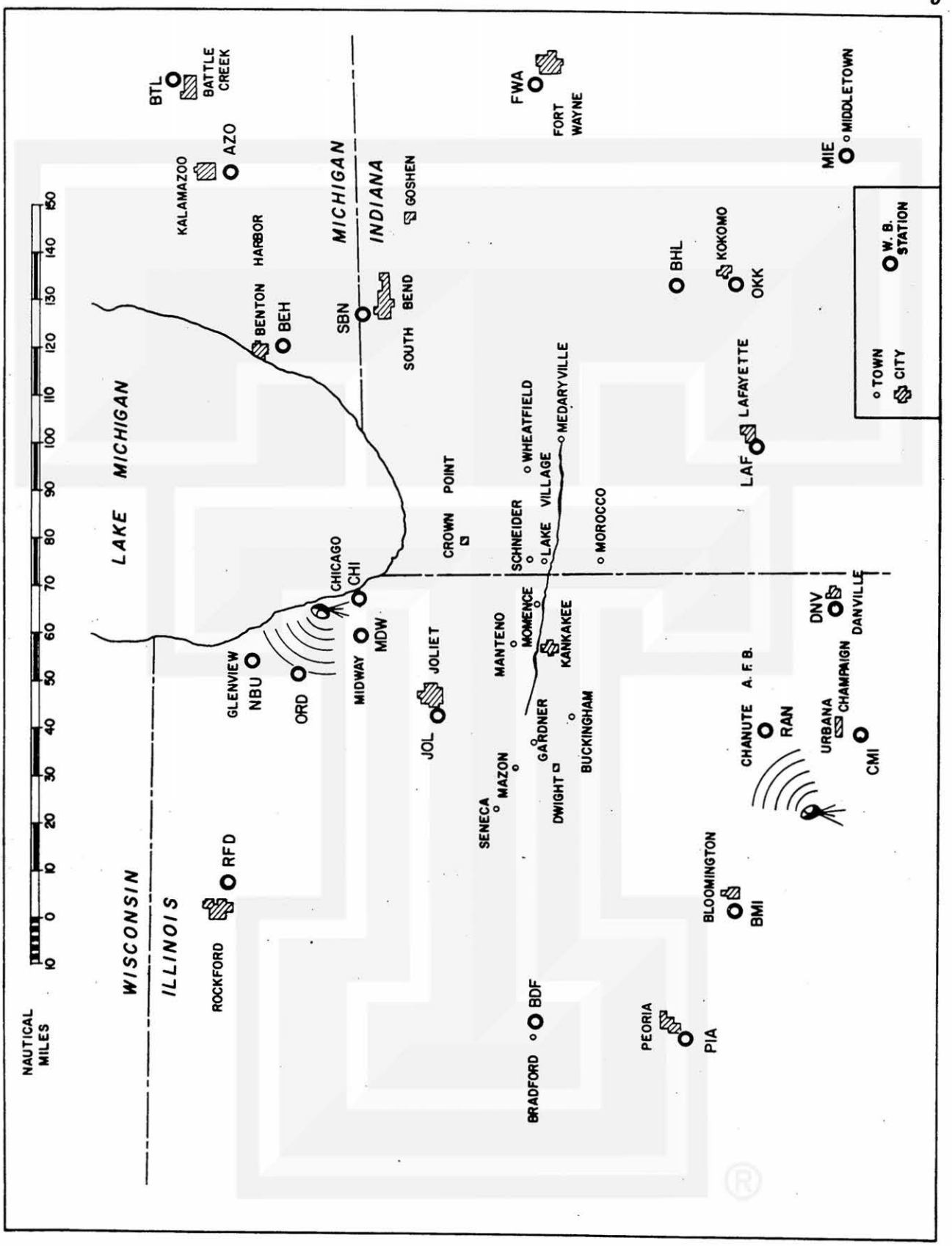

Fig. 1. Map of the area surrounding the 17 April 1963 tornado damage path. Note the distribution of Weather Bureau stations and the locations of the radar stations.

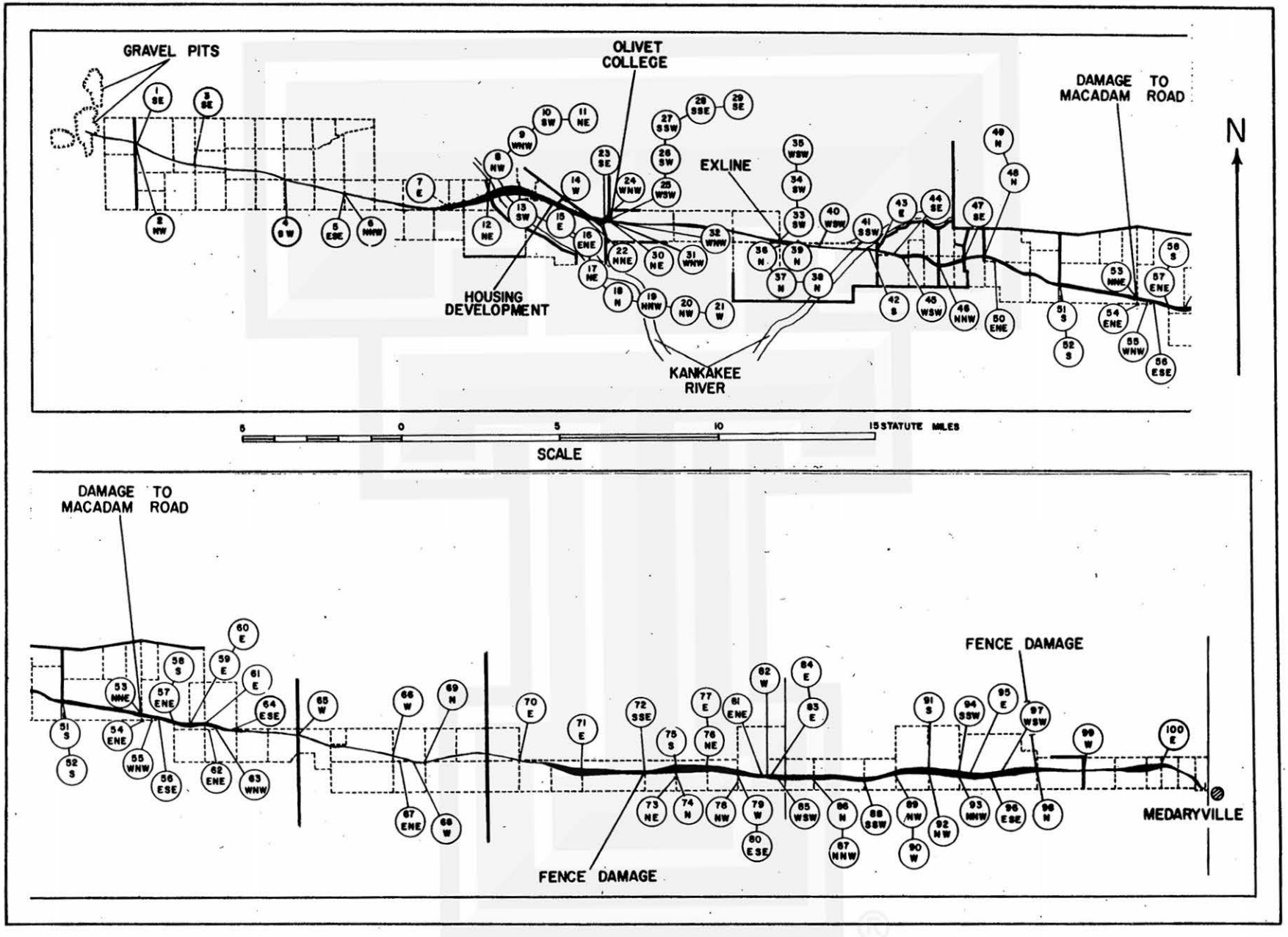

Fig. 2. Map locating the damage pictures taken while on the survey.

42 S

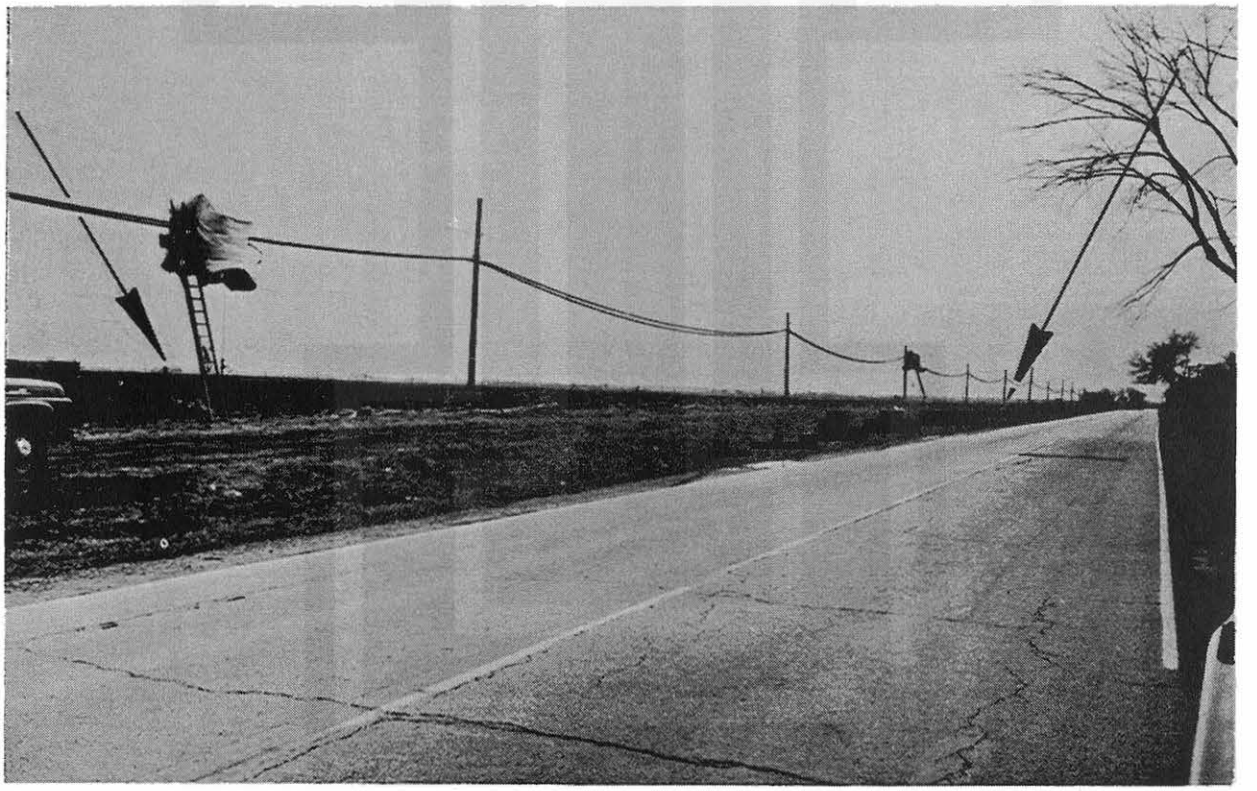

47 SE

Fig. 3. Damage photographs 42 S showing inward collapsed walls of a frame house and 47 SE showing width of tornado path and effects of circulation.

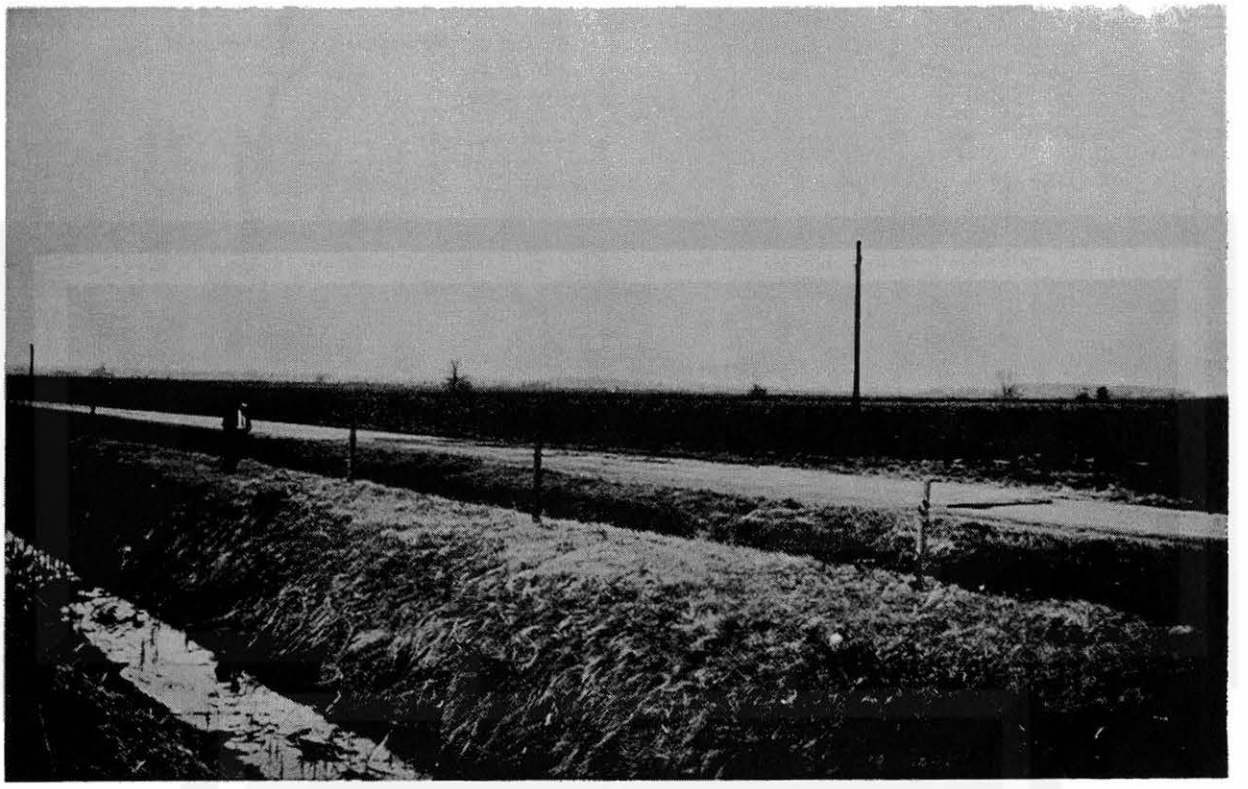

53 NNE

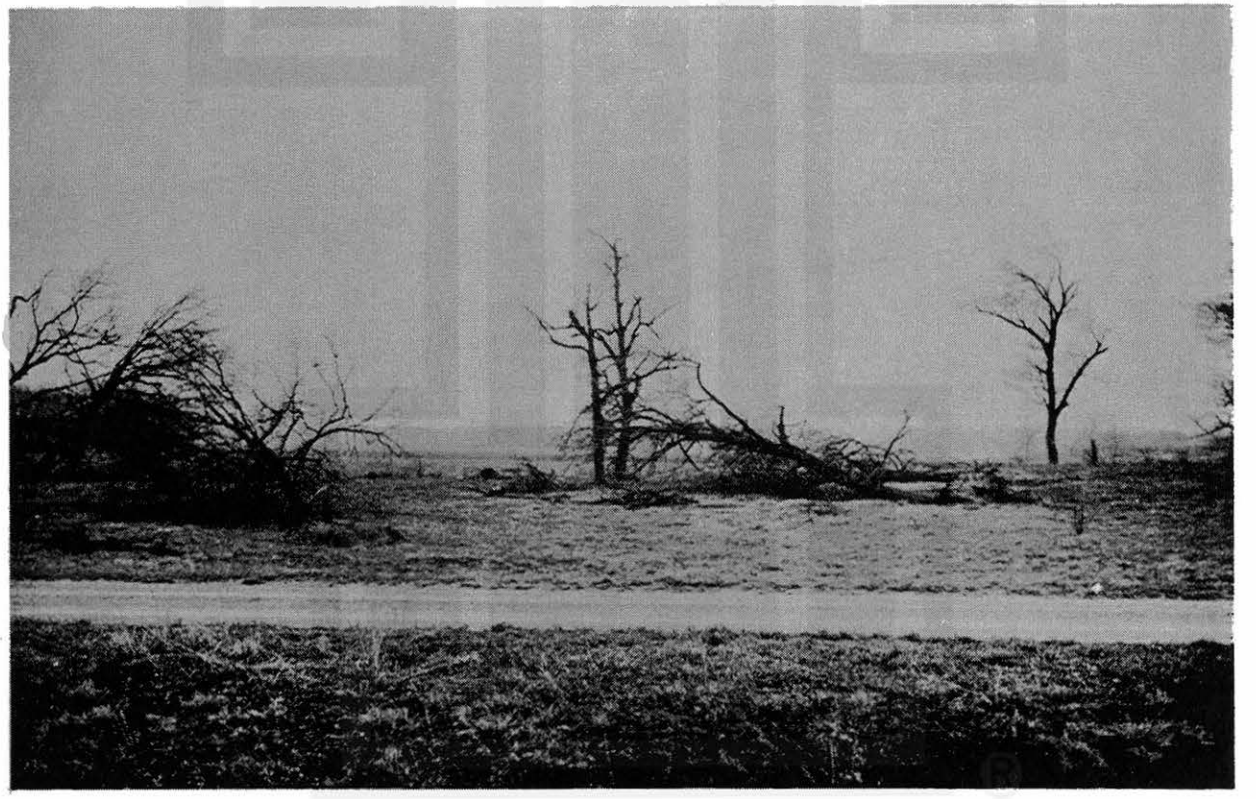

60 E

Fig. 4. Damage photographs 53 NNE of defaced macadam road whose surface was strewn across the neighboring field and 60 E of uprooted trees with their orientation toward the center of the path.

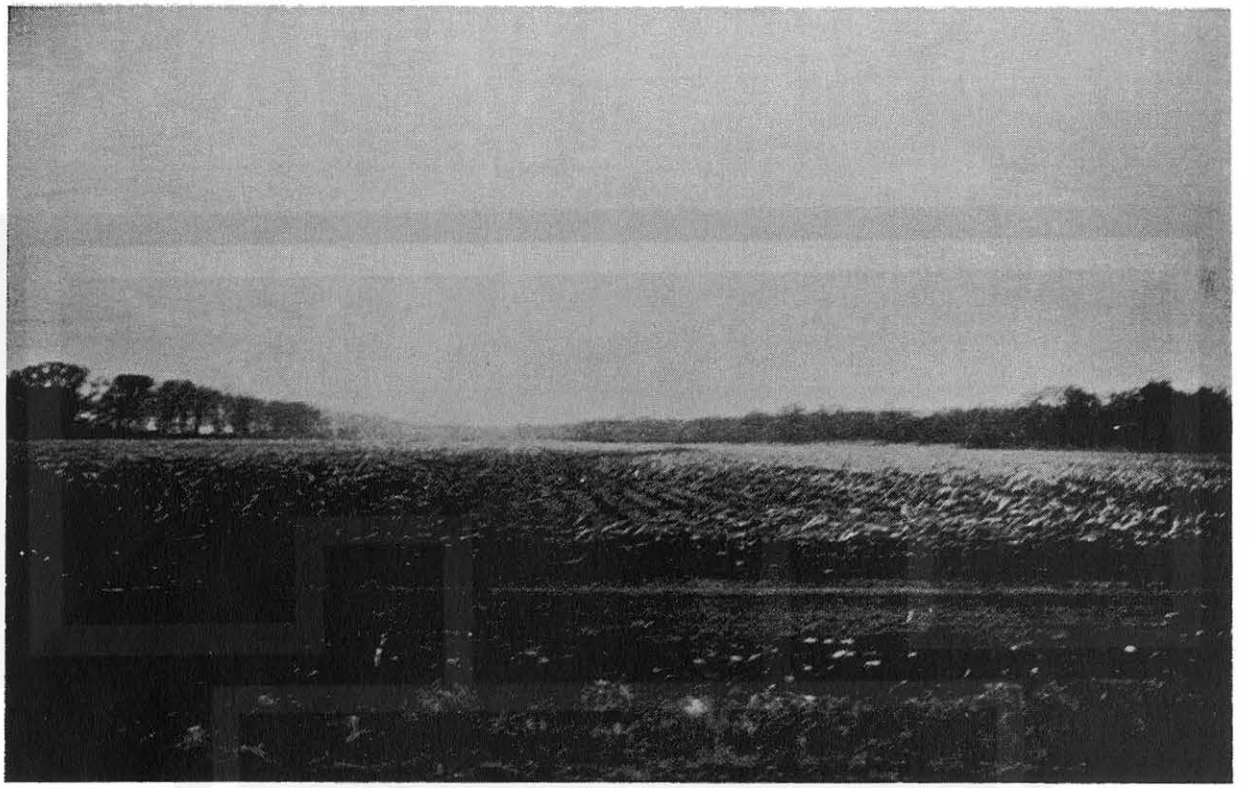

66 W

69 N

Fig. 5. Damage photographs 66 W of the damage swath through a cornfield and 69 N of the orientation of damaged fence.

98N

100 E

Fig. 6. Damage photographs 98 N showing fence damage evidence of counterclockwise circulation and 100 E showing the disposition of corn stalks in the path across a field.

III. Radar Analysis — 17 April Tornado

Radar coverage of the 17 April tornado was effected by two units located north and south of the damage path. The radar north of the path was a WSR-57 (10 cm) operated by the U. S. Weather Bureau in Chicago, and the radar south of the path was a CPS-9 (3 cm) operated by the Illinois State Water Survey in Champaign. As was explained in the preliminary report, the Champaign radar (CMI) followed the storm from an area before the funnel's first contact with the ground to the region of Lake Village, Indiana. The Chicago radar (CHIF) followed the storm from a point after its contact with the ground to the tornado's termination. The distance from the storm echo to CHIF was approximately 40 n mi and to CMI, 70 n mi. Throughout the observation period both radars were penetrating local echoes as well; therefore, the presentation of echoes at varying gain steps are approximations in absolute value of power and should be considered only in a relative sense.

In the literature of tornado radar echoes, the distinguishing portion of the echo that is usually related to the occurrence of tornadoes is called either a "hook echo" or a "pendant echo." In this study a distinction is made between these otherwise synonymous terms: the pendant echo is that portion extending from the large echo of the main cloud located in the southwest quadrant of an eastward moving main cloud; the hook is the element within the echo-free region between the pendant and the main cloud called the "echo free vault," (Browning, 1963).

The film of the CMI radar, containing a number of PPI presentations at various gain settings and elevations, shows that quantitative measurements of reflectivity are inhibited due to the factors of attenuation and beam width accompanying the 3-cm wave length radar. Unfortunately the CHIF radar films had few presentations at varying elevations so that comparisons of the two radars at varying elevations have not been made. In Fig. 7 are time composites of the CMI radar presentations. Throughout the period of observation the automatic gain stepping was not consistently applied to successive elevations so that the echoes shown for indicated times at various gain settings have been confined to zero elevation. Assuming average refraction conditions (4/3 R function), the heights of the zero-elevation echoes range from 2800 to 5000 ft. This means that the CMI radar had no chance of picking up the wide debris portion of the lower part of the tornado and if it intercepted any part of the tornado vortex at all it had to be the upper portion, or that part of the tornado system called the wall cloud.

The various gain settings, shown in Fig. 7 by the gradations of stippling,

correspond to values listed in Table I. The outlines of the first echo correspond to gain steps 1 through 5. The additional echoes have gradations bounded by steps 1, 3, and 4. The time scale in Fig. 7 is valid for each horizontal row of echoes, and the space scale is valid at each time. To compute the velocity of any portion of an echo, merely translate it perpendicularly to its position relative to the north line of the time of interest. The distance between the two echoes is now measurable with the space scale. The direction can be obtained from the north line and the time difference obtained, of course, from the noted values. The noted times are the central times of the periods covered by the indicated gain steps.

Table I

CMI Radar calibration of 19 April 1963 (Courtesy Illinois State Water Survey)

Gain Step	Power Reading (dbm)	10 log Pr/Pt (db)
1	-82	-132
2	-78	-128
3	-72	-122
4	-64	-114
5	-54	-104
6	-36	-86

The effect of attenuation becomes evident as one views all the echoes in time sequence. As can be seen, the earliest echo shown has five gain steps; whereas the later echoes have fewer, indicating a general decrease in echo intensity. However, one would expect the echo intensity to be greater during the latter period of the storm when the tornado was touching the ground and hail was falling. This expectation is borne out at least partially by the fact that the CMI radar had to penetrate echoes located near the station throughout the entire period of observation and that these interfering echoes remained on the scope after the tornado associated echo had been "gain-stepped" out.

The change in intensity of the intervening echoes is shown by the partial attenuation at 1605 1/4 which seems to have increased sufficiently to reduce the size of the echo to that of the next gain step. Although a calculation of probable drop size might

be attempted from the data shown, it is believed that attenuation due to the penetration of intervening strong cells and to the long path length of 70 n mi or more would make such an estimate too ambiguous to be of value. We can, however, observe the relative change in position of the echo core with time and, from this change in position, surmise a motion for the region that is believed to be that portion of the tornado system called the wall cloud.

In general the radar echoes consist of two main cores which seem to rotate about each other as they progress eastward along the cloud path. The arrows in Fig. 7, showing direction to the radar set, are drawn to assist in visualizing the attenuation in the core region. In the echoes from 1543 3/4 CST onwards, it seems as though the core of the pendant echo is partially attenuating what would be a portion of the core of the main or large echo; this is probably the case for most of the echoes. However, at 1551 1/2 the angular separation between the east edge of the pendant core and the west edge of the main core is about 1.5 deg; therefore, the core of the pendant could not have attenuated that much of the main core. There exists a possibility that attenuation from one of the intervening penetrated echoes caused this (more or less) perfect separation, but that seems remote. A more likely assumption would be that the core of the pendant is separated from the core of the main echo, as was the case with the Champaign pendant echoes of 9 April 1953 (see Fujita 1957). In the case of 17 April 1963 the distance between the pendant echo and the main echo was generally 2 n mi, and the pendant seems to have remained in a fixed position with respect to the main core once it had achieved the location (right flank and to the rear of the core of the main echo) shown by the echo at 1543 3/4 or 1551 1/2. These are also the times that the core of the pendant echo became separated from the core of the main echo.

A continuous chronological sequence of radar presentation might show that the core that was to become the pendant core separated from the main core at its trailing end and moved to the observed position (right-rear flank) by 1543 3/4. This interpretation leads to speculation regarding the motion of the pendant: whether it is propagating with respect to the main cloud or revolving about the main core under the influence of external steering forces. The speed with which the pendant revolves about the main core is about 3 kt, which is certainly slow enough to be considered propagation. However, deciding between the two motions in this study is impossible due to the lack of adequate upper air data.

Between the times shown for the gain-stepped echoes, there were elevation runs taken with the echo intensity at full gain. Figure 8 is a time composite of some of the elevation contoured echoes; the indicated times are central times of each period

over which the indicated elevation runs were made. These echoes are displayed in the same manner as those in Fig. 7, and the computation of echo velocity may be done by using the technique described previously.

The rather striking change in shape of the 0- and 4-deg elevation contours with time is believed to be due primarily to changes in attenuation caused by the intervening echoes mentioned earlier. At the higher elevations (above 1 deg) a greater attenuation would be expected since the radar would be penetrating the higher intensity regions of intervening storms which were 10 to 20 n mi distant from the radar. In particular, the rate of change in shape of the 5-deg contour indicates a large variability in attenuation. This is shown best by the disappearance of the 5-deg elevation contour at 1541 and 1555 CST and with its reappearance, at the later times, when the cloud is farther from the radar. Probably the noticable elongation of the low elevation contours in the direction of the echo's motion is due to attenuation at the echo itself. If reference is made to the gain-stepped echoes presented in Fig. 7, the elongated main cores of the echoes are seen to be oriented in the direction of motion of the storm and would, therefore, be an important factor in attenuating the power of the radar at points beyond that range. An example of this attenuation is the zero-deg elevation contour of the echo at 1639 CST in Fig. 8 and the orientation of the main cores of the later echoes in Fig. 7.

Even with this rather large attenuation factor, one characteristic of the radar observation did remain evident: the relatively unvarying location of the top turret of the cloud with respect to the hook. This location was pointed out by Browning and Ludlam (1962) in their analysis of the Wokingham Storm as being almost always directly above the wall of the echo free vault. In terms of the 17 April case, the wall would be on the north side of the hook area. The positioning of the top turret of the cloud with respect to the hook is shown in the vertical section of Fig. 9. For each echo time, three parallel sections spaced at 1-mi intervals are shown. The orientation of the cross-section lines through the center of the turrets for the various times are shown in Fig. 8. All the cross sections were taken at a constant angle, which was determined by the direction of the hard core of the pendant echo from the western point of the main echo after 1605 CST. As can be determined from Fig. 8 the motion of the echoes in the vertical cross section is not entirely perpendicular out of the plane of the figure; all would have a small component from left to right. As can be seen in the figure, the sections are drawn by connecting the incremental 1-deg elevation data points with a smoothed solid curve and by extrapolating these curves (dashed lines) where the extensions between and beyond data points seem obvious. The

attenuation of the echoes becomes evident by the diminishing volume of echo with heights on the right side of the vertical line. A rough estimate of the attenuation for the more distant parts of the cloud (right side of line) is as high as 7 db, assuming the intervening echoes to be composed of heavy rather than moderate showers.

An interesting comparison can be made of the vertical sections at 1639 with the photograph of the Chicago Radar RHI scope shown in Fig. 10. As is indicated the time of the photograph, 1628, corresponds to 1640 on the CMI radar's clock. This difference of 12 min is due to a slow clock at CHIF. The range markers are intervals of 20 n mi, and the vertical coordinate labeled on the right is in thousands of feet. As can be seen in the photograph, that portion of the cloud to the north of a hypothetical vertical line extending through the hook and the turret above is much greater than is indicated in the vertical sections of Fig. 9. The azimuth angle of the RHI presentation is 182 deg and a comparison of the path lengths through the cloud by the two radar beams would show a longer path length for CMI since it is penetrating the cloud at a greater angle to the minor axis than is the CHIF radar. Also the cross-section line is at an even greater angle to the minor axis (which can be assumed to be oriented north-south) than is the penetration angle of the CMI radar. Therefore, by all accounts the path length along the cross section should contain more cloud volume than is shown in the RHI picture; however, since it does not, we must conclude that this appearance is due to attenuation.

In an effort to visualize the movement of the tornado within the radar echo the path of the center of the highest point of the echo was plotted on a map containing the damage path. Although the difference in resolution of the radar path and the damage path is large, a comparison of the paths is made. The paths, presented in the same scale, are shown in Fig. 11. If the entire radar echo was plotted at various points along the path, the tornado damage path would intersect the pendant echo at all points.

An interesting feature of these plotted paths is that in every instance the few observations and estimates of giant hail that were made appear north of the damage path. Also, the largest of the giant stones seem to be distributed along the path taken by the center of the highest echo. Photographs of two of these large stones are shown in Fig. 12 and the plot of the giant stones is included in Fig. 11. Although the general study of the Kankakee tornado did not include hail as a major topic, a few remarks regarding its location and distribution with respect to size can be made.

Eyewitnesses were not questioned specifically about hail occurrence; nevertheless, information obtained from still shots, moving pictures, and unsolicited eyewitness information indicates that no hail fell on the ground south of the damage path. The

largest stone in Fig. 11 has been apprehended in a still photograph and moving pictures; its size can be compared with the nearby tread widths of tractor tires. The second largest stone was preserved in the freezer of a meat packing company; since it was kept in a plastic bag, it is assumed that the stone had not enlarged and could have decreased slightly in size before the picture in Fig. 12 was taken. Smaller hailstones were found preserved at the Lake Village Airport. Photographs taken at location 37, indicate that large hail (about 1 to 1-1/2 inches in diameter) fell prior to the occurrence of the tornado. Since there was no information concerning the length of time between the photograph and the actual hail shower, even a reasonable estimate of the original size of the photographed stones would be difficult; nevertheless, they must certainly have been larger than the size observed in the picture.

Although no information regarding the occurrence of hail was volunteered by residents at either end of the damage path, it may be assumed that no giant hail fell far from the region north of the path's mid-point. The region covered by the circles in Fig. 11 can therefore be considered a good estimate of the area on which the giant hail fell with the size spectrum consisting of an increase in hailstone diameters northward to a maximum at the path of the main radar echo and an associated decrease north of that path.

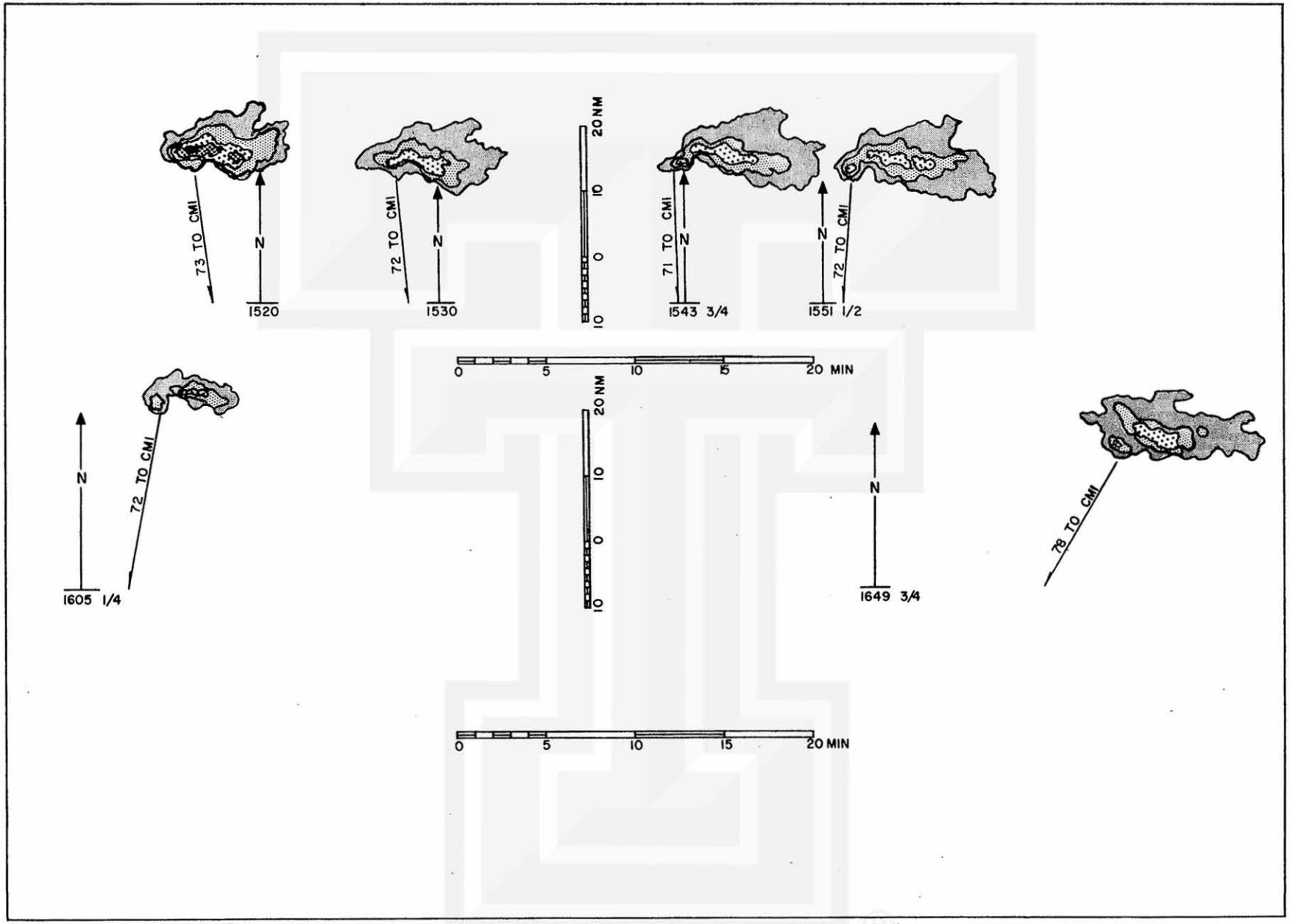

Fig. 7. CMI composite radar echoes at varying gain steps and zero elevation.

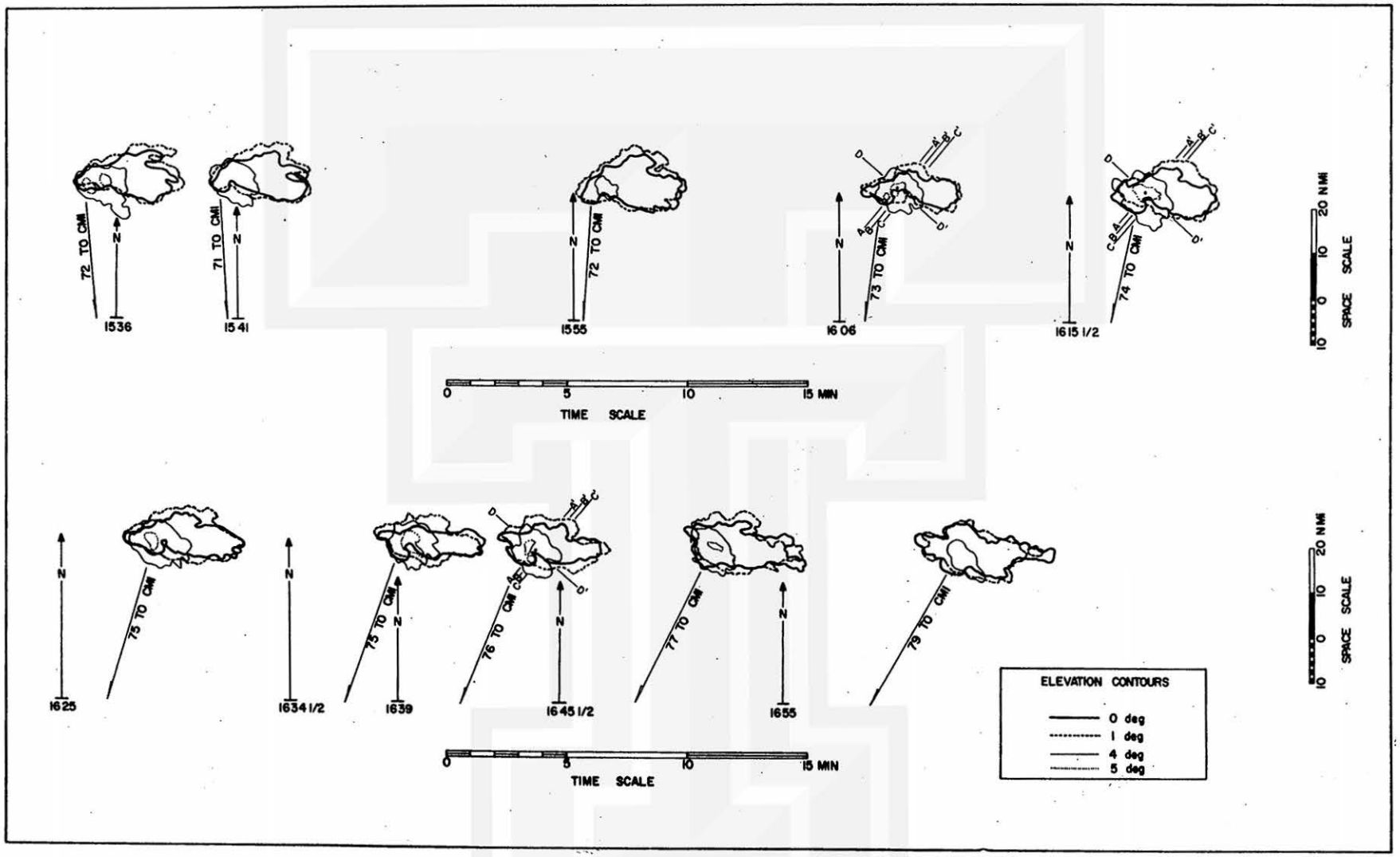

Fig. 8. CMI composite radar echoes at varying elevations and full gain.

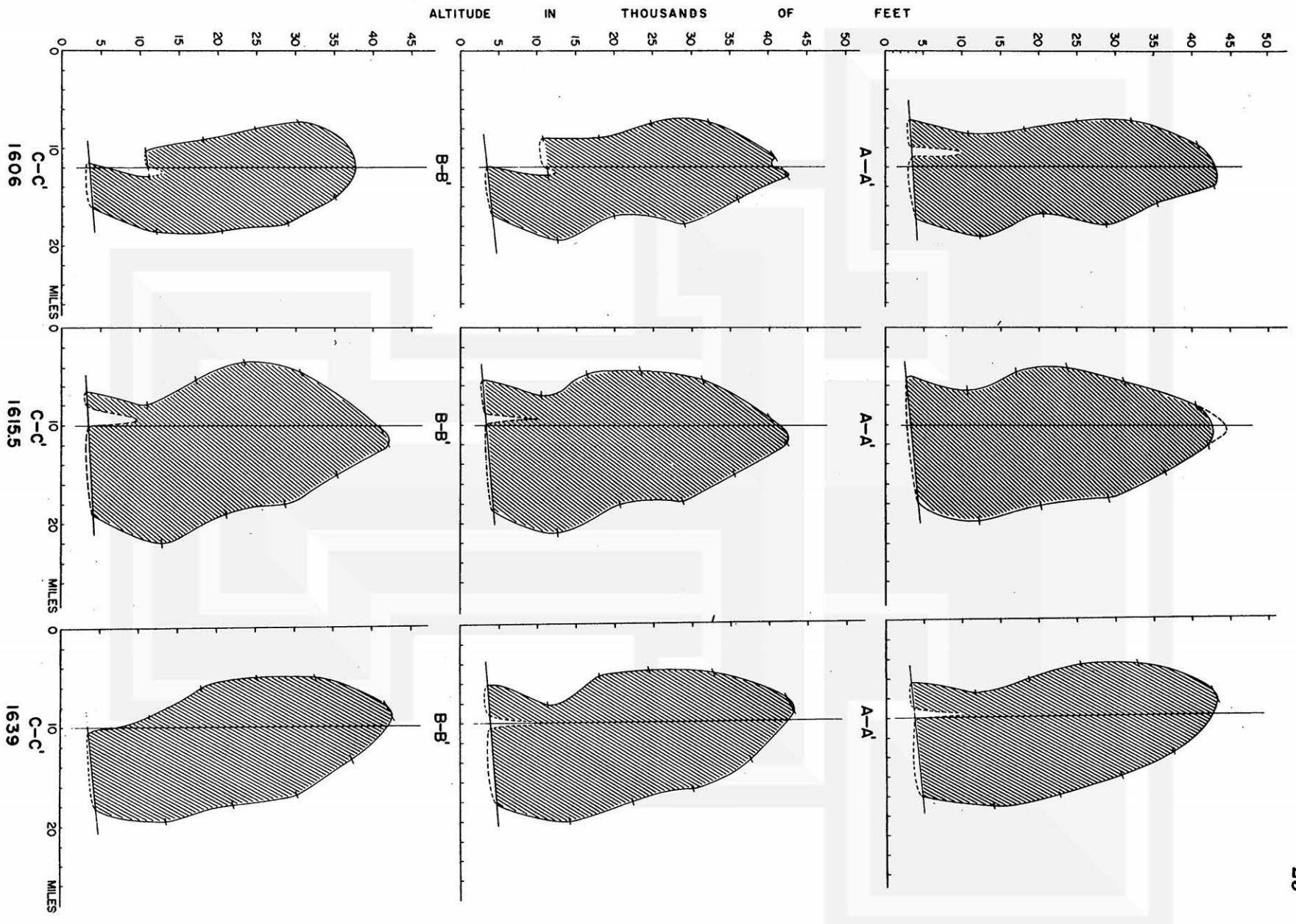

Fig. 9. Vertical sections along the lines indicated in Fig. 8 computed from the CMI Radar observations.

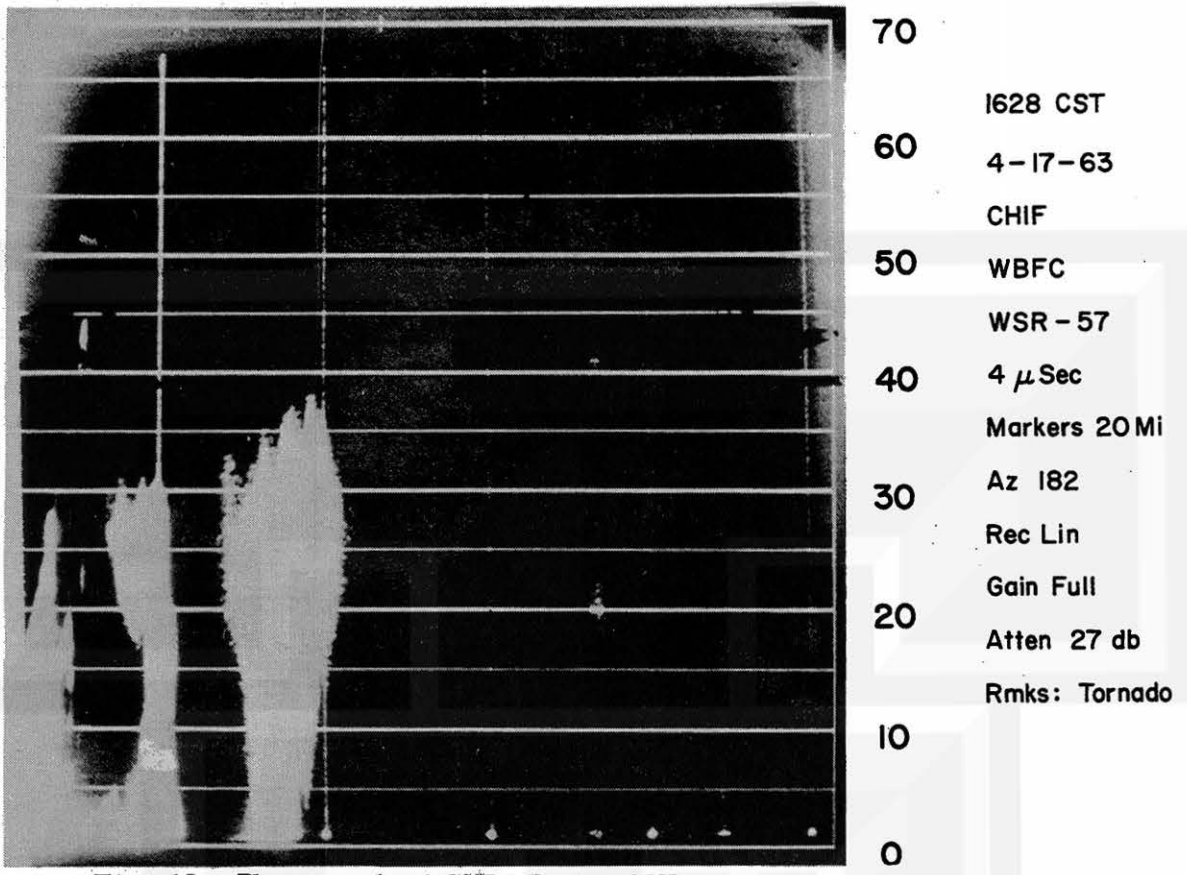

Fig. 10. Photograph of CHIF Radar RHI scope.

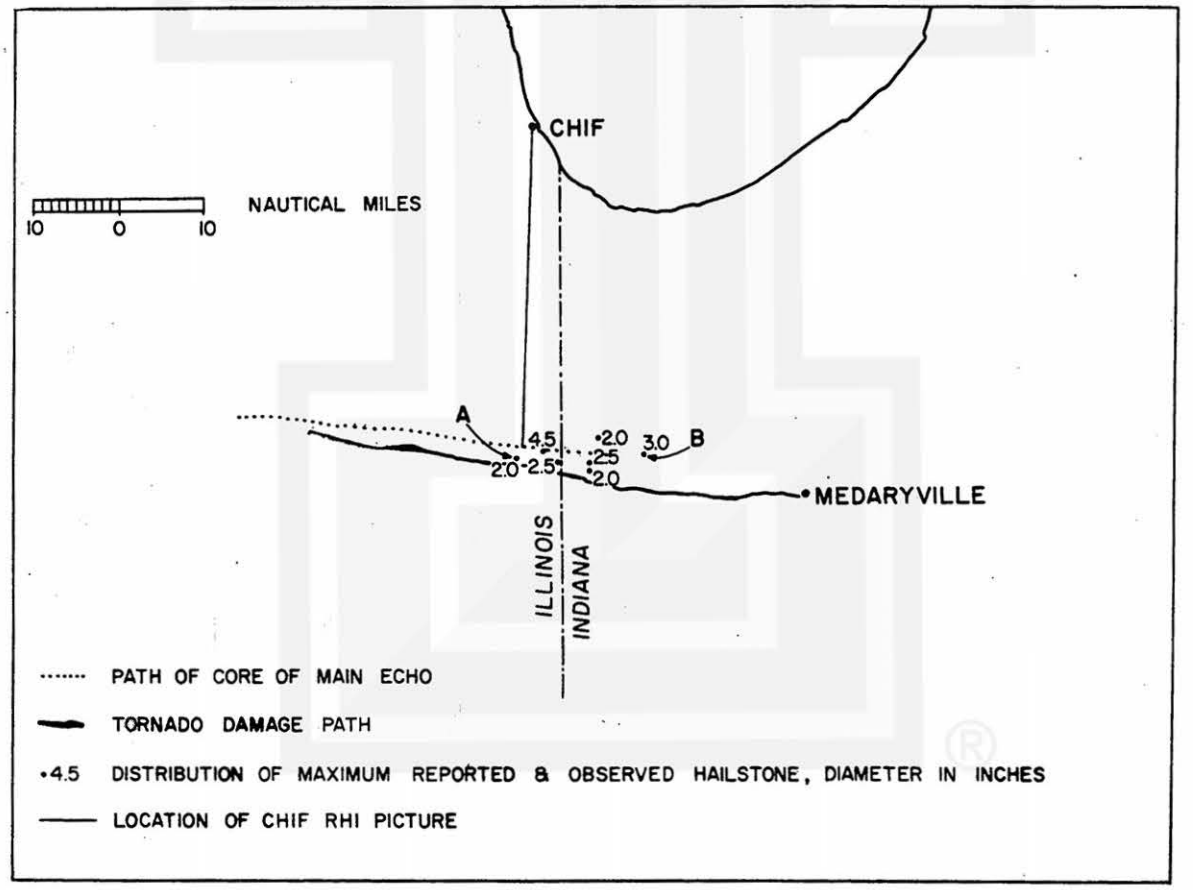

Fig. 11. Distribution of largest giant hail with the path of the main radar echo (dotted curve) and the tornado damage path (solid curve); orientation line of CHIF Radar RHI photo in Fig. 10.

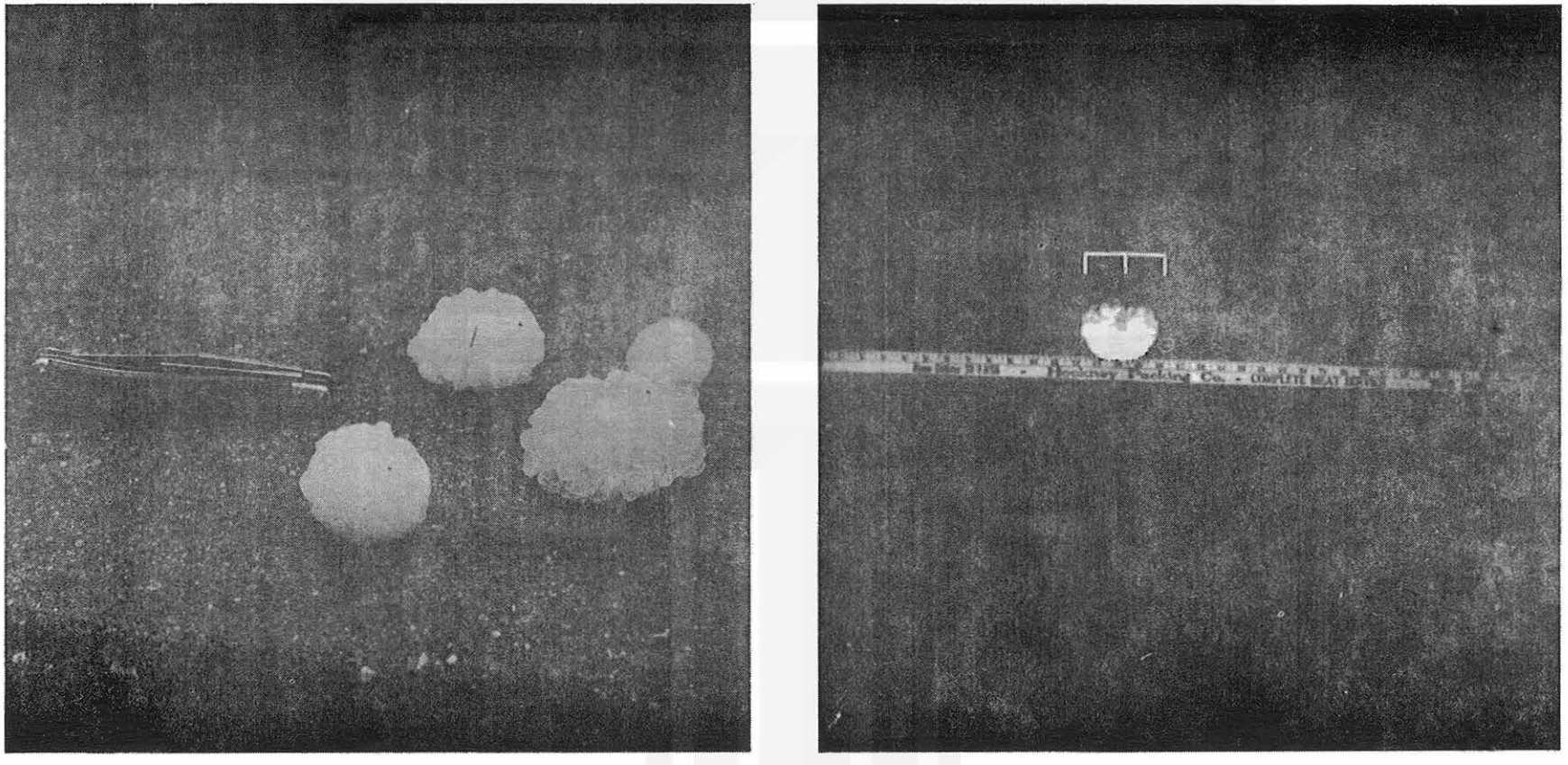

Fig. 12. Photographs of some of the giant hailstones referred to in Fig. 11: A, courtesy J. McQuown; B, courtesy Hockley Packing Co.

IV. Photographic Evidence of the 17 April Tornado

While surveying the damage path of the 17 April tornado, the survey team spoke with citizens in some of the larger communities near the damage path. The first indication of the existence of tornado cloud pictures taken by the public came from residents in Momence, Illinois. Upon returning to Chicago the team decided that a general appeal for cloud photographs should be made through the vast communication media of radio, television, and newspapers which cover Northeastern Illinois and Northwestern Indiana. In addition, a form letter was prepared and sent to various officials of the communities in the proximity of the damage path asking for their aid in locating people who had taken pictures of the tornado cloud. These appeals were reinforced by the efforts of the local television and radio weathermen who repeated our appeal for photographs a number of times throughout the course of this study.

The response to this initial effort was encouraging; approximately 40 cloud photographs and 20 ft of 8 mm movie film were obtained. Since the prints received lacked the contrast and definition necessary for photogrammetric measurement, the loan of the negatives as well as any original movie film became imperative. As a result of personal correspondence with each photographer additional requests for original film and negatives were complied with in every instance. After making enlarged prints of appropriate size and quality in order to distinguish permanent objects in the photographs, pictures taken with a precisely calibrated lens were shot from the exact locations assumed by the original photographers. During this calibration phase of the field study, much more direct contact was made with the photographers and their neighbors which resulted in an increased general public interest in both the cloud photographs and their potential value for a photogrammetric analysis.

At the request of the Davis Flying Service, whose members were personally involved in events related to the tornado, a public meeting was held at their airport in Lake Village, Indiana, to show what photographs had been obtained and to explain how these could be used for purposes of research. As a result of this, and additional meetings at the Grange Hall in Lowell, and again at the Davis airport the total number of still shots and movie film submitted to us increased significantly.

The abundance of photographic data with the accompanying information necessary to a photogrammetric analysis has made possible the following study of the characteristics of this tornado. Figure 13 is a map locating all the photographs of the Kankakee Tornado including the specific still shots of the tornado which are shown in the order of their occurrence on subsequent pages. As a guide for locating the still shots the path

is divided into sections wherein similar characteristics of the tornado cloud were observed and photographed (Fig. 14).

Picture 1 of Fig. 15 is the first photographic evidence of the tornado. The image looks like an ordinary heavy rain shower emanating from the base of a cloud with a light rain shower to the rear. (The "asterisk" or "x" on this and other photographs have been superimposed and should be neglected when considering image characteristics). Eyewitness accounts of this portion of the storm generally agree that the tornado retained this shape, resembling a rain shower or a wide column of smoke, for a significantly long period, so that little alarm was raised until the storm crossed the Kankakee River on its way to Bourbonnais. In picture 20A, a view from 14 miles east of the tornado, the shape of the extension toward the ground is barely distinguishable. At Momence, the location near which the picture was taken, eyewitnesses recounted that the vortex dropped from the cloud at the approximate time picture 20A was taken. This interpretation is understandable since the details of the tornado system of clouds only became distinguishable from smoke or haze after the first picture in the sequence was taken from location 20, and can now be illustrated by viewing the first few pictures of that sequence.

From picture 4A the title for this section of the path was gleaned. As can be seen in the close-up view, the smooth edged funnel, usually made visible by condensation, is not apparent in the photograph and the outline of the vortex, although funnel shaped, is formed by the debris that is associated with it. Moving pictures taken of the tornado near its location at picture 4A indicate large vertical motion near the base of the vortex and debris spewing out of the vortex at higher levels. Pictures 6A and 6B of Fig. 15 contain evidence of some of the characteristics that pertain to this section. The motion of the tornado (direction from left to right) can be surmised from the displacement of the tornado with respect to the background clump of trees protruding above the horizon. As can be seen, the width as well as the density of debris changed rapidly during the short interval between pictures 6A and 6B. In 6B the debris is less dense through the horizontal section in the lower part of the vortex. These and other such photos (the remainder of the photographs from locations 4 and 6 in Figs. 2 and 3, for example) lack evidence of an apparent condensation funnel by the absence of opaque debris or condensation products extending continuously toward the ground from the base of the cloud. In 6A are seen some of the general characteristics of the tornado system of clouds: the lower vertical extension called the vortex or funnel, and the upper portion called the wall cloud, with clouds that seem to hang along its edge. The spewing of debris from the middle and upper part of the tornado vortex, so characteristic of this

section, is shown clearly in 6A as well as in the photos which were taken from a closer vantage point. In photos 6C and 6D (Fig. 16) there is evidence of condensation which extends from the cloud above to within the debris cloud at or near the top of the picture; however, this was very short-lived since additional photos 10A and 10B (Fig. 18) showed no apparent condensation in the upper part of the tornado, but only at the wall cloud.

An interesting feature evident in pictures 10A and 10B is the tilt of the vortex from the vertical; almost all photos taken in a southeasterly direction had an excellent view of the tilt, which is northeastward with height. This tilt is also evident in pictures 13A through 13C (Figs. 19, 20, and 21). The spewing out of debris can also be seen in these photos where the main outflow is located on the leading side of the vortex (motion is from right to left). Photographs taken from the south side of the path indicate some of the motion features along the edge of the wall cloud. All shots taken from location 11 show the cloud wisps (or "cloud tags") along the edge of the wall cloud to be rotating counterclockwise about the center; also a strip of moving pictures taken from location A shows the motion of the cloud wisps in pictures 11E through 11G (Fig. 20).

Another feature that was characteristic of this section of the path is the tail cloud that was only photographed from positions east of the vortex. Almost all the photographs taken from location 20 (Figs. 22 and 25) show the tail cloud to be extending toward the west-northwest. Since it is rather diffuse as well as close to the base of the main cloud, the tail cloud is difficult to distinguish in close-ups that have the main cloud as background. It seems to emanate from the wall cloud but, unlike the large dense tail cloud of the Fargo Tornado, it appears to retain its location relative to the vortex without rotating about the wall cloud.

A feature that is also evident in the series of photographs from location 20 is the indentation of the visible edge of the vortex near the ground. In pictures 20H and 20I (Fig. 23) this indentation is shown with increasing degrees of clarity; as can be seen in the other photographs, it is confined to the north side of the funnel, while the spewing of debris at higher altitudes is evidenced on all sides of the funnel. Close-up photographs of the vortex, such as those from location 24 (Figs. 26, 29) show the indentation on the leading side of the vortex. Pictures 24B and 24C indicate an increase in diameter of the visible vortex by a factor of about two in a few hundred feet; rather than being an indication of the shape of the vortex, this feature is thought to be due to a large convergence of air near the ground around the vortex. Pictures 30A and 36A (Fig. 30) are the last photographs taken of this section of the path.

The change in general characteristics of the vortex from wide (with no apparent condensation funnel) to narrow (with a distinct continuous condensation funnel) was

depicted rather vividly by motion pictures as taking place within a very short distance along the damage path. At the time of the damage survey, no obvious differences in soil density or general vegetation, which might explain the clearly sudden decrease in debris, were noted. Therefore, the narrowing of the vortex might be considered more a characteristic of the motion of the system than merely the mutually, interacting effect of ground surface and air motions.

The section of the path along which the continuous condensation funnel existed is shown clearly in pictures 36B and 34 (Fig. 30). These pictures are among moving picture strips taken of the funnel from locations 34 and 30 which showed the additional small vortex in 36B to be wound about the main vortex. The small finger-like protrusion from the leading side at the base of the cloud in picture 34 is not the small vortex in picture 36B. The former appeared to be stationary with respect to the main funnel while the smaller funnels, called perturbation vortices, moved about the main vortex and seemed to dissipate as they contacted this finger-like protrusion. Moving pictures taken from location 30, on the north side of the path, indicate that the motions described were not due to improper perspective. Although it is not apparent in picture 36B, the finger-like protrusion should be in that part of the cloud located in the upper foreground. In picture 30B (Fig. 30) the existence of debris about the condensation funnel, coupled with the distance factor, makes its outline fuzzy. Motion pictures taken of this section indicate that the area covered by debris varied in breadth. However, these variations reflected short time intervals whereas the diameter of the condensation funnel, although it shrunk rapidly, retained its narrow shape for periods long enough to be considered characteristic. Additional evidence for the narrow shape of the tornado is shown in pictures 33 through 37A (Figs. 30 and 31).

Pictures 33 through 37D (Fig. 32) also depict an interesting but unexplained phenomenon that has been confirmed by eyewitness accounts for this part of the damage path: it appears that the funnel does not touch the ground. This has often been referred to as a funnel aloft in many observations. It has been established by our detailed survey that the damage path, although becoming narrow at various points, remained continuous throughout its length. In effect this means that the photographs, as well as the visual observations indicating funnels aloft, have been misleading. A close scrutiny of specially prepared prints of photographs shows evidence of debris in each of them; however, this evidence was not corroborated by all eyewitness accounts probably because certain background settings may have obscured the distinction between haze and debris at great distances. On the other hand, special treatment of photographic impressions may prove even reliable professional observations to have been incorrect. Perhaps the

significance of the "funnel aloft" observation is overemphasized and the concept should be abandoned.

Another phenomenon shown in the series of photographs including picture 30B are the giant hailstones that were evident on the north side rather than on both sides of the damage path. Although the stone in picture 30B (Fig. 30) barely visible near the tree stump in the foreground was not the largest in the immediate area of the photographer, it is representative of some of the larger stones that were photographed and collected by residents near the damage path. The largest hailstone is to the far left in the picture; large stones also appear in the foreground of picture 31A (Fig. 31). The distribution of giant hail stones is shown in the radar section of this study.

In picture sequence 35 through 37J (Figs. 31 through 33) another characteristic of the tornado system of clouds is seen: an additional protrusion of cloud from the base of the main cloud which has been referred to as the adjoining wall cloud in the preliminary report of this study. In pictures 35 and 31B (Fig. 31) this cloud is clearly distinguishable from the main wall cloud but, unlike its counterpart, it has no tornado vortex emanating from its base. These are the only pictures of the adjoining wall cloud taken from west of the tornado vortex. The series 37A through 37J (Figs. 31 through 33) shows the position of the adjoining wall cloud relative to the main wall cloud and the tornado vortex as seen from positions east and northeast of the storm. The change in position of the main wall cloud relative to the adjoining wall cloud could not be attributed solely to a rotation of the main wall cloud about a center between the two protuberances, as was suggested in the preliminary report. There are other motions that can account for the changes in its position as seen in the various image planes of the photographs. In an effort to explain the changes in position between the main and adjoining wall cloud, while retaining the visible structural features of the adjoining wall cloud, it was assumed that the adjoining wall cloud had an elliptical shape with its major axis oriented about 30 deg west of north. Even with this shape the measured changes in size of the adjoining wall cloud could not be accounted for without including a large rotation rate of the type described previously or a large horizontal extension of the cloud with time.

A variation in width of the tornado is also evident in pictures 37F and 37G (Fig. 32); the funnel seems to broaden before it goes into the discontinuous part of its path. A noteworthy point in picture 37G is the region of light in the center of the photograph that seems to be emanating from a region between the adjoining and main wall clouds. In pictures 37H and 37I (Fig. 33) the cloud mass visible above the wall cloud in the foreground resembles the cloud mass seen in photographs of the recent tornado in Wichita Falls, Texas, reprinted in Weatherwise (1964). It seems possible that the

congested cloud form, depicted clearly in picture 37J (Fig. 33) above the wall cloud, is a characteristic of tornadoes.

Picture 37J is the first photograph of the tornado as it began that portion of the path where the condensation funnel became discontinuous. The funnel portion of the cloud in picture 37J seems to have split into two vortices which cross each other in the image plane (i. e., not necessarily intersecting with one another). The vortex that is more nearly vertical seems void of any condensation whereas the vortex at a larger angle to the vertical clearly contains condensed water vapor. The fact that the rectangular-shaped region in the upper portion of the tornado and the light horizontal layers in the middle portion appear to be free of condensation provokes fresh speculation on the nature of the dissipation of tornadoes.

In picture 37K (Fig. 33) is an example of a condensation funnel that has no apparent connection with the cloud above; the motion pictures which include the scene of this photograph indicate many discontinuous vortices becoming alternately visible and invisible with condensation while changing their size and orientation in an apparently random fashion as they move generally upward (the differences in contrast between photographs in this series is due to the varying exposures made by the photographer). Picture 37N (Fig. 34) resembles some of the photographs taken of an earlier stage of the tornado when there was no apparent condensation in the tornado vortex. A clear region between the circulating debris below and downward extension of the cloud from above resembles the photographs lacking a condensation funnel; as can be seen throughout the rest of the photographs taken from position 37, the condensation into cloud particles and the evaporation of these particles continued throughout this period to the point where the tornado crossed the highway, shown in picture 37T (Fig. 35). Motion pictures taken of the tornado when it was east of this position indicate that the same processes evidenced by the still shots continued as the tornado progressed on its path eastward.

Apparently, however, this was not the dissipation activity of the tornado since photographs of the tornado at its location farther east showed it to be once again a continuous funnel made visible by condensation. In 40A (Fig. 35), for example, the tornado is a continuous condensation funnel similar in shape to the "elephant trunk stage" of the Dallas Tornado whereas 40B shows the condensation to be almost cylindrical in shape and only narrow close to the ground near the roof of the building in the center of the photograph. The pattern of debris circulating about the condensation funnel is not the same shape found in photographs of the vortex when it was west of its location in picture 40B.

Pictures 41A and 41B (Fig. 35) contain the rope funnel which is the usual structure attained by the vortex prior to receding into the cloud at the end of its damage path. Moving pictures taken of the rope funnel show it emanating from a portion of the cloud that was light in color relative to the surrounding parts of the main cloud. Unfortunately no still shots including the point of extension of the funnel from the cloud could be obtained to verify this. The smooth edge of the rope funnel indicates some condensation in the funnel; the vortex at this stage is at its narrowest (measured diameter about 50 ft.), yet the winds about the vortex are sufficiently strong to sustain the debris shown in 41B. An additional interesting point concerning the rope funnel stage was evidenced by motion pictures: the film strip illustrating condensation in the rope funnel is followed by additional footage (taken by the same photographer at a time presumed to be immediately after the first strip) that contains evidence of a circulation near the ground but without a visible condensation funnel.

From the photographic evidence shown and from the movie film collected, a nearly continuous picture of the Kankakee Tornado has been revealed. In the first photographs, the tornado vortex, consisting mainly of debris particles, gave the appearance of being a column of smoke or a rain shower in the distance. A typically well-defined smooth edge to the funnel, generally attributed to condensation, was lacking during a major part of its lifetime. At times, after the tornado passed east of Kankakee, the funnel appeared to be continuous, but circulating debris enclosing the outer visible portion of the tornado vortex disallowed verification of the familiar condensation funnel which may have existed within the circulating debris. During this period some photographs taken from the north side of the path looking westward contained evidence of a tail cloud. The wall cloud was photographed from almost all angles to the tornado, appearing in every photograph where it might possibly be observed. The orientation of the vortex was not vertical: photographs taken from locations northwest and southeast of the vortex contain the largest tilt angles for the tornado, indicating a northeastward slope with height or a tilt toward the center of the main cloud above. Although the visible tornado vortex was more cylindrical than cone-shaped, there was a noticeable decrease in the width of the vortex (made visible by the circulating debris) close to the ground involving even abrupt changes in width at particular points along the path.

The transition from a wide vortex, with no sharp outline nor apparent condensation, to a narrow continuous condensation funnel took place rapidly near the half-way point in the damage path. Although the length and duration of the continuous condensation funnel portion of the path is short, it contains additional phenomena not usually observed in tornado cloud systems: in both still photographs and moving pictures a perturbation

funnel was seen wound around the main funnel; the adjoining wall cloud, from which no tornado vortex extended, was shown clearly from locations north and east of the tornado; also this portion of the path contained photographic evidence of giant hailstones. Although hail of all sizes has usually been found to accompany tornadic storms, the great size of some of these stones confirms previous hypotheses regarding the relation between giant hail and tornadoes.

The beginning of that portion of the path characterized by a discontinuous condensation funnel is shown by a still shot of what appears to be two vortices of equal width crossing each other on the plane of the image. All subsequent photographs, including moving pictures, showed the vortex to be changing its characteristic size and circulation, either by condensation and evaporation (influx of drier air) or by deteriorating into a group of small vortices. Although the visual evidence pointed toward the tornado's dissipation, the main tornado circulation became visibly reorganized as a continuous condensation funnel prior to the appearance of the rope funnel. The length of the damage path during the rope funnel stage was short, relative to the duration and length of the other portions; however, the clear existence of the funnel with rope characteristics is substantial enough in this case to add to the mounting evidence confirming the rope funnel as the characteristic of a general stage of development (the deterioration phase) in tornadoes.

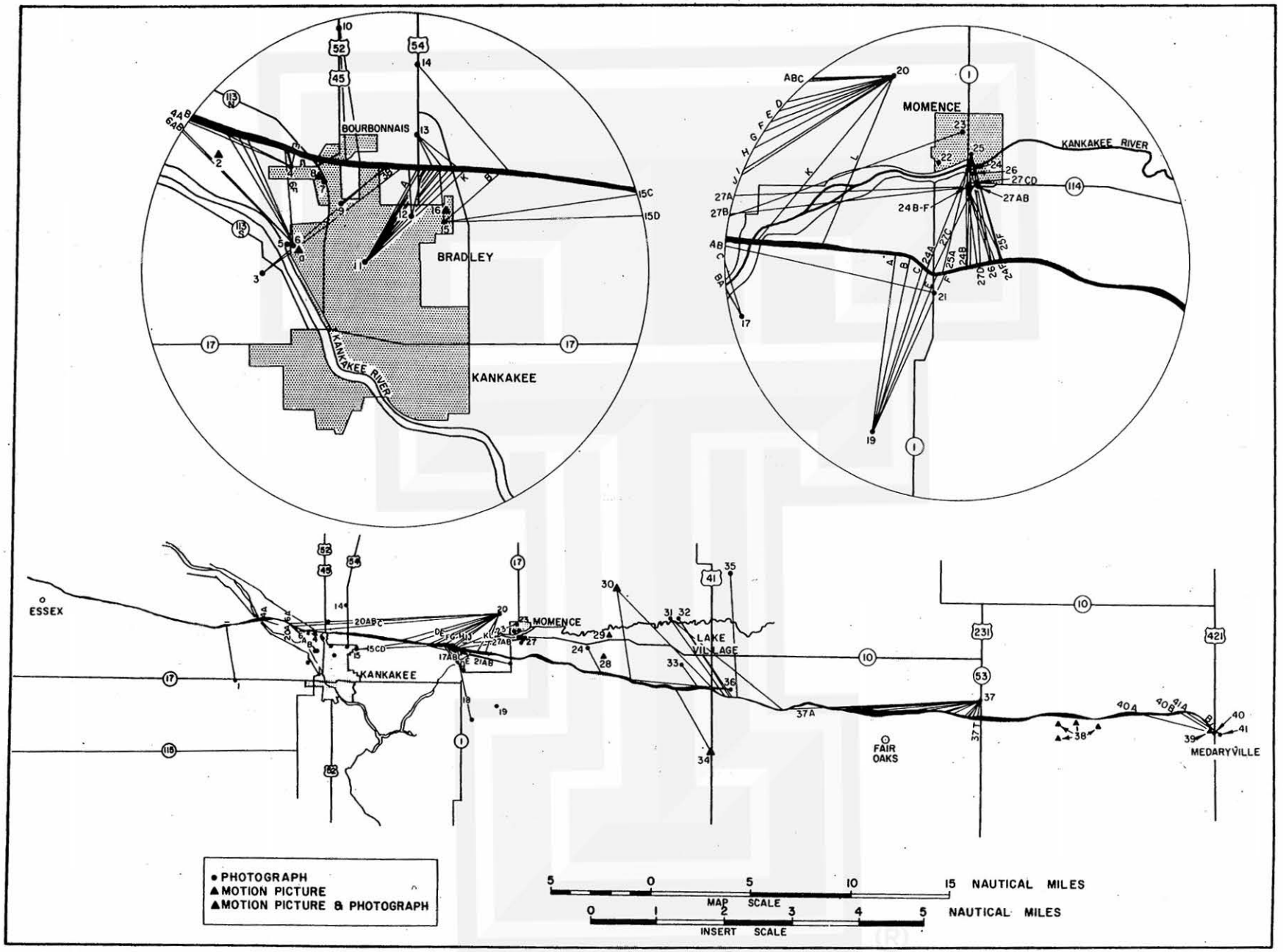

Fig. 13. Locations of tornado cloud photographs with azimuths to the tornado along the damage path.

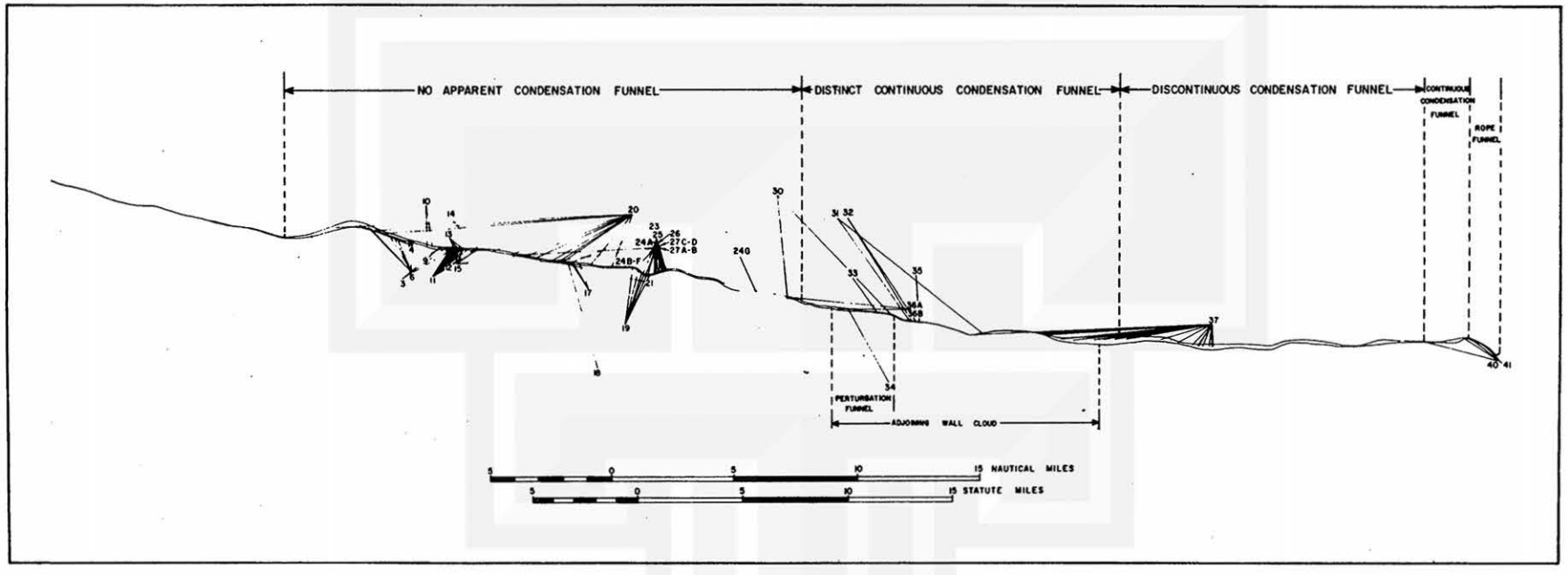

Fig. 14. Locator map for still photographs on a sectionalized damage path.

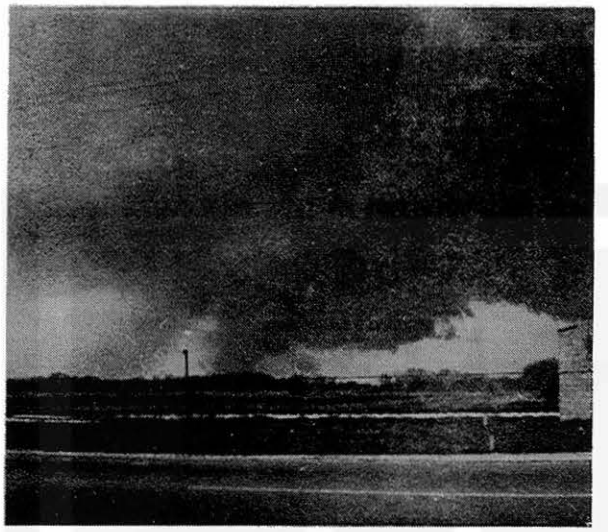

1

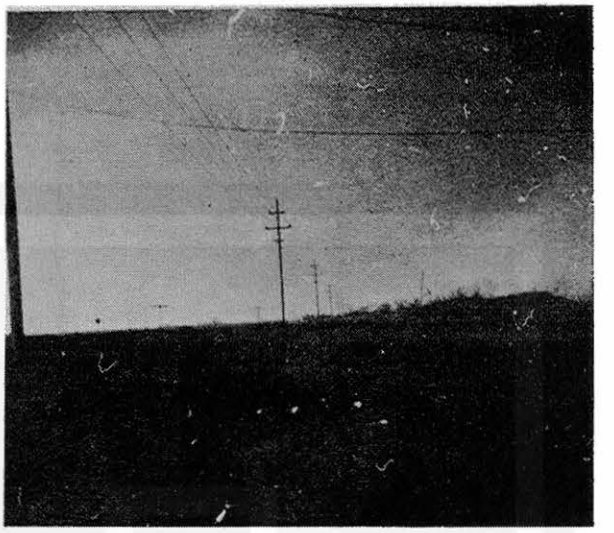

20A

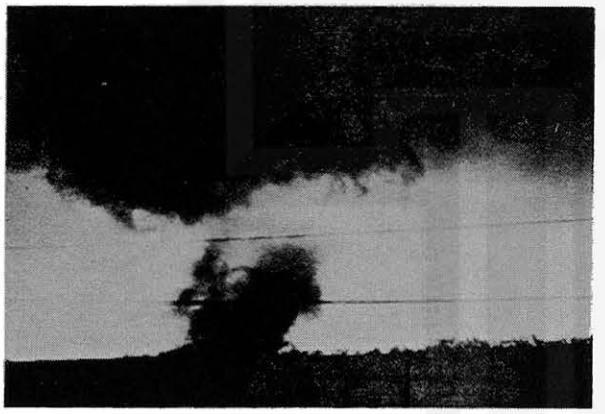

4A

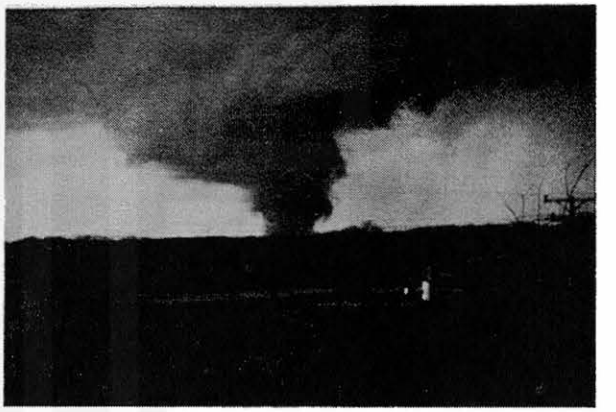

6A

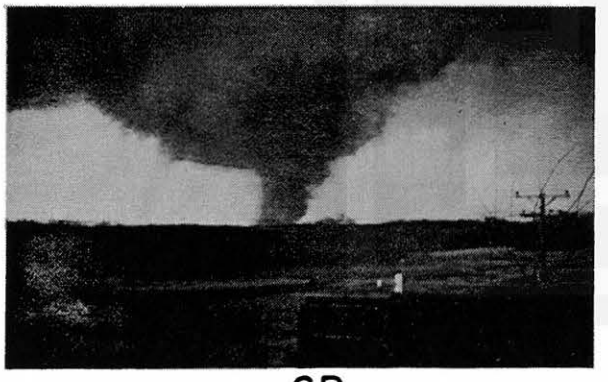

6B

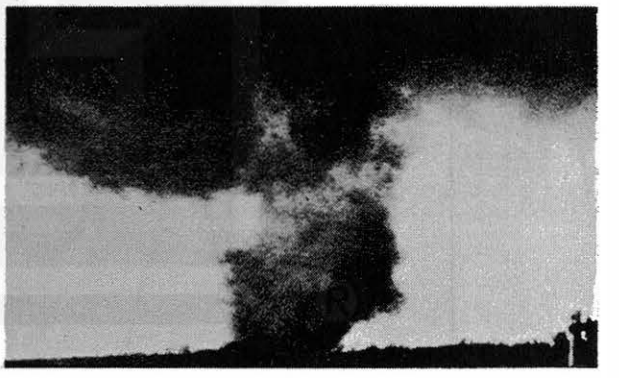

4B

Fig. 15.

20B

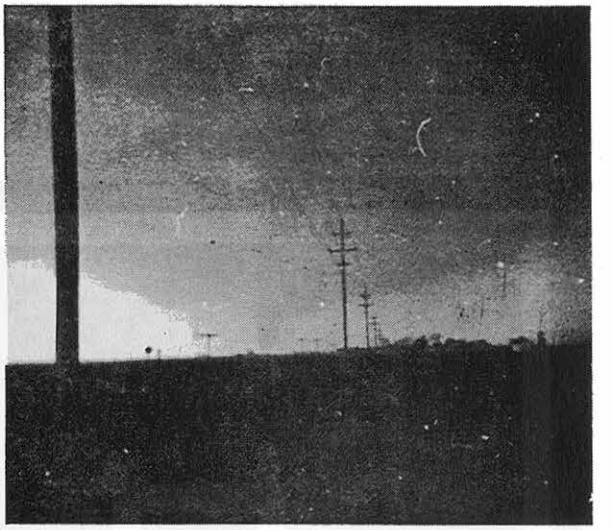

20C

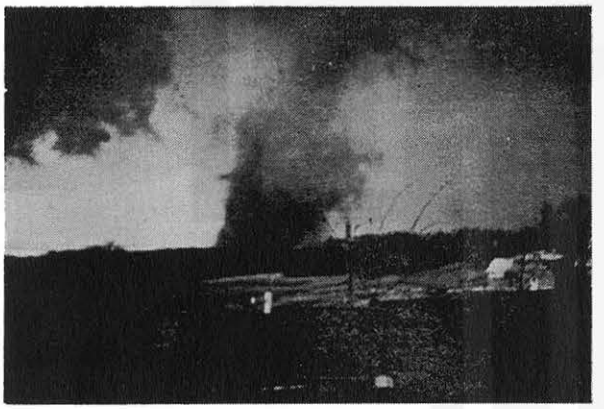

6C

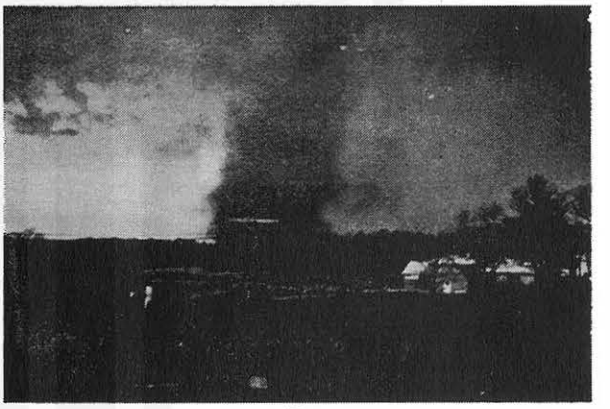

6D

6E

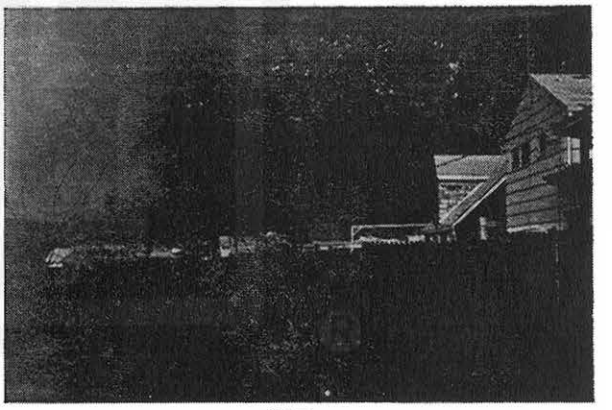

6F

Fig. 16.

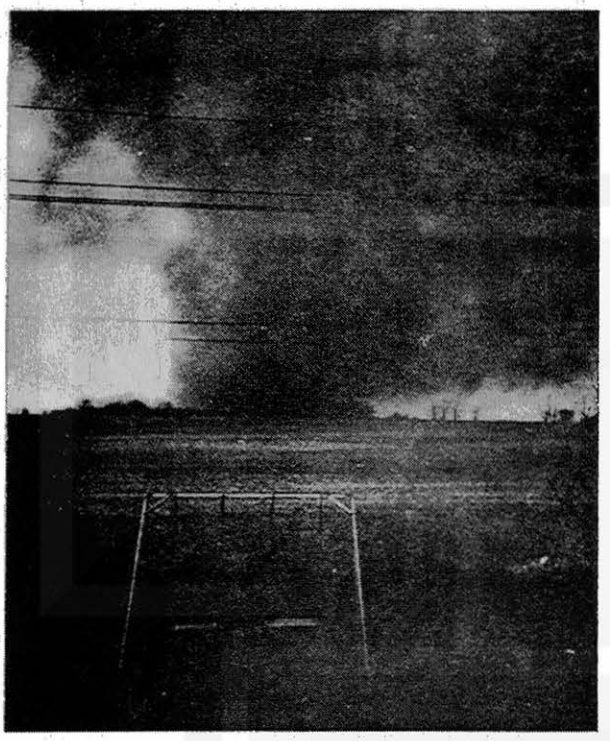

4C

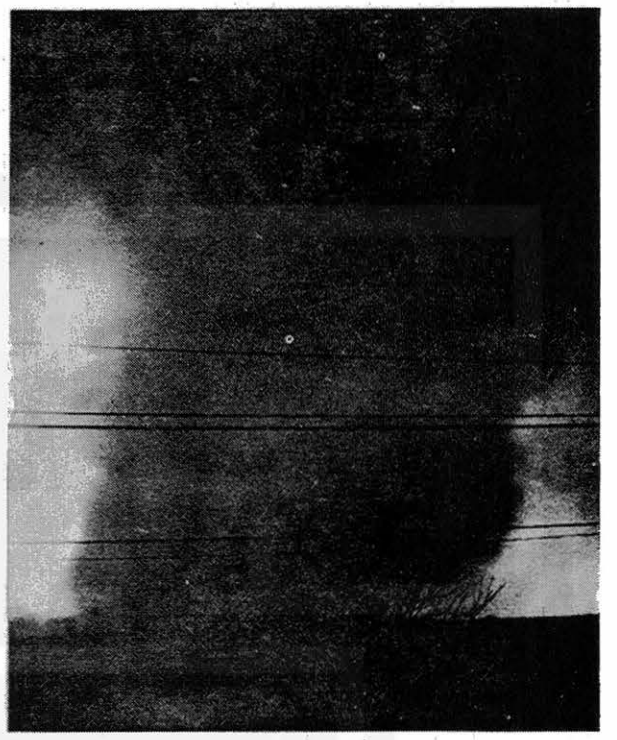

4D

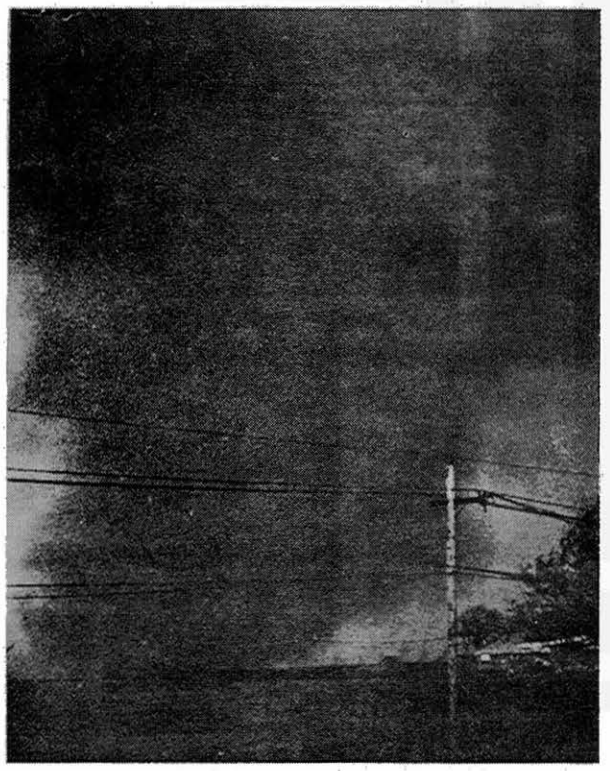

4E

5A

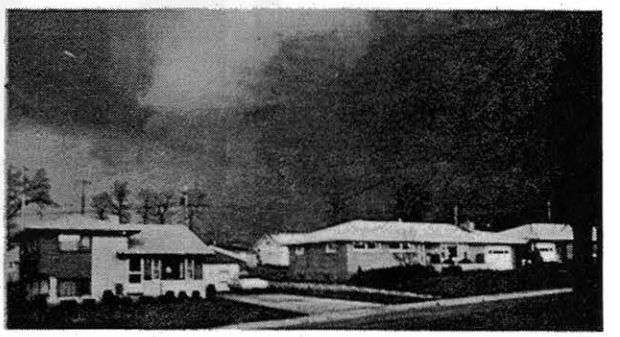

5B

Fig. 17.

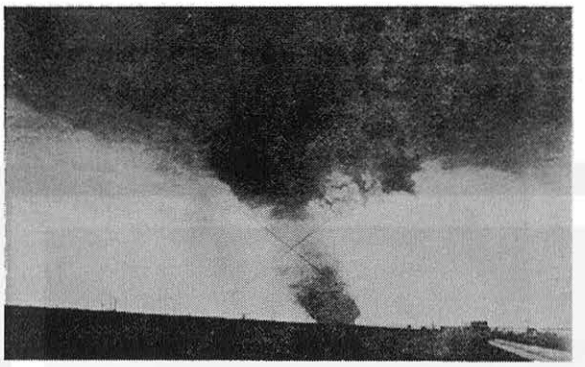

10A

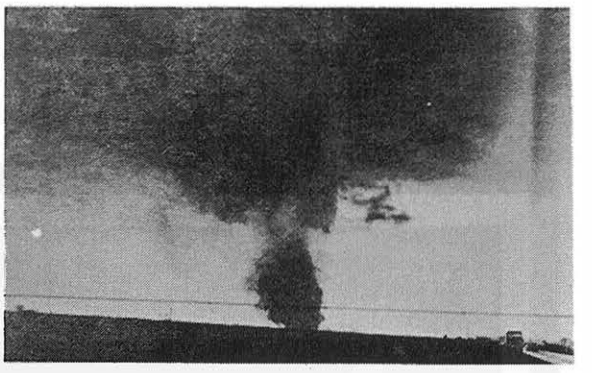

10B

9

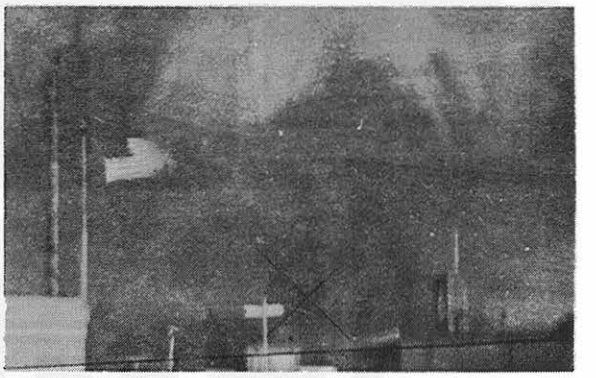

7A

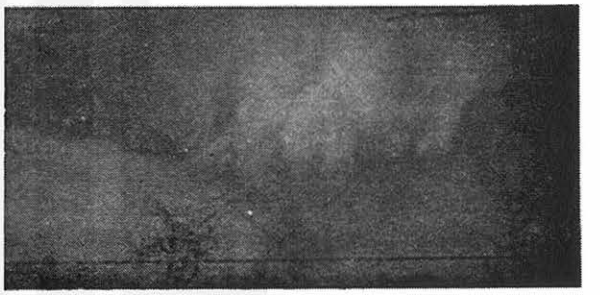

3A

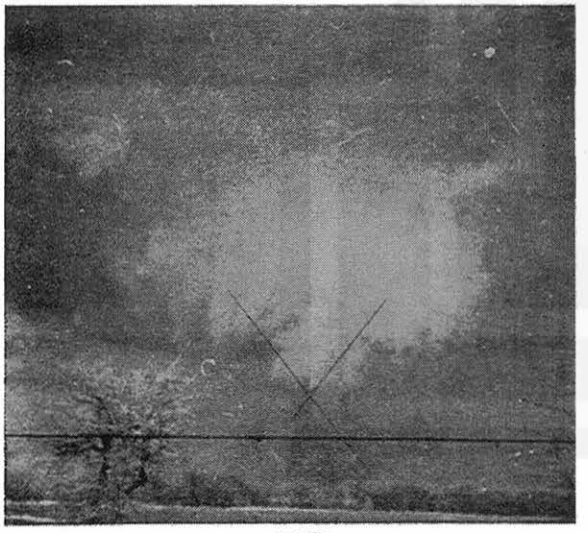

3B

12A

Fig. 18.

11A

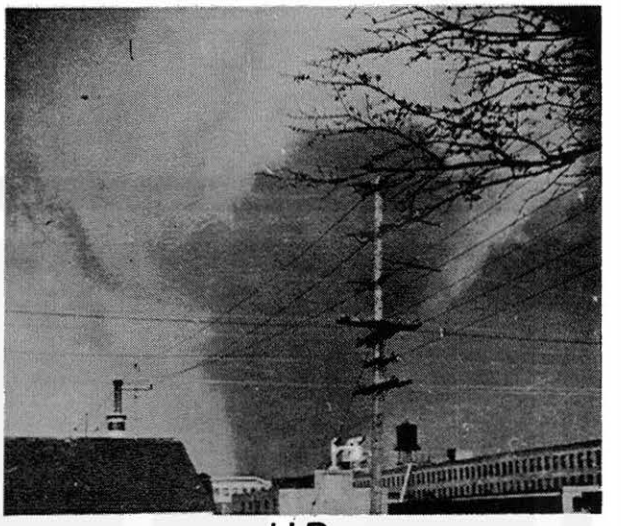

11B

12B

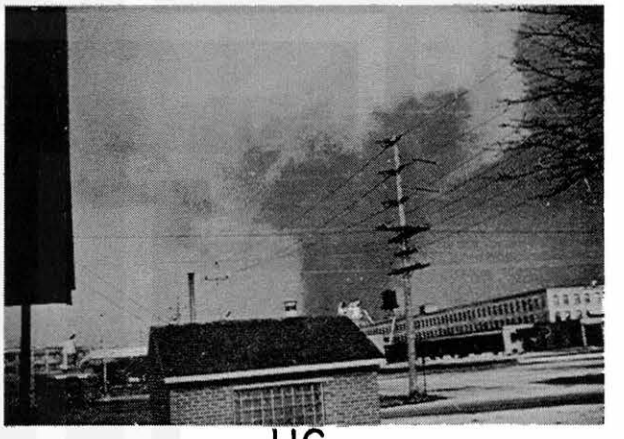

11C

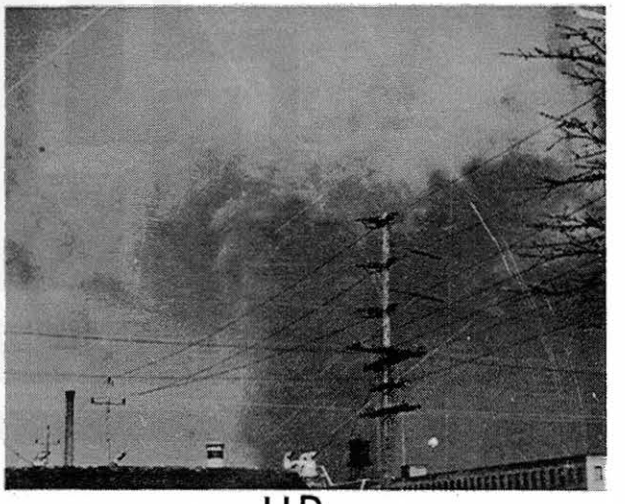

11D

Fig. 19.

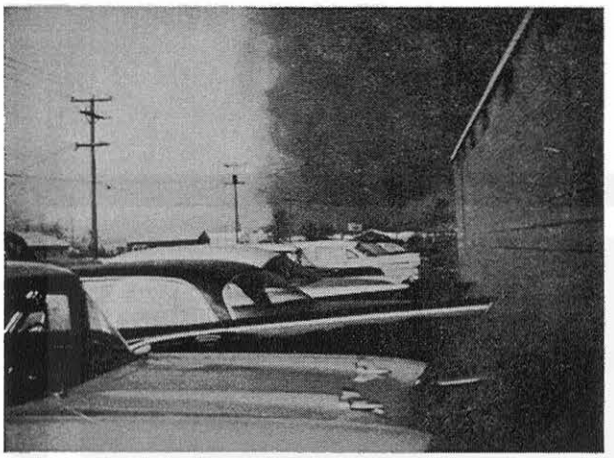

15A

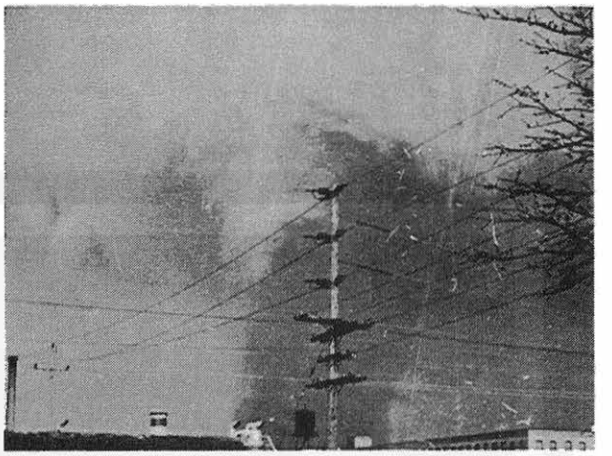

11E

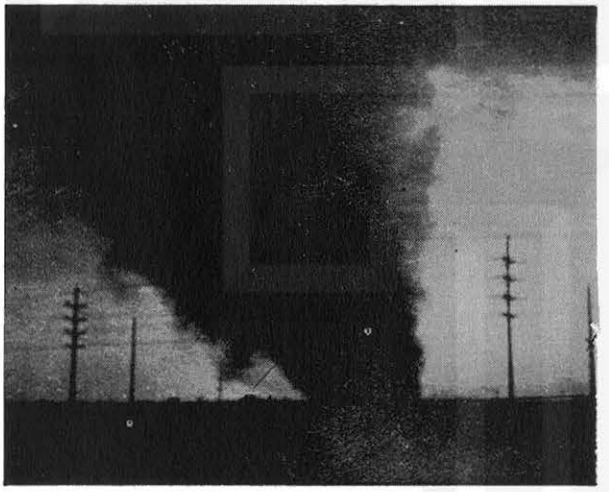

13B

7B

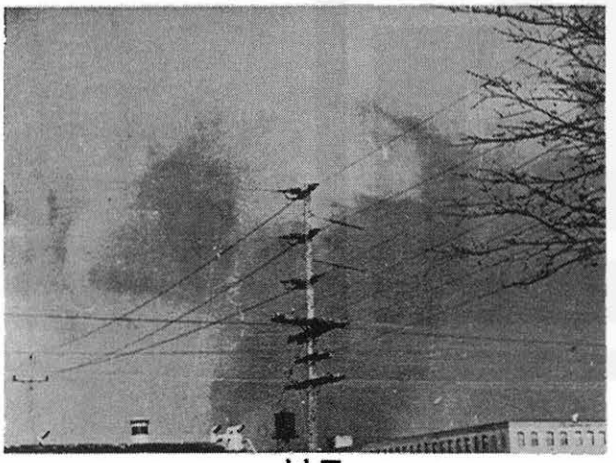

11F

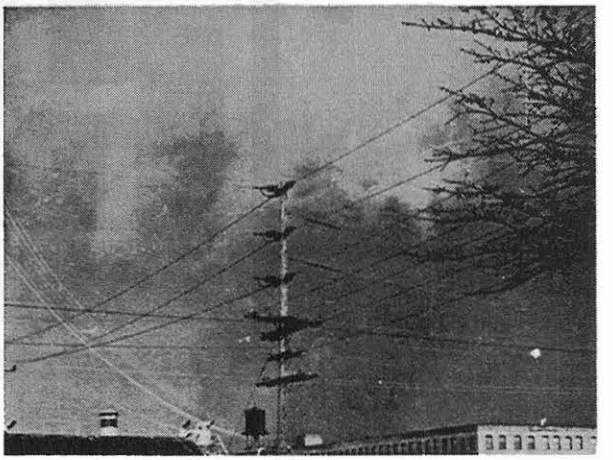

11G

Fig. 20.

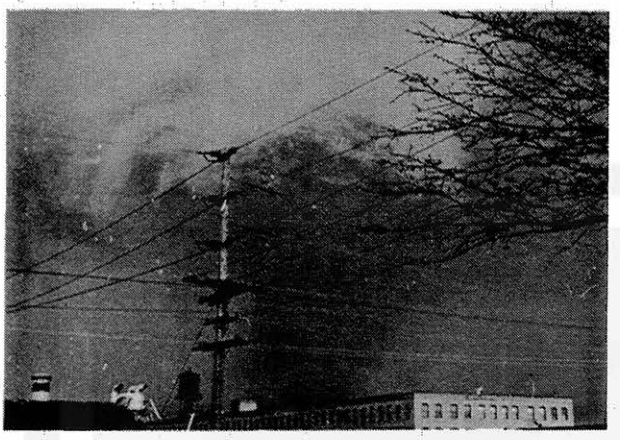

11H

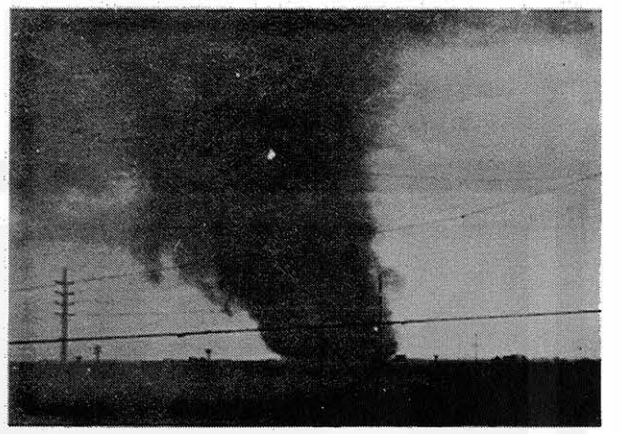

13C

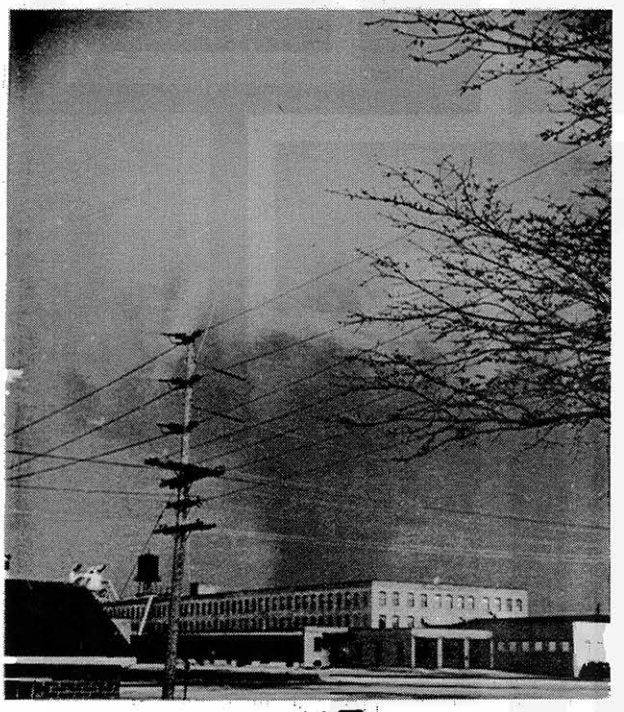

11I

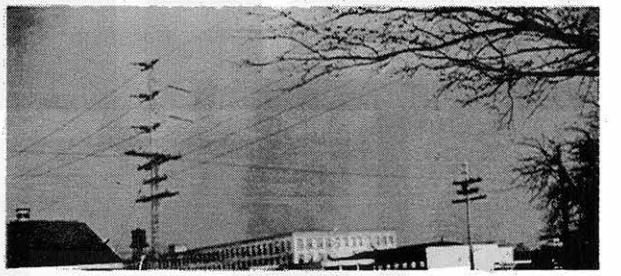

11J

11K

15B

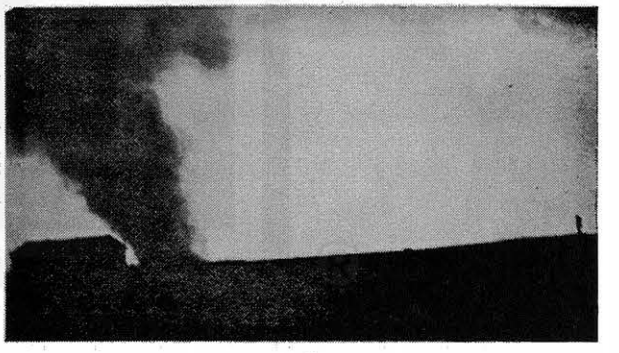

14

Fig. 21.

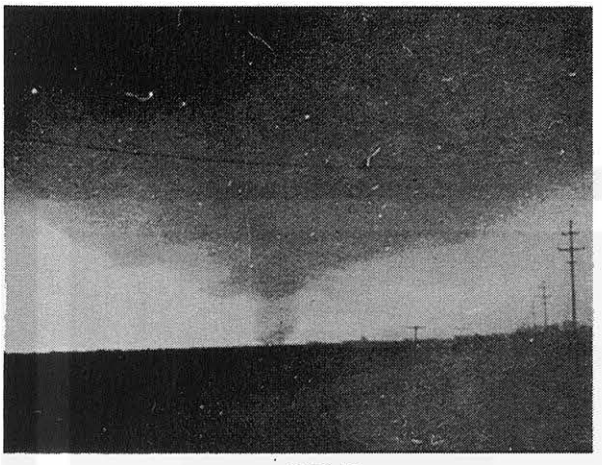

20D

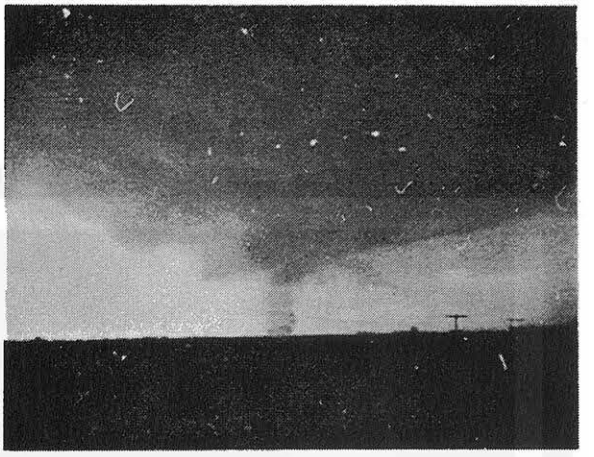

20E

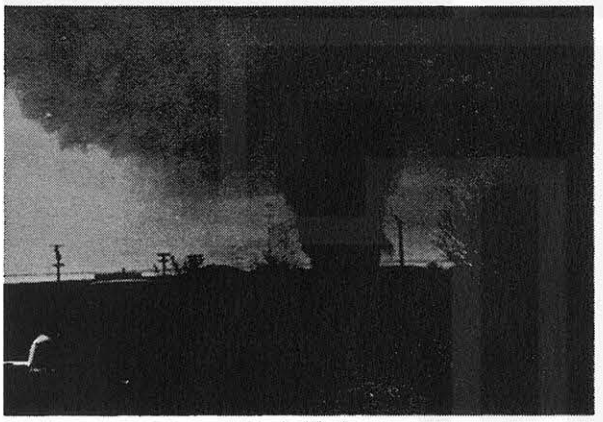

27A

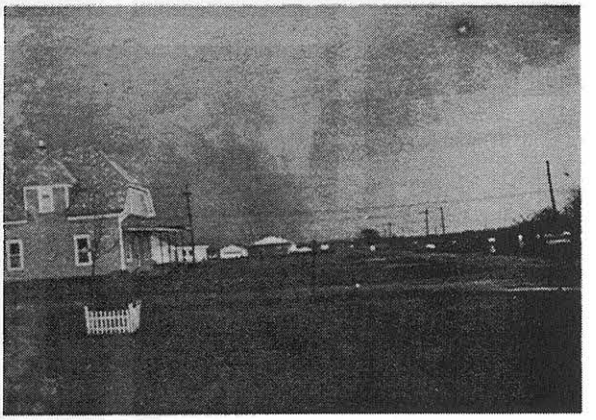

15C

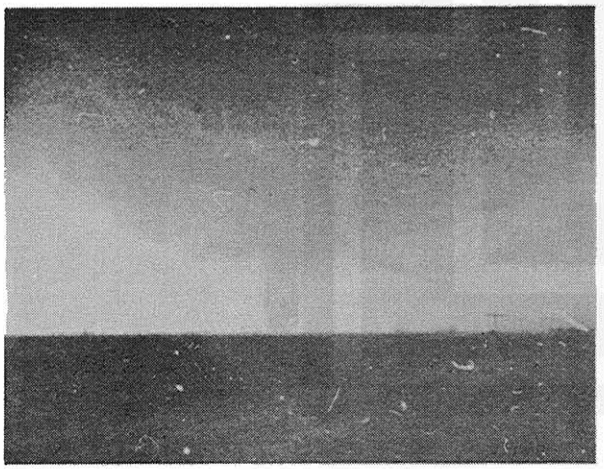

20F

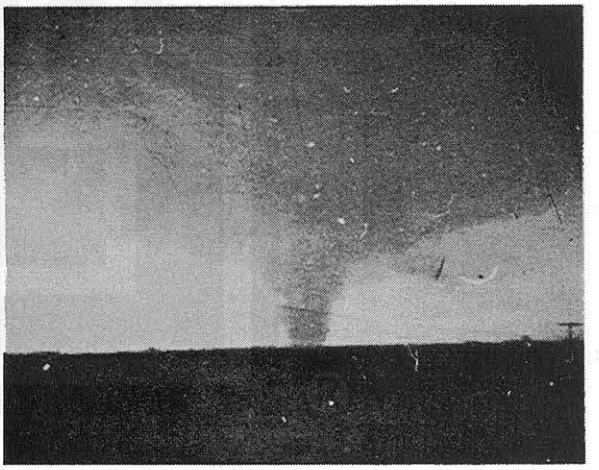

20G

Fig. 22.

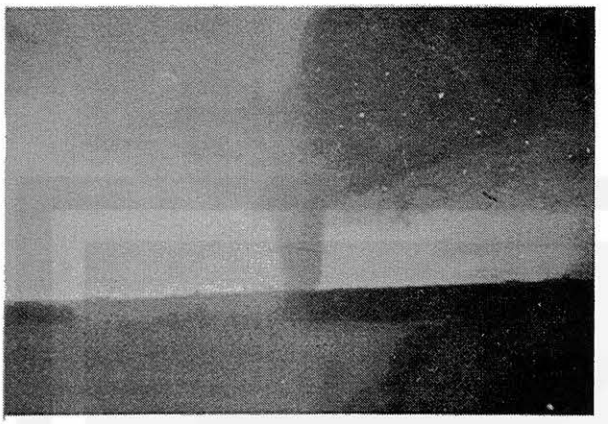

20H

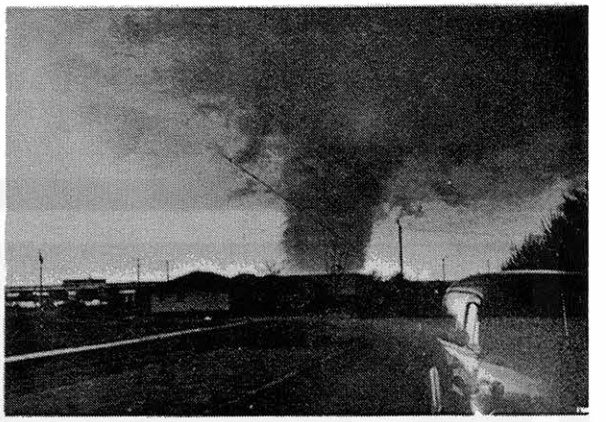

27B

15D

21A

21B

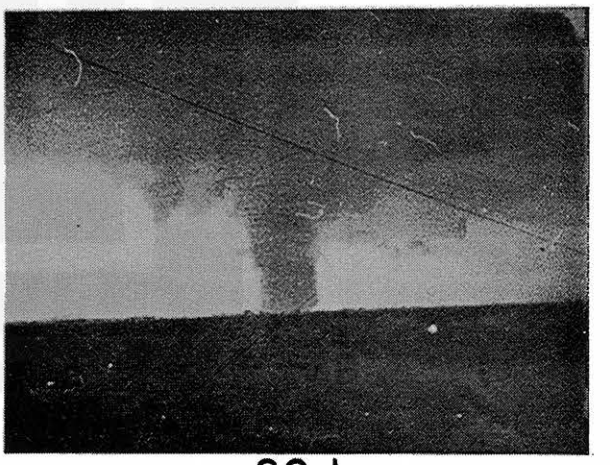

20 I

Fig. 23.

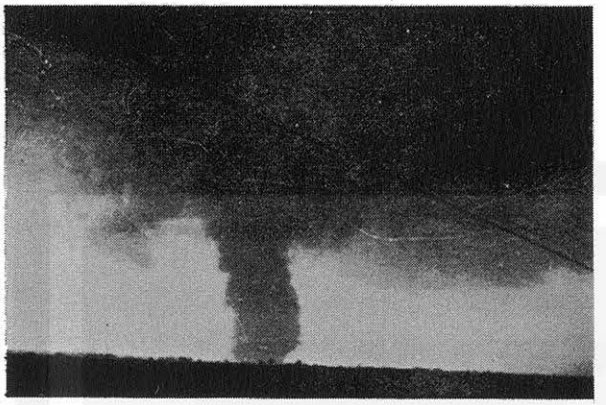

20J

18

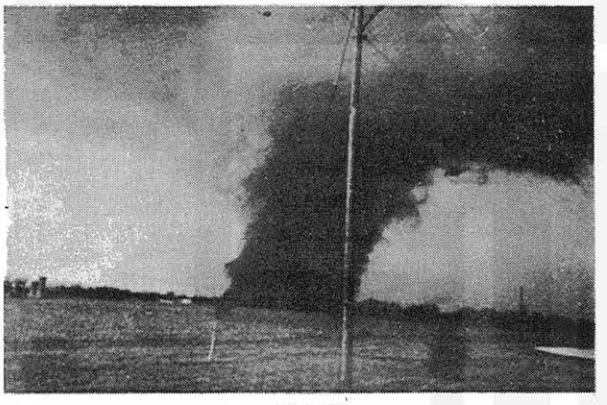

17A

23

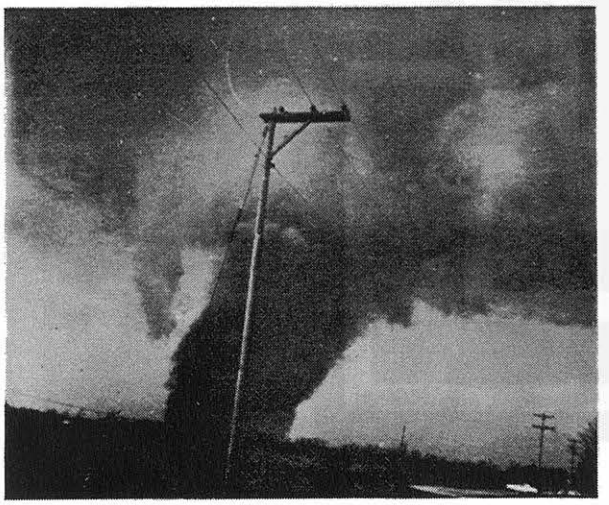

17B

17C

Fig. 24.

17D

17E

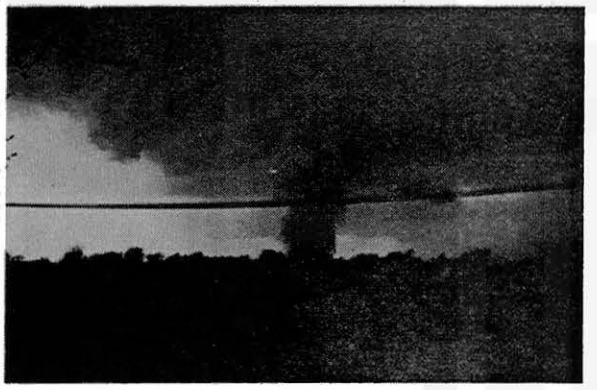

22A

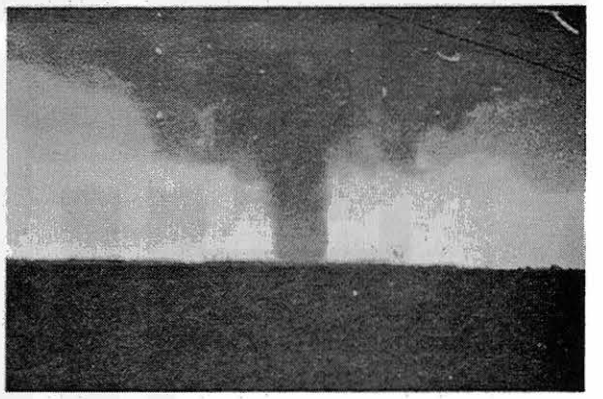

20K

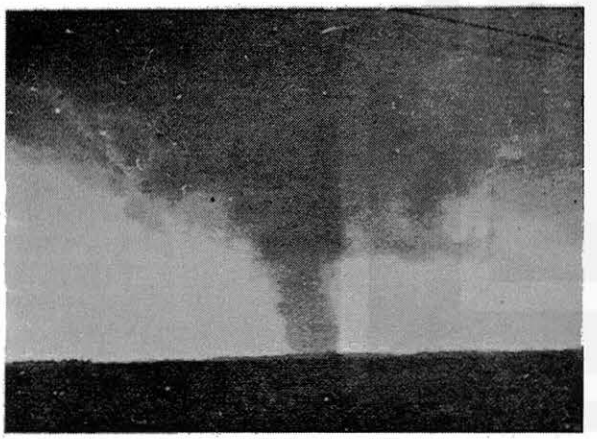

20L

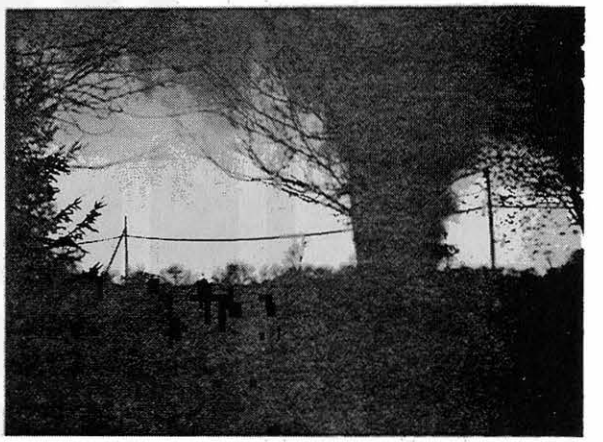

22B

Fig. 25.

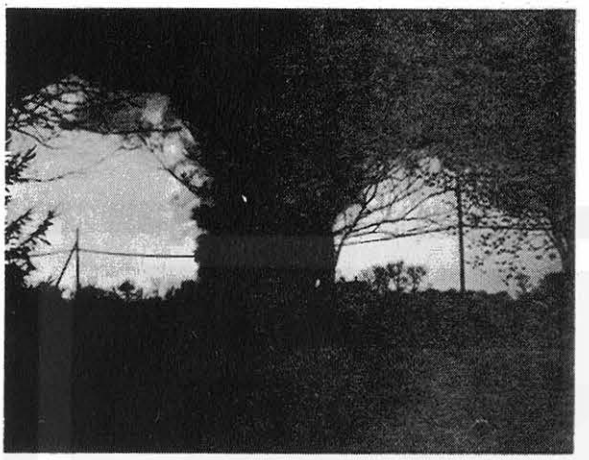

22E

19A

19B

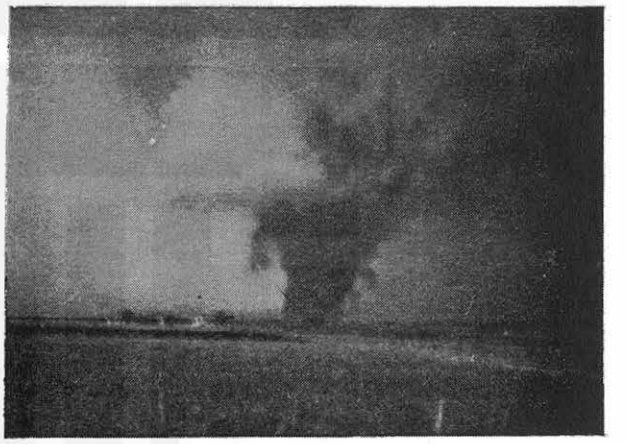

19C

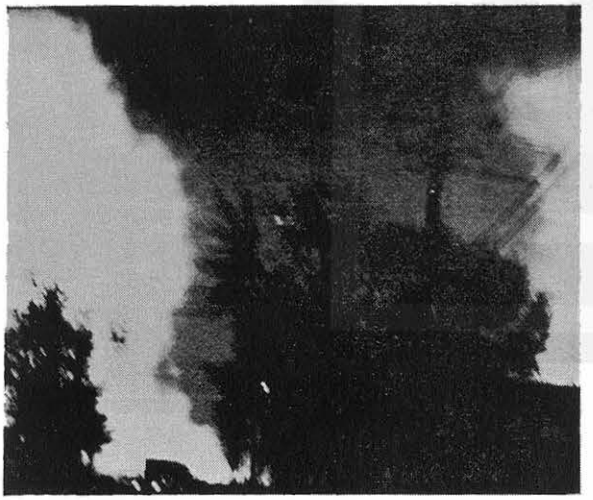

24A

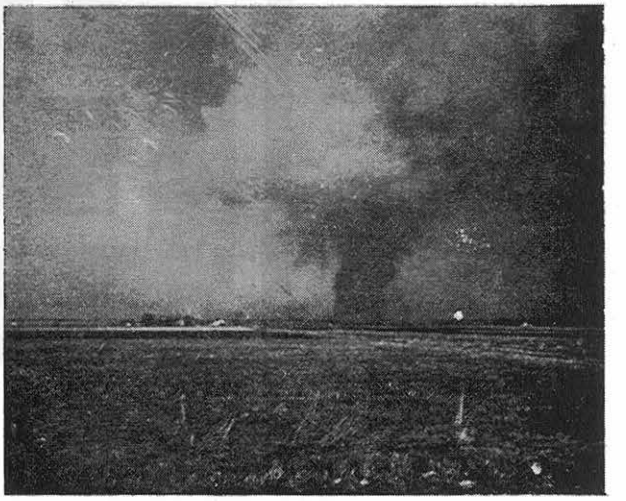

19D

Fig. 26.

27C

19E

25A

19F

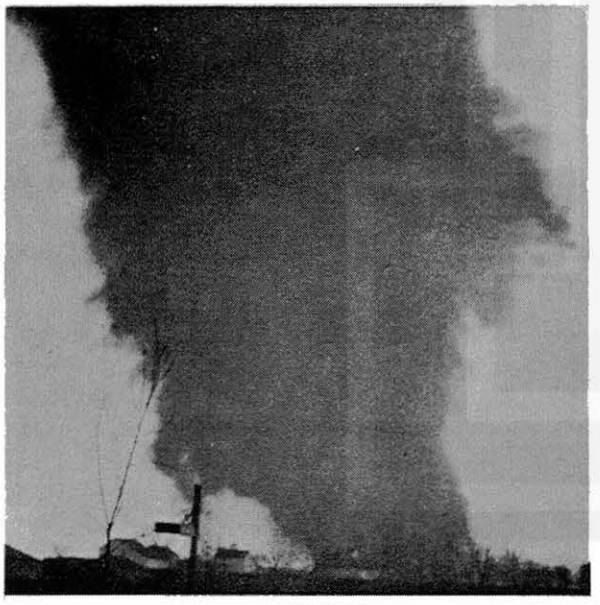

24B

25B

25C

Fig. 27.

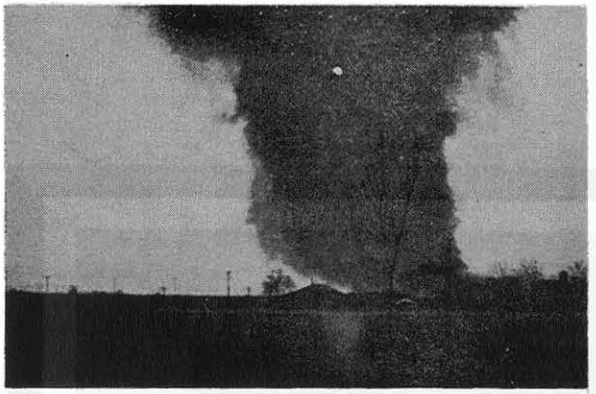

24C

27D

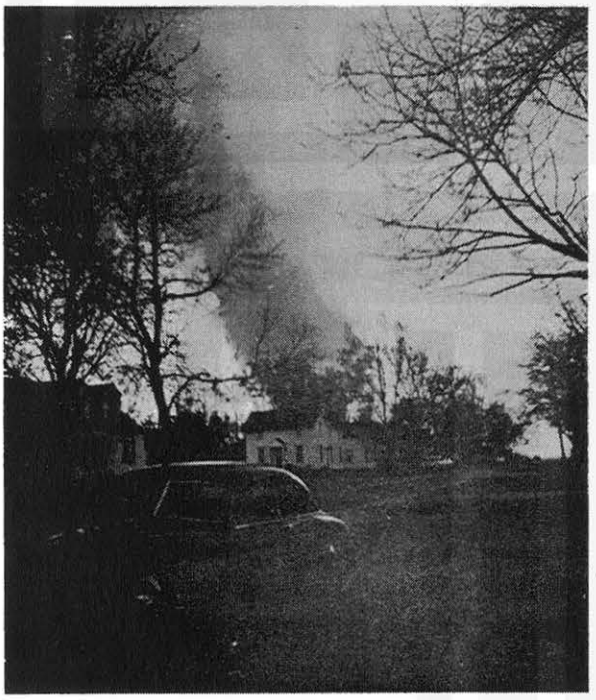

26

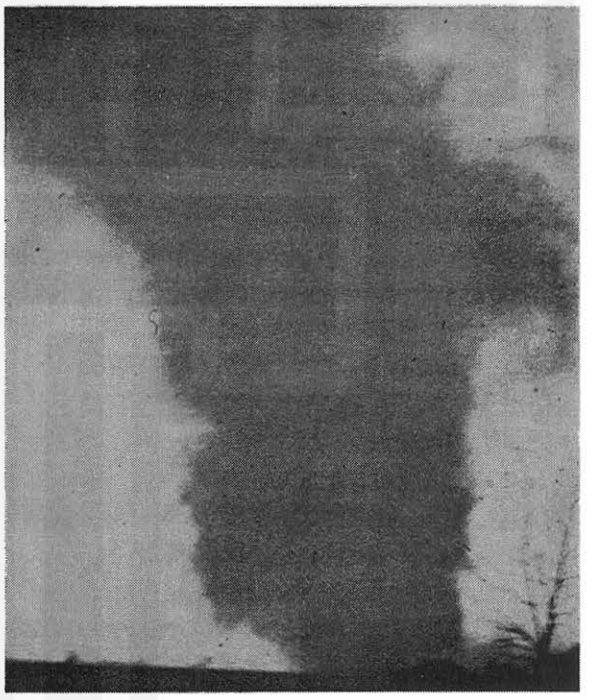

24D

25D

22D

Fig. 28.

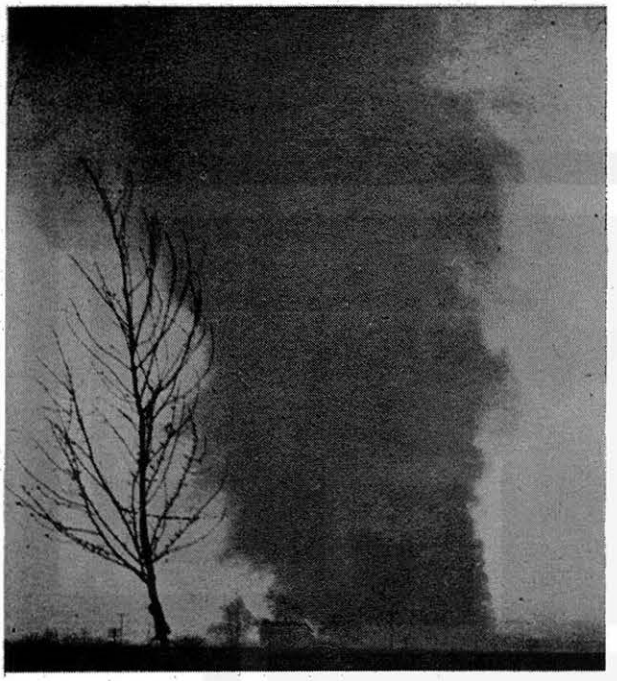

24E

25E

25F

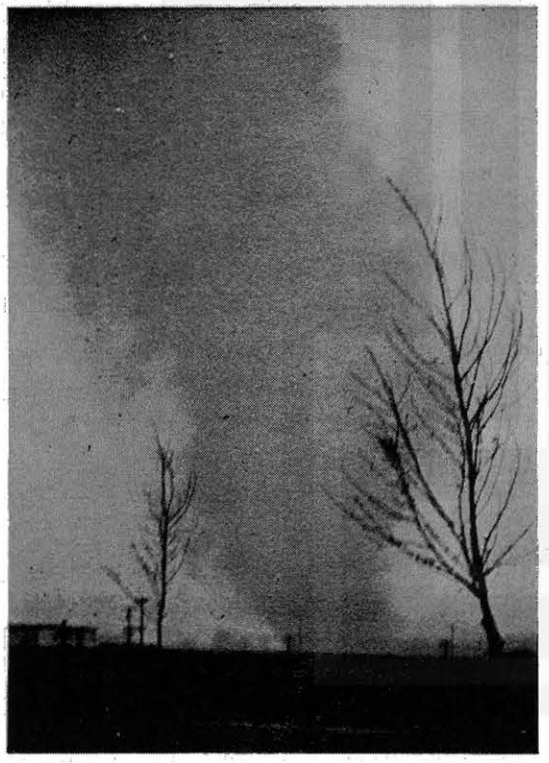

24F

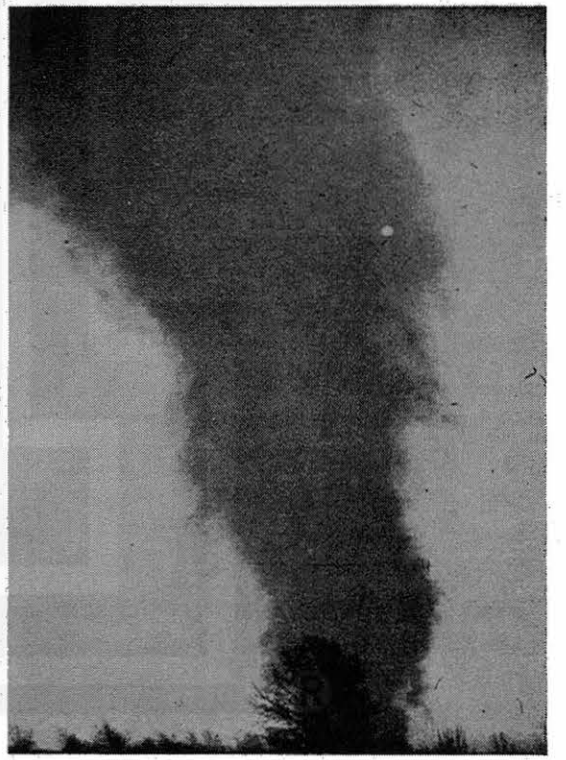

24G

Fig. 29.

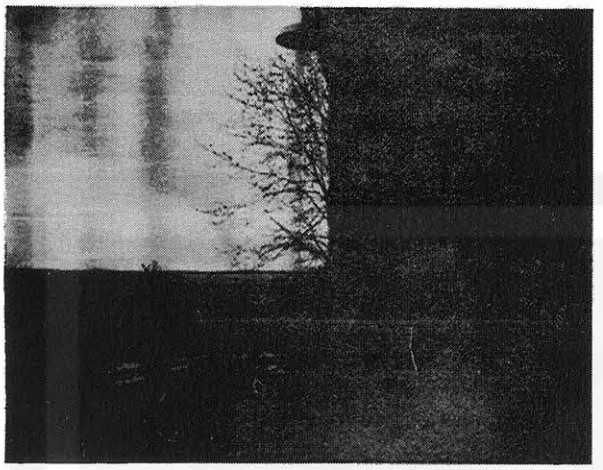

30 A

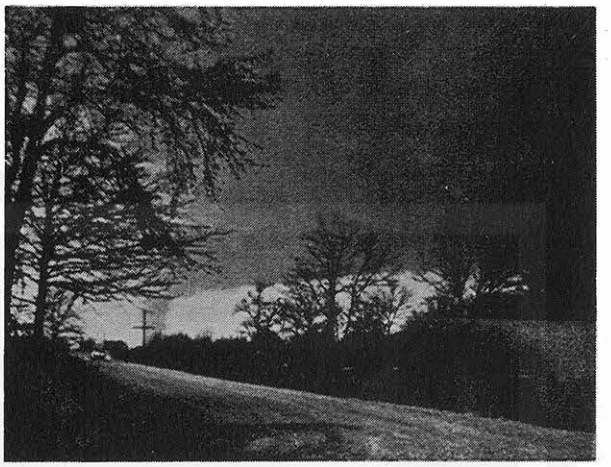

36 A

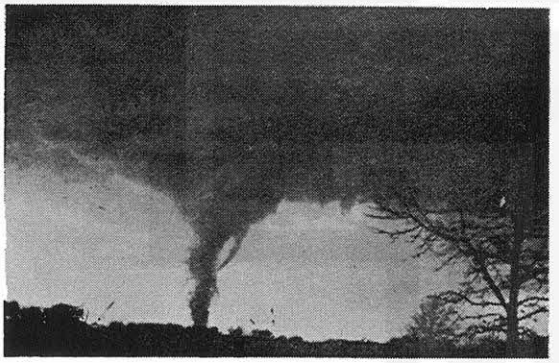

36B

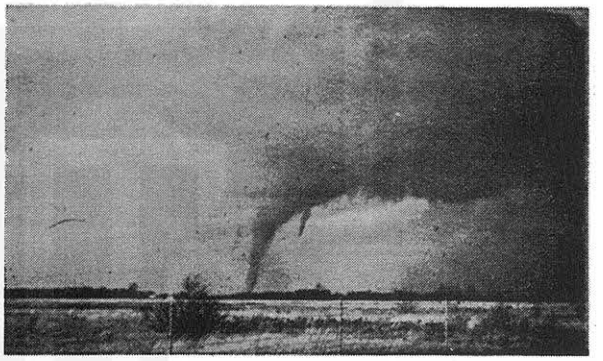

34

33

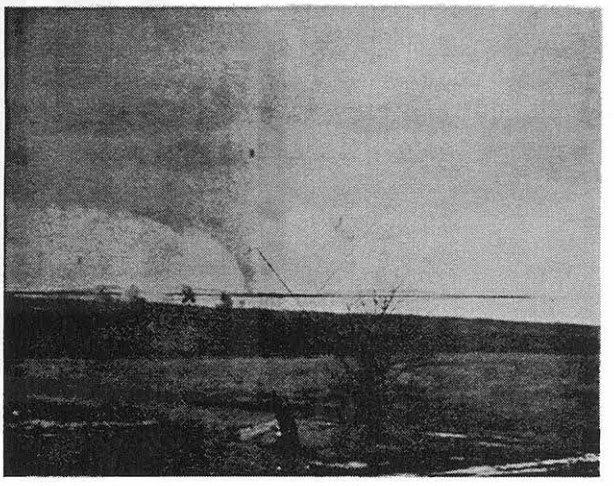

30B

Fig. 30.

31A

32 A

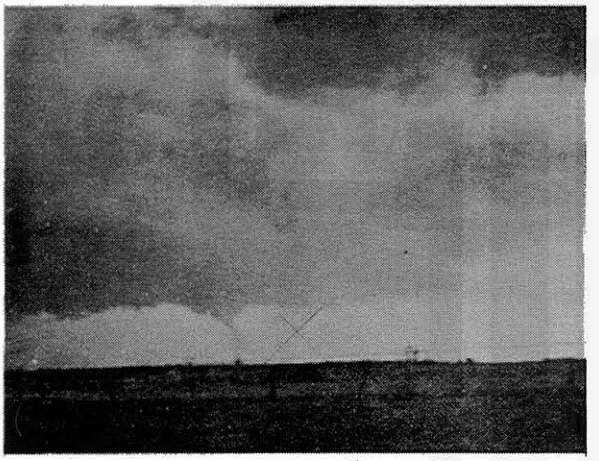

32B

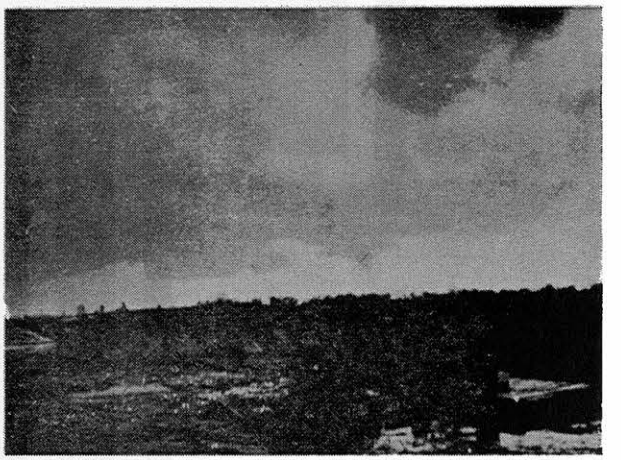

35

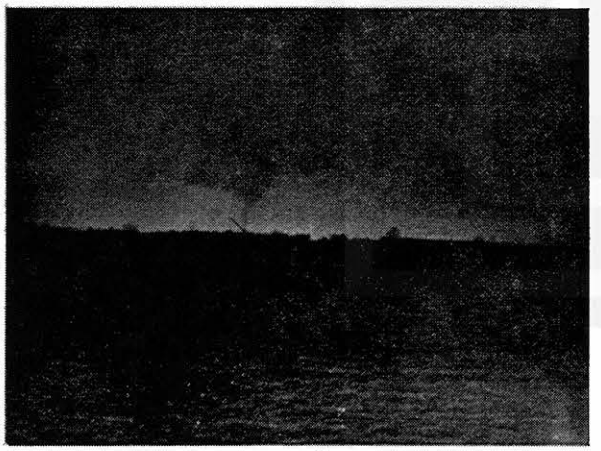

37A

31B

Fig. 31.

37B

37C

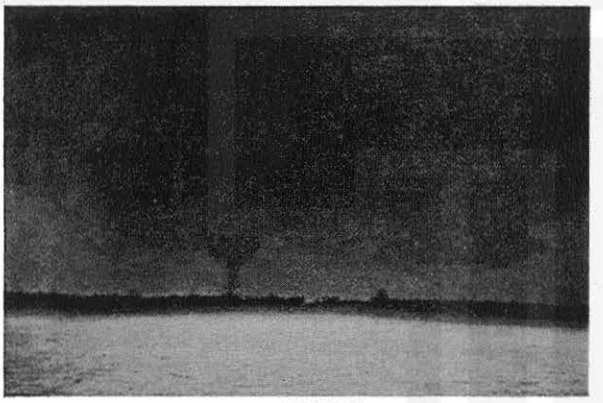

37D

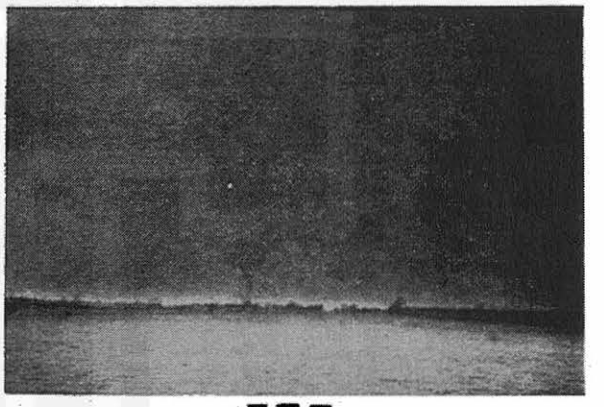

37E

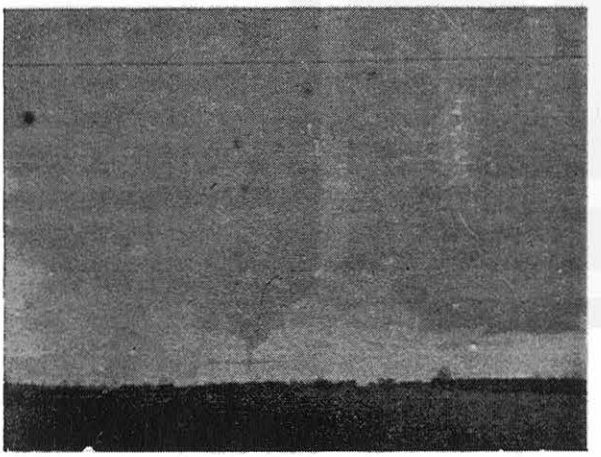

37F

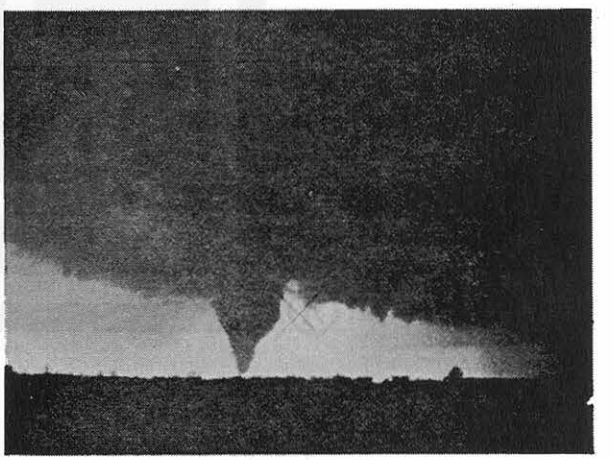

37G

Fig. 32.

37H

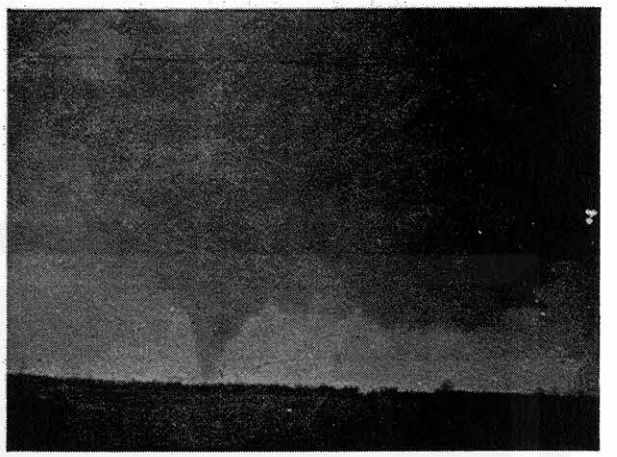

37 I

37 J

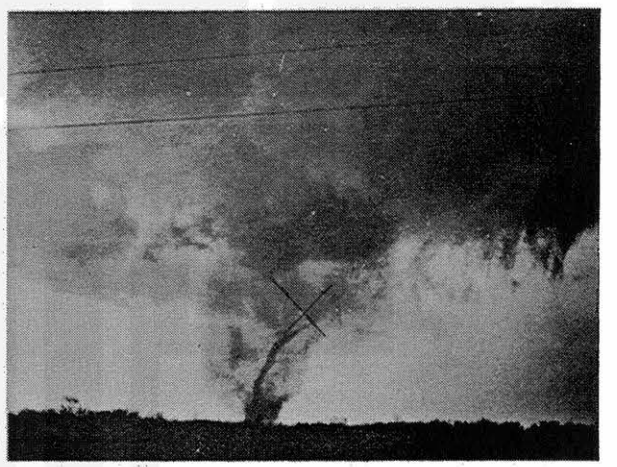

37 K

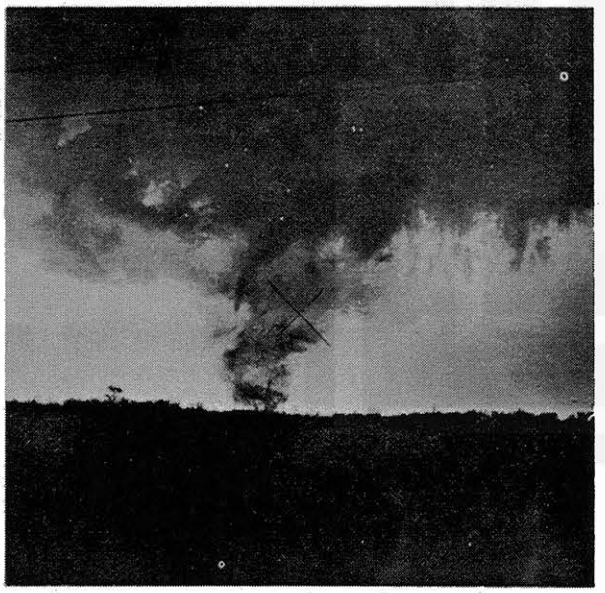

37 L

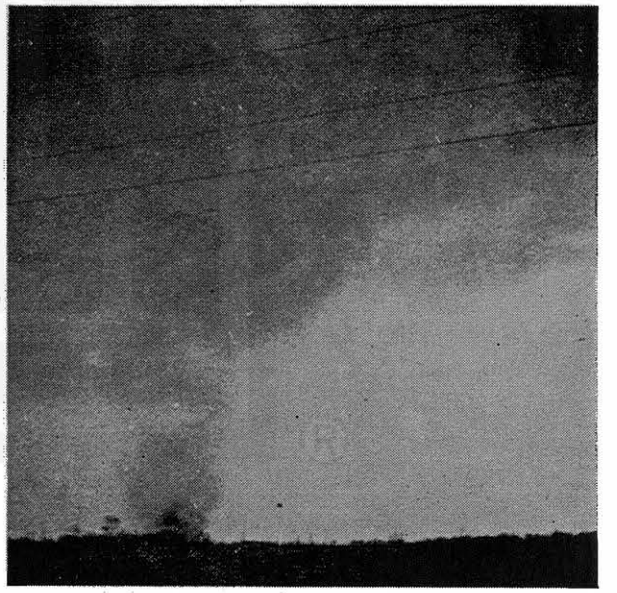

37 M

Fig. 33.

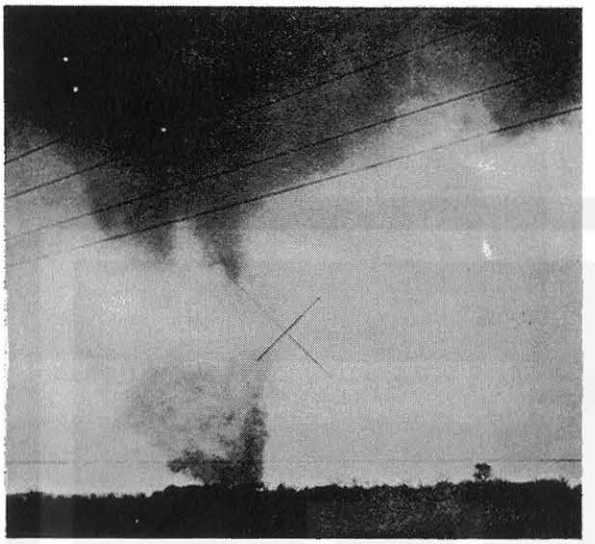

37N

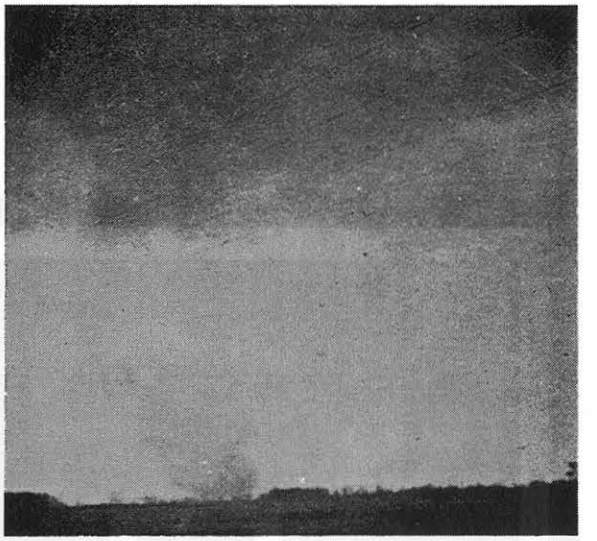

37 O

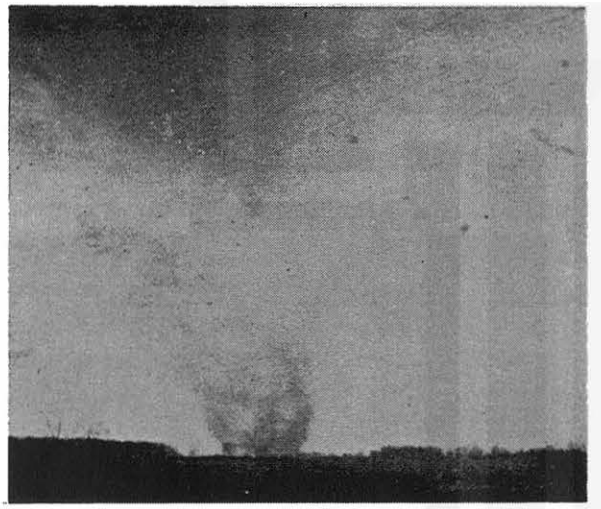

37 P

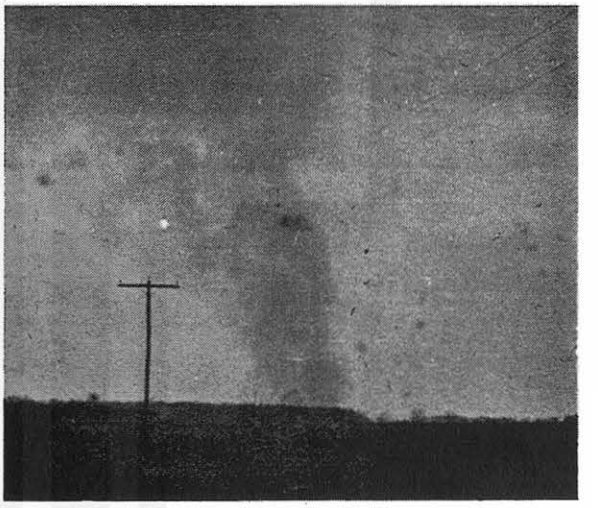

37 Q

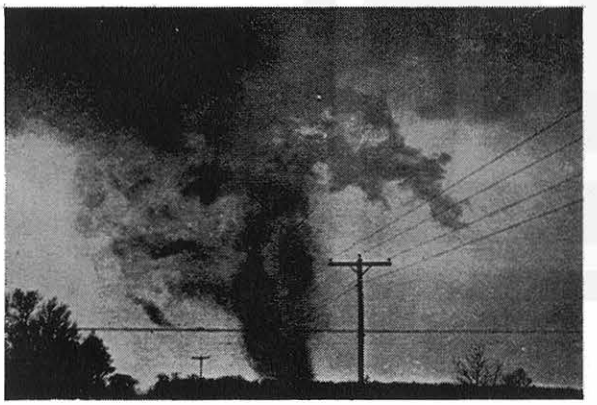

37R

37S

Fig. 34.

37 T

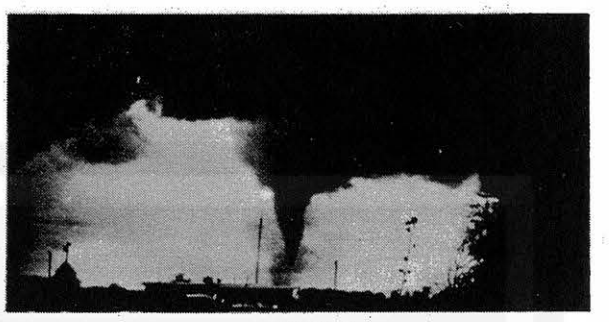

40A

40B

41A

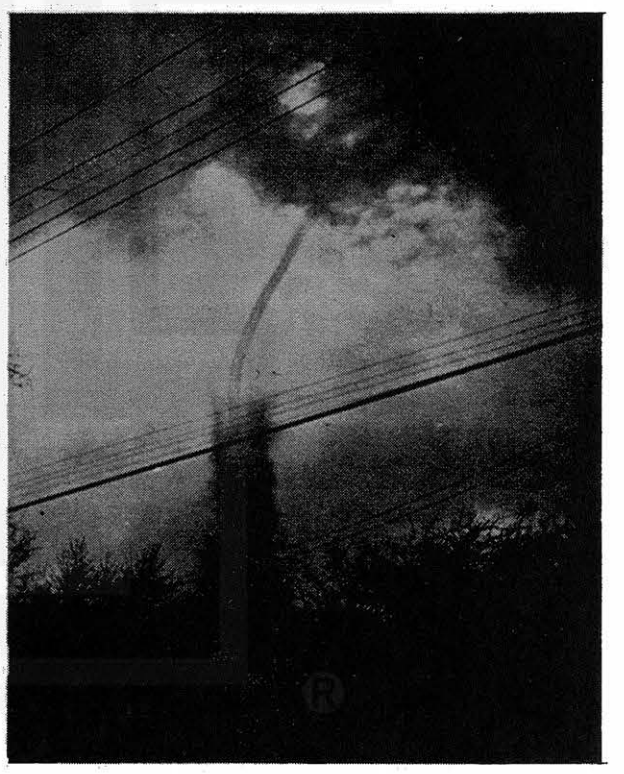

41B

Fig. 35.

V. Photo-Rectification Process

In order to rectify tornado cloud photographs the three essential factors are: the location, the orientation, and the focal length of the camera lens. Since many of the cameras used by the photographers in this study had no easily ascertainable values of lens focal length and since the manufacturer's quality control on fixed-focus camera lenses is poor considering the accuracy needed, the necessity for knowing the focal length of the camera lens with which the cloud picture was taken had to be circumvented. This problem was met by reshooting the original view using a camera lens that had been precisely calibrated. Since this method may be the rule rather than the exception for rectifying tornado cloud pictures of the type in this study, the process used is outlined and explained as follows:

1. From the tornado picture negative a print is enlarged so that fixed objects can be easily discerned.

2. Using a calibrated camera, a picture is taken from the exact location and in the same direction as the original tornado picture; the direction of the picture is ascertained and the elevation angle of the focal axis is established, especially in cases where foreground objects obscure the horizon.

3. After calibration photos are enlarged to a predetermined size, the image length between fixed distant objects are measured; this is done with three or four objects.

4. The ratio of image lengths in the calibrated photo to image lengths in the enlarged original photo is then calculated.

5. Prints from the original tornado negative are then enlarged to the lengths prescribed by the measured distances between objects in the calibrated photo.

1) The most important point is obtaining the negative so that the principal point (geometric center of the image) of the photograph can be determined accurately. In numerous cases of the photographs obtained for this study, there were assurances made by the cloud photographers (who were professionals in many instances) that the prints sent to us for analysis had not been cropped. When the negatives were obtained later, all cases had some cropping of the prints, usually uneven, leading to a displacement of the principal point. Another important reason for obtaining the negative is that prints made commercially (usually on a mass production basis) may not have the quality or contrast that might be attained with individually handled pictures wherein the processor would be guided by specific goals. In two cases the images on the negatives were too faint to be printed by conventional methods. However, by using unconventional methods the images in these cases were made discernable and they proved to be valuable additions to the data for assessing the

shape and size of the tornado cloud.

2) The need for using a calibrated camera lens cannot be over-emphasized. Generally lens manufacturers will mark the lens focal length on the lens housing in broadly rounded units to the nearest half millimeter, whole millimeter, whole centimeter, or even whole inch! For aerial and ground based cloud photogrammetry the lens focal length to the one-tenth millimeter is desirable, and an error of less than five-tenths of one percent in the focal length is desirable for use with the tilt angle grids used in this study.

The exact location of the photographer becomes increasingly important as the distance from the photographer to the tornado decreases. The entire photogrammetric analysis depends on angular and distance measurements. The location of the tornado at the time of the photograph is determined by the intersection of the line made by the angular measurement to the tornado funnel (in the image plane) with the surveyed path. If the angular measurement and the subsequent measurements of arc lengths of specific objects is assumed to be accurate, then the error factor in computing the size of objects is inversely proportional to the distance from the object. In the case where the original photographer cannot remember his precise location, the juxtaposition of foreground and background objects in the image should aid in determining the location.

The tilt angle of the particular photograph is determined from the angular distance between the principal point and the true horizon measured along the perpendicular to the true horizon. Since all photographs in this study were ground based, the true horizon and apparent horizon are identical. Then, in order to select the proper tilt grid, the apparent horizon must be made discernable either in the calibration photograph or by measuring the elevation angle to the principal point. If the tornado photograph is taken from a rural area then a calibration photo using a wide angle lens might be sufficient to determine the horizon. However, if taken from an urban area, a measurement of the tilt angle will most likely be needed.

3) Enlarging the calibrated photos to a specified size should be done with great care since the ensuing measurements from the calibrated photos will be the basis from which all cloud measurements are made. The size to which the photos are enlarged is specified in this case by the focal distance of the prepared tilt angle grids (94.7 mm). After enlarging the calibrated photo, identical objects in the original and calibrated photo should be found and their respective sizes should be compared. In order to avoid errors due to lens distortion, objects away from the edges of the photo should be chosen. However, errors in measurements of distances between objects may necessitate choosing objects in the region of the photo where lens distortion may be significant. In such cases a number of distance measurements between distant objects should be made. It is also important that the objects measured and compared are background objects in the photo. The problem of exact location becomes significant if foreground objects are used to calculate distances. If there is a choice between various objects in the photograph, preference should be given to background objects whose image distance is large enough to be measured with an error of less than five-tenths of one percent.

4) The ratios or the calibration image distances to the original photo image distances are then computed. If the ratios for differing distances are equal then the measurements are accurate, and the proper enlargement of the original photo can be made. If the ratios are not equal, then errors should be investigated. The most common error found in this study was in the choice of objects. In the case where the image distance between foreground and background objects is used, the exact location of the original photographer became important, and the comparison of these ratios made the error in location evident. Preference was then given to the ratio computed from the objects most distant from the photographer (i. e., closest to the horizon). In cases where more than one tornado picture is taken by a photographer and the enlarged prints are the same size, the enlargement ratios should be the same for each photo since the only significant variable is the lens focal length which is assumed the same (in the absence of information to the contrary) for all pictures taken by an individual photographer.

5) The last step in the rectification process is enlarging the original tornado photograph to the size specified by the focal distance of the tilt grids. This can be done more accurately if the distance ratio is applied to a line in the photograph such as the horizon line. If the ratio is applied to the horizon line, the roll angle of the original photo should be considered since the length of the horizon line varies as function of this angle. Especially in the case where a number of pictures were taken by an individual photographer, particular attention should be paid to the differences in length of the horizon line, and a separate enlargement should be computed for each of such pictures.

The tornado cloud photographs can now be considered rectified and the photogrammetric measurements of objects in the image can now be made. Since the coordinates on the tilt grid are angular units, geographic distances from the observer (or photographer) to the various image objects are necessary before absolute linear dimensions can be applied to the objects. The one distance point known is where the tornado vortex makes contact with the ground. This point was determined from the surveyed damage path. If the vortex has no slant angle (i. e., extends vertically to the base of the cloud), the distance to all points along the vortex is also known, and the linear dimension of the vortex can then be computed. If the vortex has a significant slant angle, then the distance to the vortex as prescribed by the distance to the damage path would not be appropriate to determine the absolute size of the vortex at points other than its point of contact with the ground.

VI. The Shape of the Visible Tornado

By using the photogrammetric techniques described previously, as well as taking into account the various tilt angles of the vortex that were depicted in certain photos, the diameter of the visible vortex at varying heights was computed from the still photographs. The computed diameters were then plotted on a chart of distance versus height along the path, and lines of equal diameter were drawn for the plotted values. A plot of the various tornado tilt angles in image planes was made to denote positive or negative distance corrections with height, after which small scale variations in the values of visible diameter were smoothed.

Due to its unusually long span the path was split into several short-length sections so that all variations in the width of the vortex could be examined. The small sections were then placed side by side and variations in the vortex width due to variations in the density of data coverage along the entire length of the path covered by photographs were considered. Some smoothing between sections was necessary since the density of data points near the edges of the short sections varied considerably. However, when viewed in its entirety, the major variations in the height and the diameter of the photographed vortex were revealed.

Figure 36 is a smoothed analysis of the diameter of the vortex along the damage path. The isolines of diameter are in units of feet, and they are presented in varying intervals to denote differences in significance. The thin vertical lines denote the locations of the data points in the various portions of the path. Since the density of data points in some parts of the path was so great that drawing lines for every observation was prohibitive, the number of lines indicating the data can be considered minimal.

As can be seen in the figure, the general slope of the lines indicates a decrease in the width of the visible vortex along its path. Although the variability in visible vortex width increases, the impression of those variations at higher portions of the vortex implies that all the low-level variations are not caused merely by changes in type and density of debris. The first portion showing a large variation over a relatively short space develops about 35 mi along the path. This section is of particular interest since the change in width was subsequently verified in strips of moving pictures taken of a small segment of that portion. Additional measurements made from the motion pictures supplemented the evidence from still shots so that the length of path over which this variation in visible vortex width occurred has been reduced to that shown. The region where apparently sustained enlargement in the width of the vortex occurred at 50 to 55 mi along the path was covered by a series of still shots

taken from the same location. Moving pictures taken of the vortex in this region and beyond verify the enlarged shape. The greatest variation in width occurs near the end of the path. The rapid change in width of the vortex including the condensation funnel at about 69 mi is computed from the measurements in two photographs shown in the previous section. The short dashed lines are drawn for those width values of the condensation funnel that could be distinguished from the width values of the circulating debris; the long dashes are for estimated width values between data points.

Since the distinct continuous condensation section in Fig. 36 includes existent debris in the analysis of the width, that portion of the path for which the condensation funnel could be measured is shown separately in Fig. 37. The vertical lines indicate the vertical extent and the location of data points. As can be seen from the intersection of the isolines of diameter with the vertical lines, the decrease in width of condensation funnel below 2000 ft altitude was manifest in more than one photograph. Also the increase in width near the end of that section of path was evident in more than one photograph. This abrupt change can be seen vividly by comparing photographs 37F and 37G (Fig. 32). The ending of that section of path occurred with a continued broadening of the visible vortex and the final breakup of the condensation funnel into many discontinuous parts that seemed to be small vortices.

Although a number of photographs contained measurable elements of cloud higher than 4000 ft, the vertical extent of the data (as indicated by the height to which the vertical lines extend in Fig. 36) varied considerably, generally below that level. Because of the decrease in the number of data points for the higher levels, the intervals between isolines of width were increased. As far as can be determined from the combined movie and still-photographic evidence there was no indicated change in patterns that could be clarified by additional isolines. In the lowest region near the ground surface the addition of isolines would necessitate an analysis of effects that embrace differing soil conditions.

The general function of these smoothed presentations can therefore be considered quantitative estimates of the continuous change in shape in the lower 4000 ft of the tornado cloud system. This estimate can be applied to the study of both time and space changes in the structure of this portion of the system and might also serve as a means of comparison between various tornadoes.

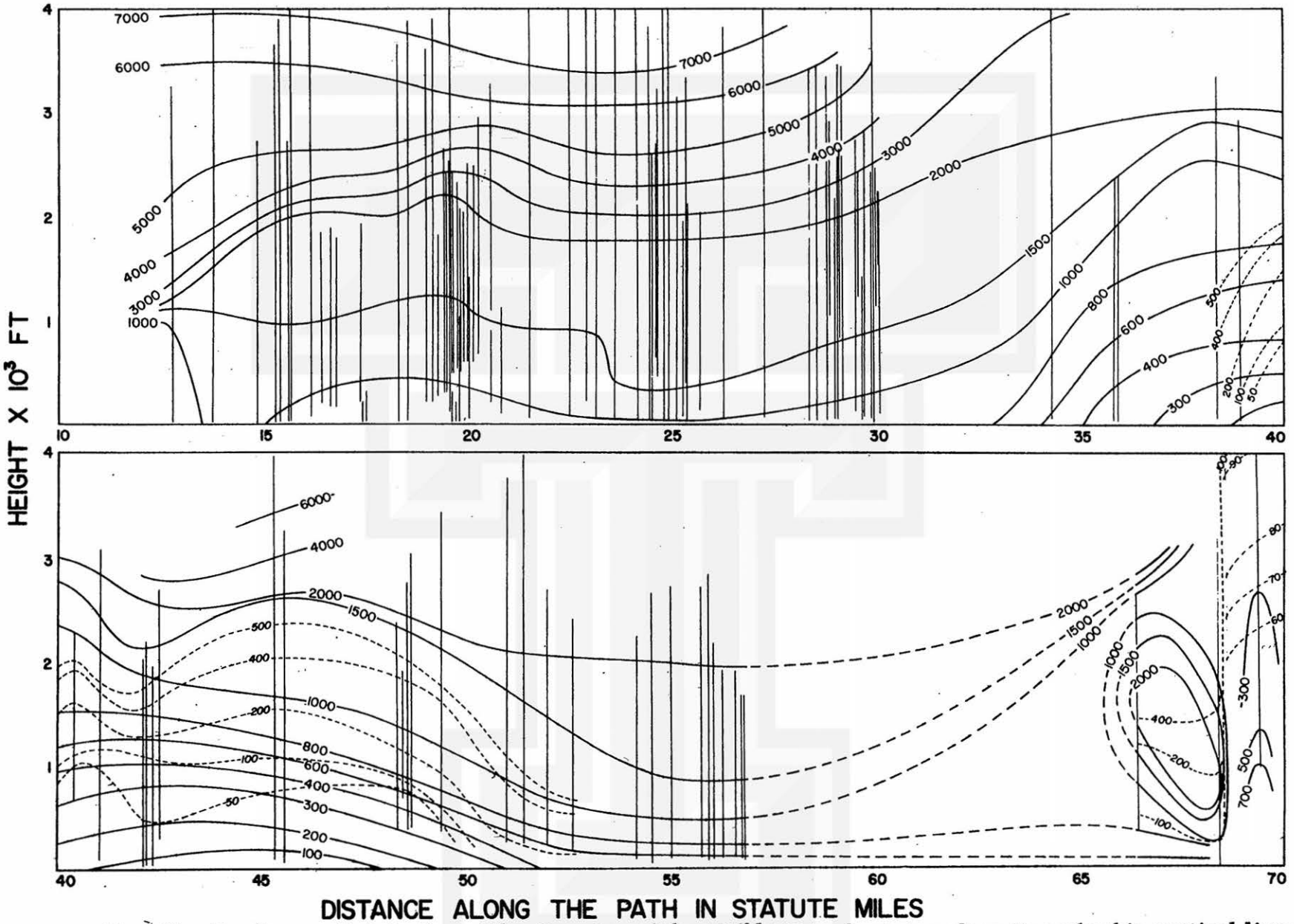

Fig. 36. Continuous distribution of the diameter of the visible tornado vortex along its path: thin vertical lines indicate the location along the path and extent of data in the vertical; solid lines represent values of visible diameter composed of debris or condensation particles; short dashed lines represent diameters of the vortex made distinct by condensation particles, large dashed lines represent the estimate of the visible diameter in the absence of data.

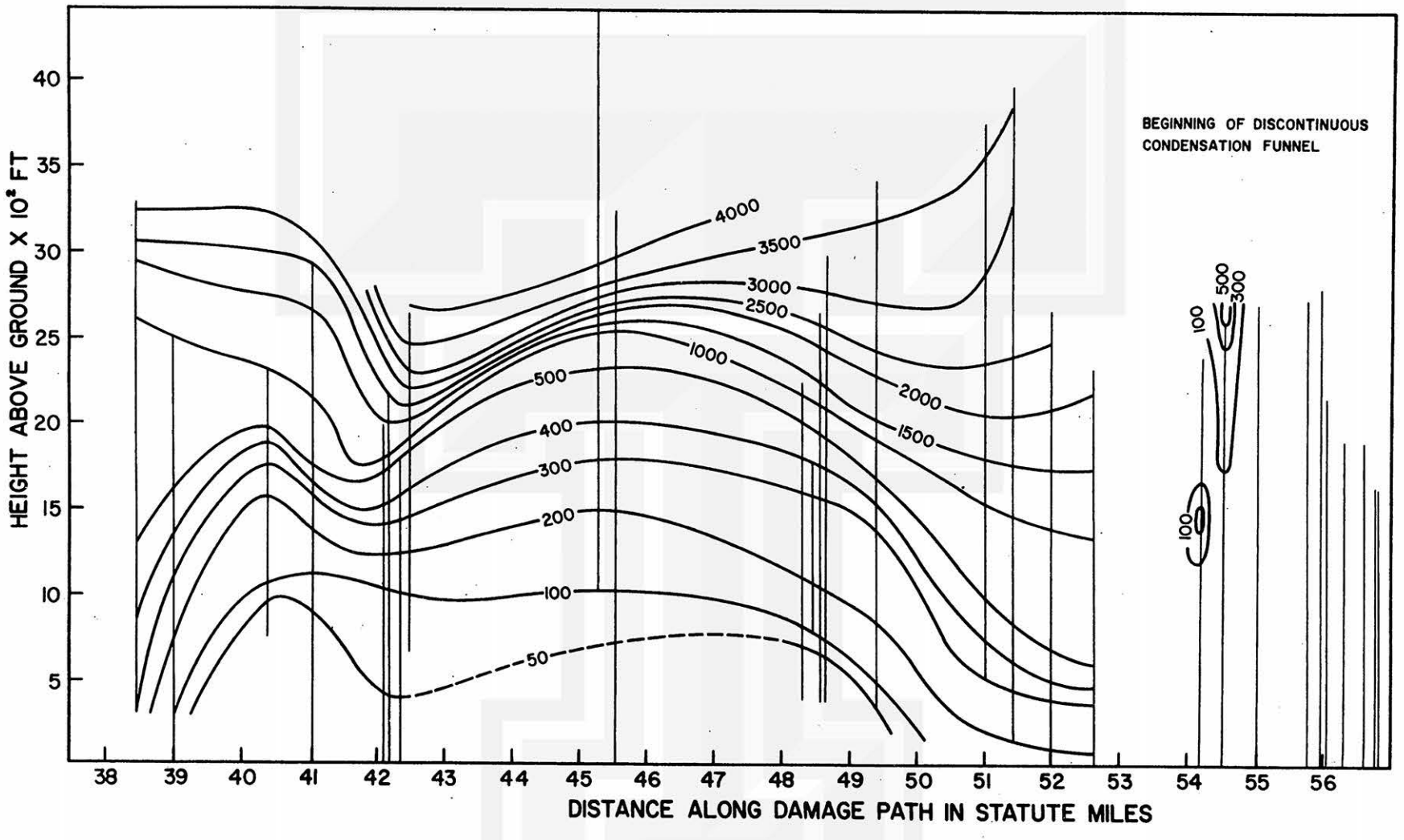

Fig. 37. Smoothed analysis of the diameter of the condensation funnel as a function of height and distance along the path.

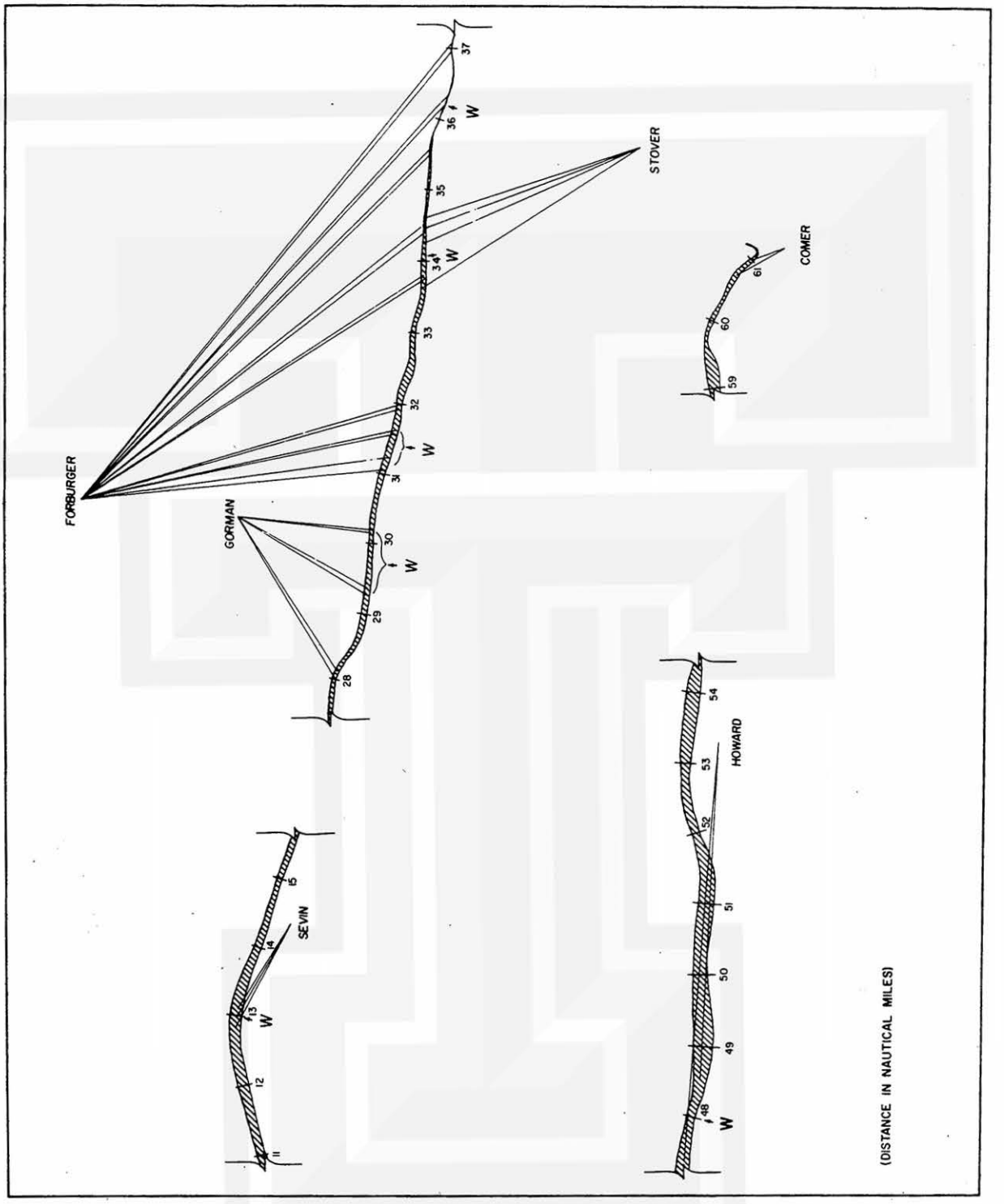

Fig. 38. Location of data points along the path with which translation speeds and motions within the tornado vortex are computed.

VII. Air Motions of and within the System

Motion pictures of cloud movements are probably the best qualitative evidence of the magnitude and sense of rotation of a tornado system. However, such pictures are usually taken by the general public and, as a result, all the shots of the 17 April tornado were on 8 mm color film, so that no distinguishable minutiae could be pinpointed as might have been possible had the original film been 35 mm. In fact, it was impossible to differentiate small objects from the grain of the film or from other particles not related to the subject of the pictures (such as dust on the film, scratches, etc.). Nevertheless, conglomerations of fine particles (probably dust) that remained in a recognizable group for an observable length of time (usually for 25 or more frames) and displayed an organized rather than a random motion were singled out and subsequently used as the data points of motion within the system. Recognizable fringes of cloud (called "cloud tags" by Hoecker) on the outside edge of the wall cloud were also used as data points from whose tracks calculations of the rotation were made.

Although objects in the motion pictures were not precisely calibrated as were objects in the still photographs, ample coverage of the tornado along its path allowed accurate measurements to be made from the motion pictures through the following method. The projected size of the tornado system and its parts from the motion picture were compared to the calibrated size of the tornado system and parts determined from the still photographs at appropriate locations along the damage path. The ratio of projected size to calibrated size was then used to convert projected displacements to true linear (geographic) displacements, with which speeds were calculated. Using this method, vertical components of the motion were also calculated. The tangential components were calculated in the same manner with the additional assumption of a circular path whose length is determined by the diameter's projection on the image plane. Since all primary measurements of displacement of data points are made with respect to the tornado or wall cloud, all of the computed air velocities are relative to the tornado's translation. In addition, the displacement of the tornado funnel along its path was measured so that its speed of progression along the damage path could be calculated, providing, as well, checks on the assumed and reported speeds at which the various movie cameras were set.

In all but one case calibration shots were made with the same equipment as was used for the calibration of the still shots. These calibration shots aided in the location of the tornado along its damage path and served as a future check on the structural measurements of the tornado cloud derived from the movies. In Fig. 38 are the

locations of the data used to calculate speeds; tick marks along the damage path are labeled so that the distribution of true geographic locations may be inferred. The calculated component motions are indicated and the linear extents along the damage path, for which computations from the film strips were used, are also shown. As is indicated in Fig. 38, the movie coverage of the tornado was apparently as limited as the still shots during the first part of the damage path (perhaps this is due to the rather indefinite shape of the funnel during its initial stage).

The translational motion of the tornado along its path was also computed from its movement indicated in many of the film strips. These speeds have been incorporated, with that calculated from two power failures along the damage path, into a single representation of the distribution of translation of the tornado at the ground along its path. This distribution is shown in Fig. 39.

Since the movie film data are valid over small distances along the path, most of the values of speed are plotted in Fig. 39 as points. In the case of the two power failures, the computed speed is interpreted as a mean speed over that section of path and appears as a horizontal line segment between the two points. The vertical extensions emanating from the points represent the computed limits of error in the speeds.

As can be seen in Fig. 38, small errors in the measurements of angles can result in large disproportionate errors in speed along the path. Since the general time interval over which speeds were computed was the order of seconds, the distances along the path were usually tenths and hundredths of miles. Errors in linear measurement of such short distances contribute significantly to the error in speeds. The errors in angular measurement became increasingly significant when the angle made from the path of the tornado and the line from the observer to the tornado approaches 180 deg. Although other factors such as camera lens distortion and inaccurate timing mechanisms for shooting speeds contribute to error, these other factors could not be computed easily and were, therefore, not included. The error computation then consisted of the contributions of errors in angular measurements at the observing point and linear measurements along the path.

The distribution of the data points in Fig. 39 does not lend itself easily to interpretation as a continuous distribution of speed. However, some conclusions regarding the variability of speeds along the path with some estimate of mean speed can be inferred. If the reported times of the power failures and their locations are accepted and the reported time of termination of the tornado is taken to be 1730 CST $\pm$ 10 minutes the mean speed from the point of the second power failure to the end of the path would be between 35 and 46 kt. This range in mean speed is shown in the figure as the area

included in the light stippled region extending from about 20 n mi. to the end of the path. If we assume, in addition, that the tornado began its damage path at 1555 CST, the limits on the mean speed for the entire damage are reduced to 35 and 43 kt. This range is shown in the figure as the heavily stippled area. All but two of the data points have some of their range in the speed within the stippled areas, and all but one of the points have some of their range in speed within the light stippled area. If the time of the first power failure is used in conjunction with the times of termination, the range of mean speed increases to 34 and 48 kt.

The lower limit of this range might be restricted for the first half of the tornado path if the distribution of radar echo speed is considered. The speeds of the radar echo were computed from fixes of the center of the highest echo contours shown in Fig. 8. Since the speeds are valid as a set of discrete averages between fixes, a continuous distribution was drawn so that the integration of the speed would produce the correct location fix and the abrupt changes in speed could be minimized. The resultant distribution of speed showed the radar echo speed to increase continuously from 30 to 38 kt. The range in speed from the radar echo position at 1555 CST to the end of the examined radar fixes, at about the path position of the last strip in the Forburger movie film, is 31 to 38 kt with a mean of 34 kt. Throughout this period of radar observation the pendant echo was seen to revolve about the center of the main echo as the entire echo moved eastward. If the tornado is assumed to be located within the pendant echo it seems reasonable to assume that the tornado vortex at the ground would describe a path including this revolving motion about the center of the main echo. For want of a better point, the center of the pendant echo is assumed to describe the smoothest and shortest tornado path to produce a lower limit of speed of translation. The mean speed of 37 kt would allow for the change in orientation of the center of the pendant echo with respect to the main echo. Since the tornado damage path is certainly not smooth, the mean speed computed for this smoothed path would be less than that for the actual path.

One other point regarding the relation of the top and bottom of the tornado vortex is the fact that at no time other than at the end of the path was the tilt of the photographed vortex from the vertical greater than 30 deg. Assuming that the photographed vortex is representative, this means that the base of the wall cloud and bottom of the tornado cannot be displaced by more than one-half mile. Considering the possible variation in the position of the damage path with relation to the center of wall cloud caused by tilt of the vortex, the maximum effect could be one mile over the assumed smooth path, thereby producing a negligible difference in the 37 kt speed.

If the 37-kt lower limit is used for the first half of the path, with the knowledge that the main radar echo increased its speed along its path, some implications regarding the variation in speed of the vortex might be gleaned. Assuming that the decreasing tendency shown by the Sevin movie data is valid, a curve might be drawn to include both of Sevin's speed ranges; then its negative slope might be decreased to account for the mean speed of 36 kt computed for the power failures. After which a smooth curve could be drawn to include at least some part of all the ranges of the data points by having it decrease to a minimum speed of about 32 kt at the third Gorman point and then increase through both of the Stover data points to a maximum of 52 kt at the next to last of Forburger's points. A decrease seems to be in order from that point to Comer's value near the end of the path; however, the lack of intervening data precludes any such implication. The restrictions of the range in mean values for the first part of the path imply a higher value of mean speed (to about 37 n mi) than for the second. This would lead to lower values of speed for the second part of the path than could be obtained by a gradual decrease in speed from the maximum of 52 kt to Comer's value of 42 kt.

The path length of 6 n mi from the minimum in speed to the maximum at about 36 n mi along the path could be a significant half cycle that repeats itself along the path; however, that seems remote since neither the influence of the river crossings nor the manifestations of the variability in the path direction fit such a short wavelength.

The importance of accurate translation speeds of the tornado along its path cannot be overemphasized since, in addition to being a characteristic of the tornado, it serves as a check on the shooting speeds of moving pictures which are important factors in the calculations of the motion relative to the tornado. This was particularly true for one film strip taken during the early part of the tornado's period of existence: in this case the shooting speed was corrected from the value reported by the photographer thus permitting representative values of component motions in the vortex to be computed.

In Fig. 40 are the data points of all the component motions computed from movie film; vertical and tangential velocity components are indicated by W and W_θ respectively. As can be seen, most of the data points are for vertical motions and, for this reason, most of the analyses of component motions are restricted to the vertical component. The data computed from various locations along the tornado's path are plotted as various symbols which refer to specific locations. A legend relating the symbols to the location numbers appears in the figure, and the locations of data points relative to each other are conserved generally by the numbering system.

Since the values computed for vertical motion are taken from various locations and times of the tornado, the assumption that the distribution of the values shown in Fig. 40 represents a distribution at a particular moment would be invalid. In order to make the values more representative of such a distribution, the data were divided into groups representing the particular portion of the path over which they were valid, and then analyzed separately. Since all of the data points used in the computation were near the edge of the visible funnel, the variations in width of the funnel in addition to the changing pattern of vertical velocity are indicated by the differences among the four analyses shown in Fig. 41. To accentuate the change in slope of the edge of the visible funnel the radius scale is twice the height scale. Time intervals over which the individual patterns extend are indicated at the top of each pattern. The time intervals between patterns are indicated at the bottoms of the charts.

In the first pattern representing the vertical motions in the early portion of the tornado's existence, the data points are concentrated at the lower levels of the vortex. As a result, the analysis of vertical velocity does not extend as high as in the later patterns. The small slope of the edge of the vortex coupled with the double maxima in the pattern casts doubt on the representativeness of this pattern. However, the slope of the edge of the vortex was found to be representative by the analysis of the shape of the vortex shown in the previous section, and the double maxima existed only in this pattern — probably a short-lived phenomenon considering the entire life cycle of the tornado.

If there exists a relationship between the change in slope of the edge of the visible vortex and the pattern of vertical motion, then the double maxima of the first pattern can be assumed to rise and merge into a single maximum at the location and position of the second pattern in the same gradual fashion that the slope of the visible vortex rises, (as shown by the smooth lines in Fig. 36). The second pattern is in the region of large change in slope of the funnel, and although the differences in patterns between the second and third seem slight, the change in pattern with time is the largest shown by the moving pictures. The fourth pattern is in the region where the condensation funnel has ceased to be continuous and the pattern of motion, as shown by visible particles, has increased significantly in radius. The speed with which this change took place can be assumed to be as gradual as is indicated from the relatively gradual increase in width of the funnel (shown in Fig. 36) near that section of path for which the fourth pattern is valid. This pattern was extended beyond the normal limits of the data points due to qualitative evidence of the lack of radial shear in the motion pictures for this portion of the tornado.

Certainly these four patterns do not depict the entire changing pattern of vertical motion in the tornado, especially since no measurements of vertical motion could be made in sufficient quantity from the movie of the rope funnel. However, if the pattern in Fig. 36 is functionally related, as assumed previously, then the four patterns can be considered to be representative of a major portion of the vertical motion within the tornado; and the following general information regarding the time and space change of the vertical motion pattern can be extracted.

During the early portion of the tornado's lifetime, the height of the maximum in vertical velocity increases with a decrease in its value of radius. In addition, the value of the maximum increases so that in general, as the radius of the vortex shrinks, the maximum in vertical velocity increases as it rises. This process is gradual and only becomes more abrupt as the tornado reaches the approximate midpoint in its path. After reaching this area the value of the maximum point in the vertical velocity pattern decreases while the height and radius of the point increase. The radius of the vortex must decrease near the end of its lifetime and, judging from the rapidity with which this previously was shown to occur, the maximum point also decreases abruptly. The change in pattern of vertical motion about the maximum point can be likened to the changes in the shape of the funnel. Where the vortex is shrunk in radius (near the midway point of its path), the pattern is tight, indicating large shear of vertical velocity; where the vortex increases in radius the shear decreases. This is excepting the large vertical shear in the first pattern, which is probably due to the proximity of the ground.

In order to normalize the four patterns of vertical velocity without losing many features of the horizontal and vertical shear that might be a function of the visible edge of the vortex, both the geometry of the visible vortex and the position of the individual maxima were used as indices. The geometry of the visible vortex was obtained by computing a mean width of the vortex over the length of the damage path between the first and last patterns. Since this portion of the path was also covered by data from still photographs, the smoothed distribution of visible vortex diameters was used to determine the representative shape of the vortex over the prescribed path length. The position (in radius and height) of the maximum was then computed from the mean height of the maxima in the four patterns, and the radius was determined from the radius at which that height occurs on the mean shape of the vortex. This value of radius was close to that obtained by the arithmetic average of the height and radius of the four maxima, as was expected, since the four patterns seem to represent the extremes in the overall shape of the visible vortex exclusive of the rope funnel stage.

Using the mean values of the heights and radii of pattern maxima, the four patterns were gridded with respect to their individual maxima using the intersections of linear increments of the height and radius taken in whole-tenth values. In order to check the effect of the various shapes of the visible vortex on the final representation, normalizing with respect to the maximum point and to the near vertical axis of maximum vertical velocity was done with the result that the changes in slope produced no more significant changes in the mean pattern than those caused by the rotation of the various patterns necessary to aline the near vertical axes.

The pattern of mean vertical velocity, determined by conserving the near vertical slope of the axis of maximum vertical velocity, is shown in Fig. 42. The isolines are in ft sec^{-1} and a curve of small dashes encloses the region containing the grid points for which mean values were computed from four values. The region outside the curve that is composed of grid points for which three values are available was also analyzed; this region is also represented by the extent of dashed isolines of mean vertical velocity. The abrupt difference in shear near the boundary between the two regions is due to the general lack of the low values of vertical velocity in the first pattern that are absent from the mean values of the region of three-value grid points. The axis representing the mean slope of the edge of the visible vortex is the near vertical thin line, and the indicated point is the maximum in the pattern whose value and location can be derived. The alternating dot and dash segment of the 100-ft sec^{-1} isoline is an extension of the line through the regi on of fewer data. The dashed line extending from the edge of the four-value region is the 100-ft sec^{-1} isoline for the mean values computed from the three-value points of that area. The difference in position of these two lines is perhaps a better indication of the differences in pattern caused by the three-value data points.

In Fig. 43 is the normalized pattern of mean vertical velocity based on the location of the maximum point (lines are as in Fig. 42). As can be seen, when the two patterns are compared, the normalized pattern based on the slope of the edge of the visible vortex contains greater radial shear in the vertical component than does the other pattern. From considerations of the original data, with which the syntheses of the four patterns were made, the normalized pattern based solely on the location of the maximum point is considered more representative of the mean field of vertical motion through the particular length of path over which the patterns occurred. The pattern based on the slope is representative of a mean field of vertical motion with respect to the expanding and contracting radius of the visible vortex.

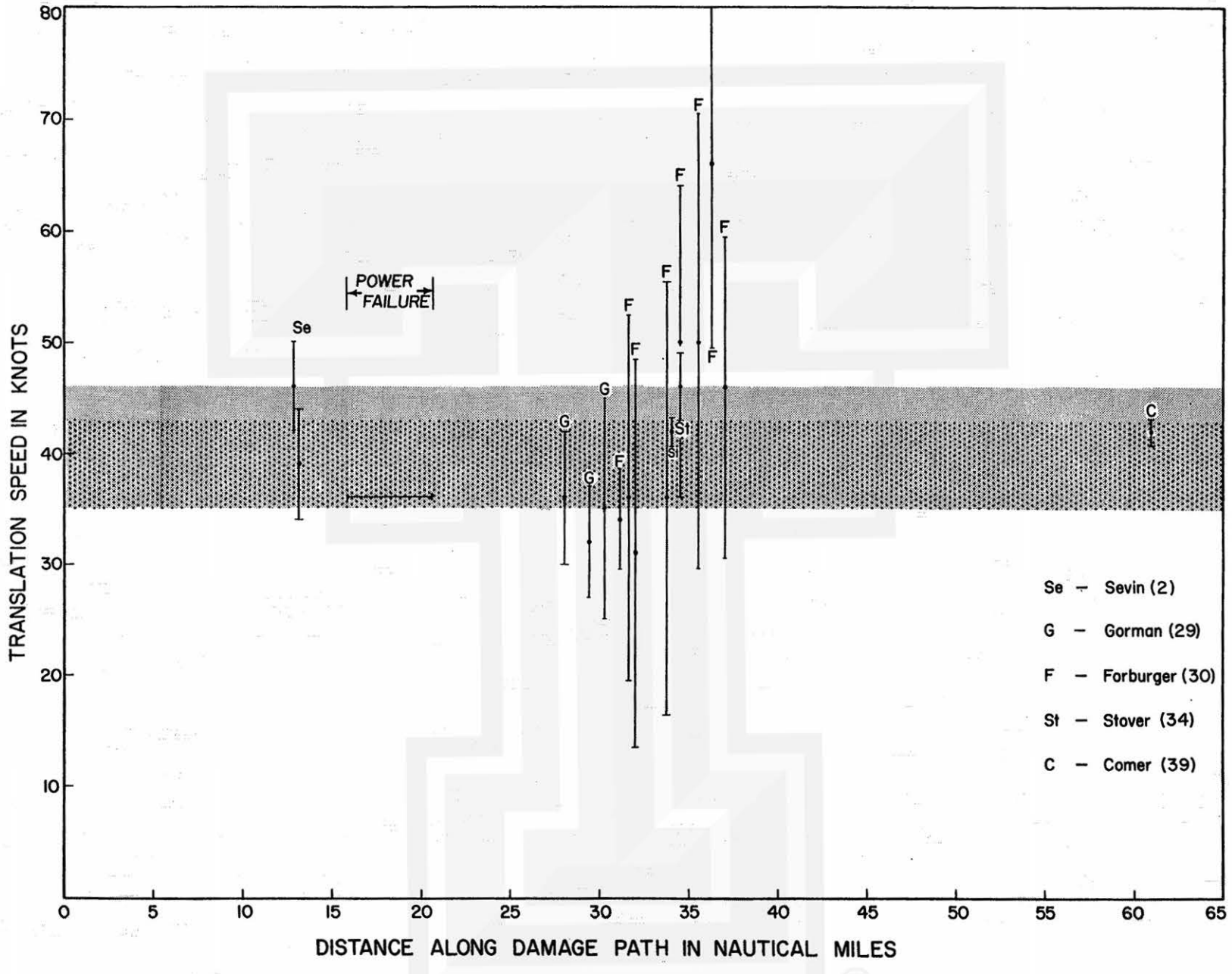

Fig. 39. Distribution of translation speeds of the vortex computed from movie film data and times of power failures.

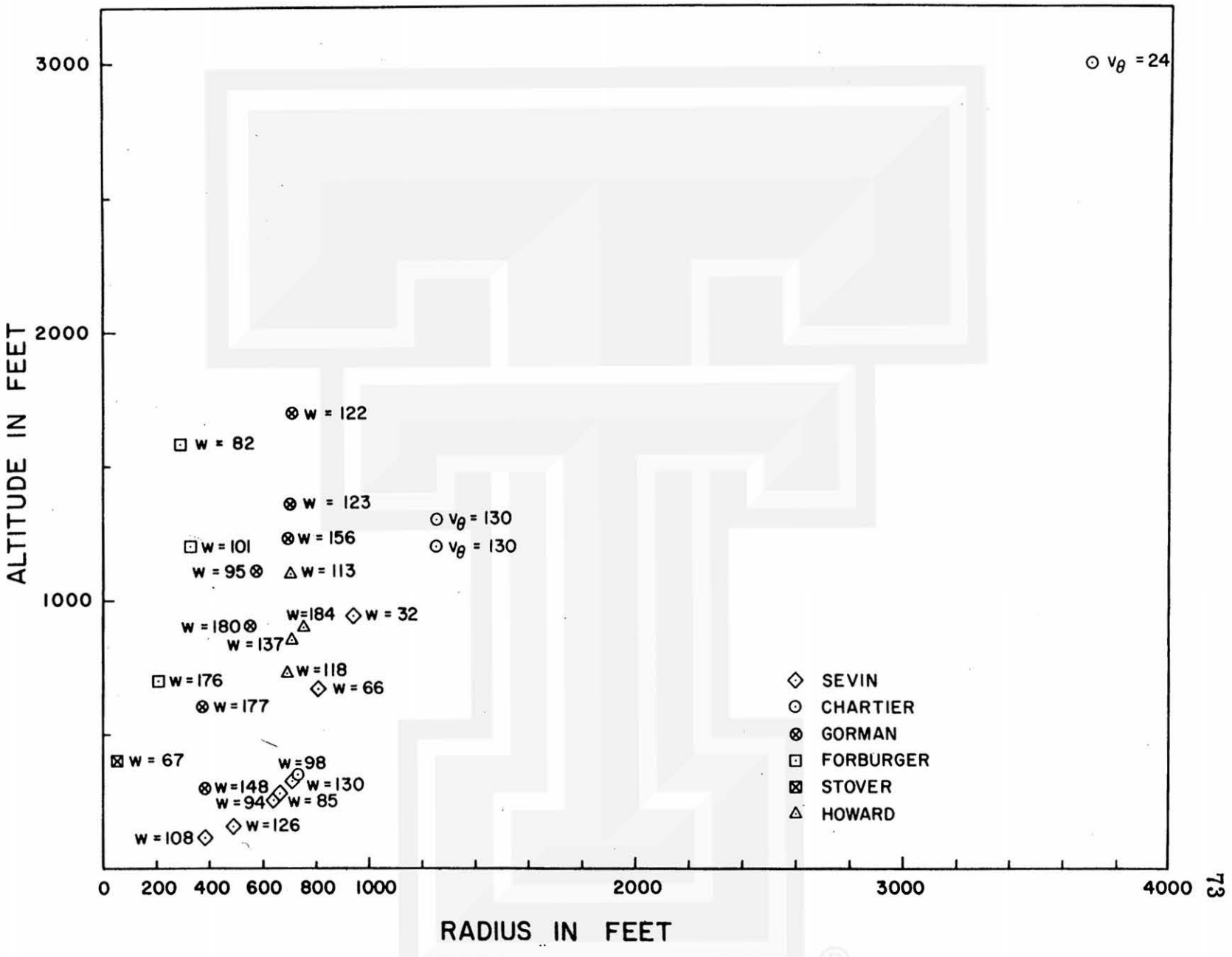

Fig. 40. Radius versus height distribution of data points with which component motions within the tornado system are computed.

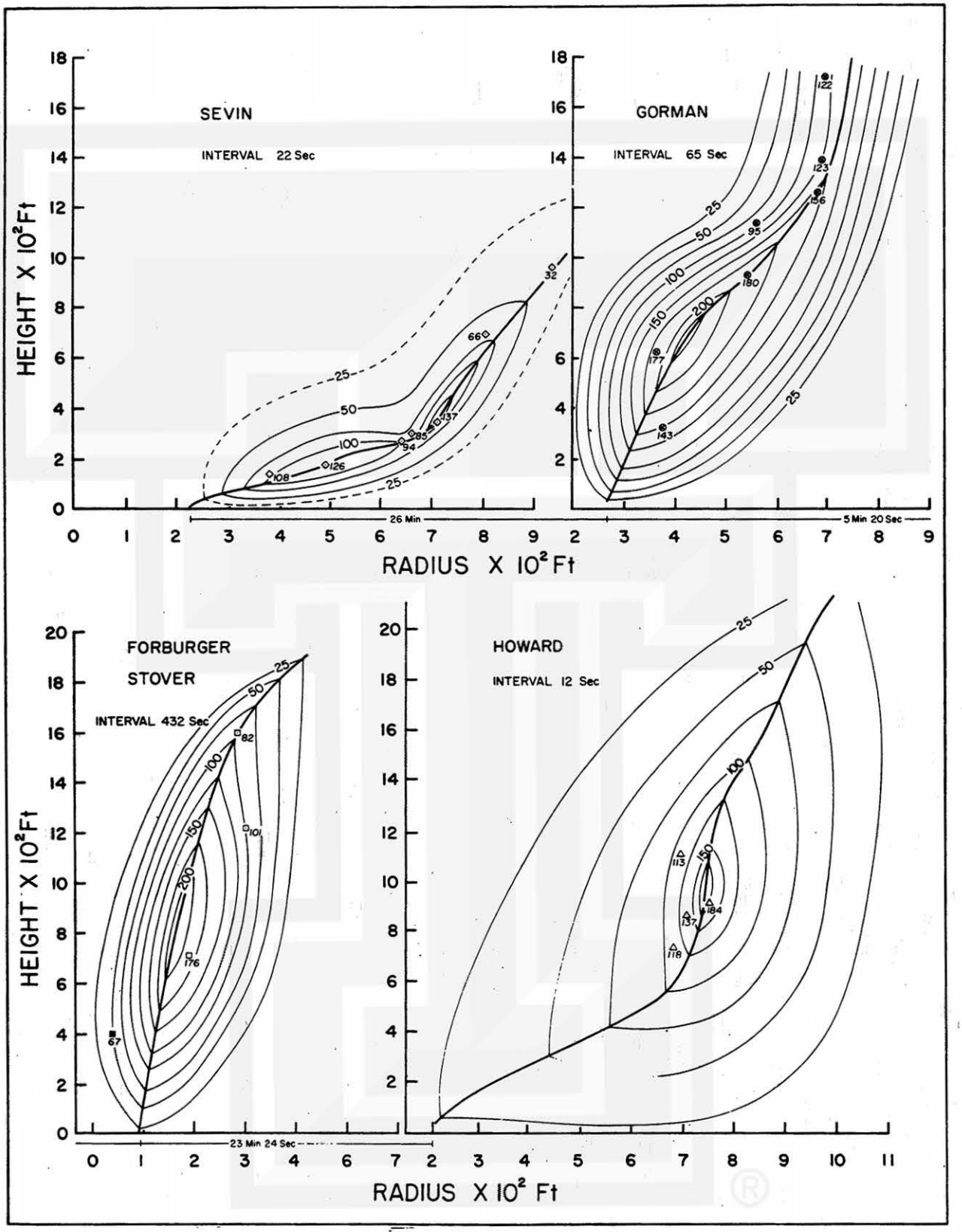

Fig. 41. Vertical velocity patterns at four locations along the damage path.

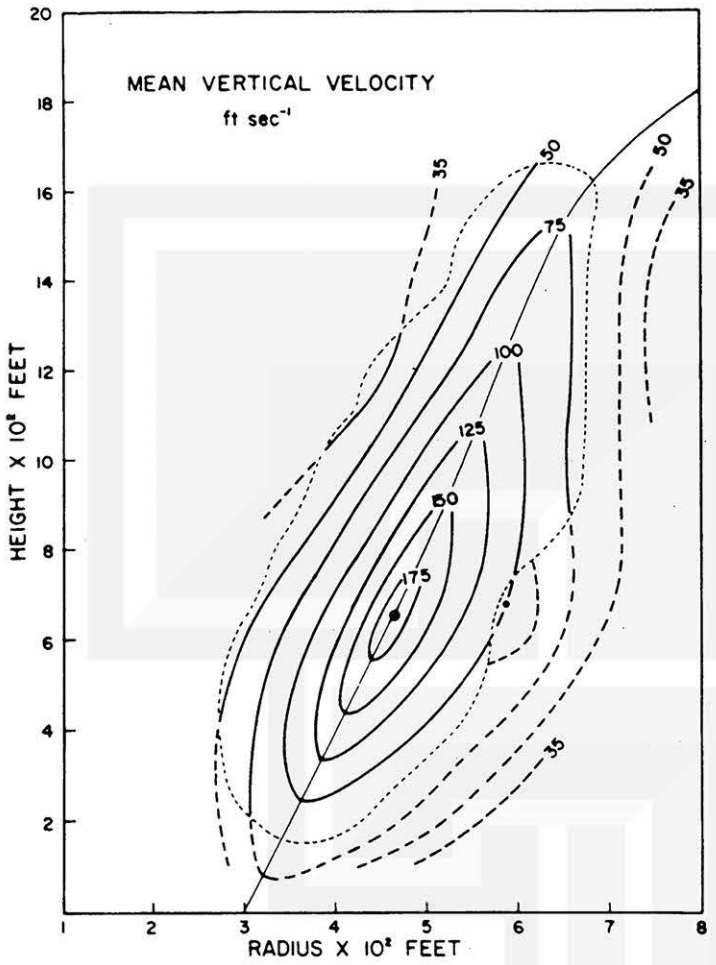

Fig. 42. Mean vertical velocity field normalized with respect to the maximum point and the axis of maximum speed.

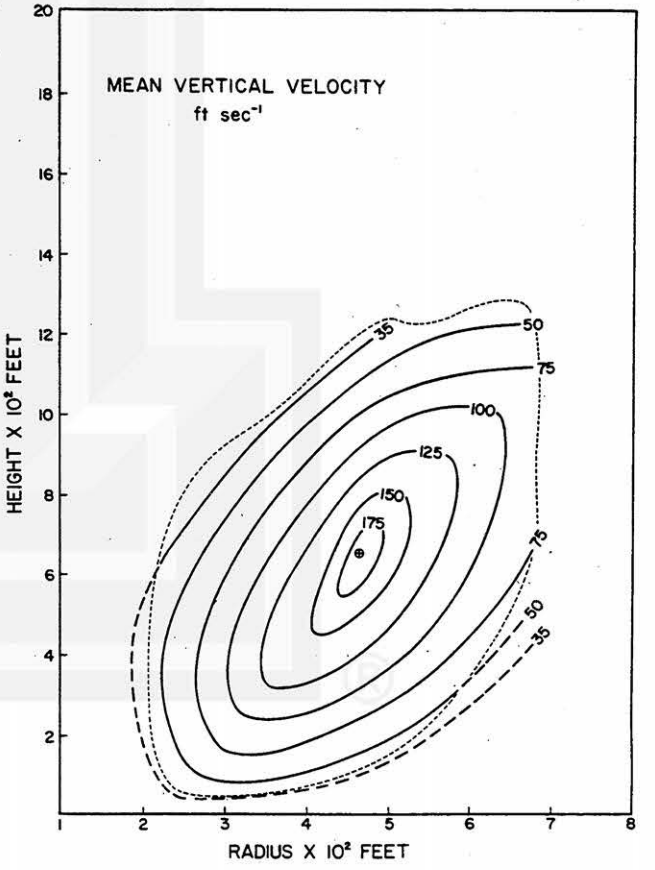

Fig. 43. Mean vertical velocity field normalized with respect to the maximum point.

REFERENCES

Browning, K. A., 1963: The basis of a general model of the airflow and precipitation trajectories within persistent convective storms. Conference Review for Third Conf. on Severe Local Storms, Amer. Meteor. Soc., Urbana, Illinois, 16 pp.

_____, and F. H. Ludlam, 1962: Airflow in convective storms. Quart. J. R. meteor. Soc., 88, 117-135.

Fujita, T., 1957: Three dimensional meso-analysis of a squall-line. Research Paper No. 1, Illinois State Water Survey, Urbana, Illinois, DA-36-039 SC-64656, 19 pp.

_____, 1962: A review of researches on analytical mesometeorology. Research Paper #8, Mesometeorology Project, Univ. of Chicago, 114 pp.

Goldman, J. L., and T. Fujita, 1963: Preliminary radar and photogrammetric study of the Illinois tornadoes of April 17 and 22, 1963, Research Paper #24, Mesometeorology Project, Univ. of Chicago, 7 pp.

Hoecker, W. H. Jr., 1960: Wind speed and air flow patterns in the Dallas Tornado of 2 April 1957. Mon. Wea. Rev., 88, 167-180.

Weatherwise, 1964: 17, 78.